

Naval Surface Warfare Center

Carderock Division

West Bethesda, MD 20817-5700

NSWCCD-50-TR-2008/040 May 2008

Hydromechanics Department Report

Potential Flow Forces and Moments from Selected Ship Flow Codes in a Set of Numerical Experiments

by

John G. Telste

William F. Belknap



Approved for public release. Distribution unlimited.

REPORT DOCUMENTATION PAGE				Form Approved OMB No. 0704-0188	
Public reporting burden for this collection of information is estimated to average 1 hour per response, including the time for reviewing instructions, searching existing data sources, gathering and maintaining the data needed, and completing and reviewing this collection of information. Send comments regarding this burden estimate or any other aspect of this collection of information, including suggestions for reducing this burden to Department of Defense, Washington Headquarters Services, Directorate for Information Operations and Reports (0704-0188), 1215 Jefferson Davis Highway, Suite 1204, Arlington, VA 22202-4302. Respondents should be aware that notwithstanding any other provision of law, no person shall be subject to any penalty for failing to comply with a collection of information if it does not display a currently valid OMB control number. PLEASE DO NOT RETURN YOUR FORM TO THE ABOVE ADDRESS.					
1. REPORT DATE (DD-MM-YYYY) 30-May-2008		2. REPORT TYPE Final		3. DATES COVERED (From - To) 1-Oct-2006 - 30-Sep-2007	
4. TITLE AND SUBTITLE Potential Flow Forces and Moments from Selected Ship Flow Codes in a Set of Numerical Experiments				5a. CONTRACT NUMBER	
				5b. GRANT NUMBER	
				5c. PROGRAM ELEMENT NUMBER 0604300N	
6. AUTHOR(S) John G. Telste and William F. Belknap				5d. PROJECT NUMBER	
				5e. TASK NUMBER	
				5f. WORK UNIT NUMBER 07-1-5500-765	
7. PERFORMING ORGANIZATION NAME(S) AND ADDRESS(ES) AND ADDRESS(ES) Naval Surface Warfare Center Carderock Division 9500 Macarthur Boulevard West Bethesda, MD 20817-5700				8. PERFORMING ORGANIZATION REPORT NUMBER NSWCCD-50-TR-2008/040	
9. SPONSORING / MONITORING AGENCY NAME(S) AND ADDRESS(ES)				10. SPONSOR/MONITOR'S ACRONYM(S)	
				11. SPONSOR/MONITOR'S REPORT NUMBER(S)	
12. DISTRIBUTION / AVAILABILITY STATEMENT Approved for public release. Distribution unlimited.					
13. SUPPLEMENTARY NOTES					
14. ABSTRACT This report describes the tasks assigned to code runners in the potential flow force study, which is part of Task 1.4 (Computational Tools) of the Phase IV Hull Form Plan. It describes the computer codes selected to perform the tasks and the data received from the code runners. It highlights the work required to process the data so that force time histories from all the codes are in phase as well as other work required to obtain comparative time history plots of forces and moments during one full period of motion. The time history plots, which are provided in appendices, compare computed quantities from all codes in the force study during one period of motion. The report also presents plots of the minimum and maximum of forces and moments versus measures of nonlinearity for the radiation and diffraction problems in the study. The plots of the minimum and maximum are contained in appendices.					
15. SUBJECT TERMS potential flow, forced motion, tumblehome, flare					
16. SECURITY CLASSIFICATION OF:			17. LIMITATION OF ABSTRACT SAR	18. NUMBER OF PAGES 104	19a. NAME OF RESPONSIBLE PERSON John G. Telste
a. REPORT UNCLASSIFIED	b. ABSTRACT UNCLASSIFIED	c. THIS PAGE UNCLASSIFIED			19b. TELEPHONE NUMBER (include area code) 301-227-1932

(BLOCK 19)

CONTENTS

	<i>Page</i>
NOMENCLATURE	ix
ABSTRACT	1
ADMINISTRATIVE INFORMATION	1
INTRODUCTION	1
TASK DESCRIPTIONS	2
THE COMPUTER PROGRAMS	11
DATA RECEIVED	15
STANDARDIZATION	28
PROCESSING	34
Dominant Periodicity	34
Data Smoothing	35
Time Histories	41
Minima and Maxima	41
OBSERVATIONS	42
Nonlinearity	42
Lack of Agreement Among the Codes	56
Hydrostatic Force and Moment	56
Submerged Deck	61
Steep Large Amplitude Waves	62
Nonlinear Strip Theory and 3D Nonlinear Theory	62
Nonlinear Versus Linear Strip Theory	62
Effect of Grid Velocity Term	62
Wave Contouring	66
Minimum and Maximum in Forced Pitch Motion	66
FREDYN	66
CONCLUSION	66
REFERENCES	85
Appendix A: Time History Plots for Prescribed Heave Motion of Model 5613 (<i>Linked PDF File</i>)	A-1
Appendix B: Time History Plots for Prescribed Heave Motion of Model 5514 (<i>Linked PDF File</i>)	B-1
Appendix C: Time History Plots for Prescribed Roll Motion of Model 5613 (<i>Linked PDF File</i>)	C-1
Appendix D: Time History Plots for Prescribed Roll Motion of Model 5514 (<i>Linked PDF File</i>)	D-1
Appendix E: Time History Plots for Prescribed Pitch Motion of Model 5613 (<i>Linked PDF File</i>)	E-1

Appendix F: Time History Plots for Prescribed Pitch Motion of Model 5514 (<i>Linked PDF File</i>)	F-1
Appendix G: Time History Plots for 0-DOF Motion of Model 5613 in Waves (<i>Linked PDF File</i>)	G-1
Appendix H: Time History Plots for 0-DOF Motion of Model 5514 in Waves (<i>Linked PDF File</i>)	H-1
Appendix I: Time History Plots for 2-DOF Wave Contouring Motion of Model 5613 (<i>Linked PDF File</i>)	I-1
Appendix J: Time History Plots for 2-DOF Wave Contouring Motion of Model 5514 (<i>Linked PDF File</i>)	J-1
Appendix K: Minimum and Maximum Plots for Prescribed Heave Motion of Model 5613 (<i>Linked PDF File</i>)	K-1
Appendix L: Minimum and Maximum Plots for Prescribed Heave Motion of Model 5514 (<i>Linked PDF File</i>)	L-1
Appendix M: Minimum and Maximum Plots for Prescribed Roll Motion of Model 5613 (<i>Linked PDF File</i>)	M-1
Appendix N: Minimum and Maximum Plots for Prescribed Roll Motion of Model 5514 (<i>Linked PDF File</i>)	N-1
Appendix O: Minimum and Maximum Plots for Prescribed Pitch Motion of Model 5613 (<i>Linked PDF File</i>)	O-1
Appendix P: Minimum and Maximum Plots for Prescribed Pitch Motion of Model 5514 (<i>Linked PDF File</i>)	P-1
Appendix Q: Minimum and Maximum Plots for 0-DOF Motion of Model 5613 in Waves (<i>Linked PDF File</i>)	Q-1
Appendix R: Minimum and Maximum Plots for 0-DOF Motion of Model 5514 in Waves (<i>Linked PDF File</i>)	R-1

FIGURES

	<i>Page</i>
1. Body plans for Models 5613 and 5514.	5
2. Isometric views of Models 5613 and 5514.	5
3. Variables record for task 1, forced heave, Model 5514, obtained from a data file received for AEGIR-1.	17
4. Edited list of zone records in a data file containing data from AEGIR-1 for forced heave motions of task 1 for one of the ships.	18
5. Edited list of zone records in a data file containing data from AEGIR-1 for forced roll motions of task 1 for one of the ships.	18
6. Edited list of zone records in a data file containing data from AEGIR-1 for forced pitch motions of task 1 for one of the ships.	19

7.	Edited list of zone records in a data file containing data from AEGIR-1 for task 2 for one of the ships.	19
8.	Edited list of zone records in a data file containing data from AEGIR-1 for task 3 for one of the ships.	19
9.	Time history of F_x^{dif} for the last period of motion as predicted by LAMP-4 together with smoothed time histories from two techniques; 21 data points used in the smoothing; $H/\lambda = 1/10$; $\lambda/L = 1$; $\beta = 45^\circ$; $F_n = 0.0$; Model 5514 scaled to $L = 142$ m.	37
10.	Time history of F_x^{dif} for the last period of motion as predicted by LAMP-4 together with smoothed time histories from two techniques; 11 data points used in the smoothing; $H/\lambda = 1/10$; $\lambda/L = 1$; $\beta = 45^\circ$; $F_n = 0.0$; Model 5514 scaled to $L = 142$ m.	38
11.	Part of the time history of M_x^{rad} as predicted by LAMP-4 together with the smoothed time history from a Fourier transform technique; 21 data points used in the smoothing; frequency = 0.2079 rad/s; roll amplitude = 65° ; $F_n = 0.0$; Model 5514 scaled to $L = 142$ m.	39
12.	Closeup of a peak in the previous figure showing part of the time history of M_x^{rad} as predicted by LAMP-4 together with smoothed time histories from a Fourier transform technique. 21 data points used in the smoothing; frequency = 0.2079 rad/s; roll amplitude = 65° ; $F_n = 0.0$; Model 5514 scaled to $L = 142$ m.	40
13.	Vertical component of the total, hydrostatic, and radiation force experienced by Models 5613 and 5514 at forward speed in prescribed heave motion of frequency 1.1 rad/sec and amplitude 80% of the draft.	43
14.	Total, hydrostatic, and radiation pitch moment experienced by Models 5613 and 5514 as they advance at forward speed in prescribed heave motion of frequency 1.1 rad/sec and amplitude 80% of the draft.	44
15.	Minimum and maximum of total vertical radiation force and total pitch moment versus amplitude of motion experienced by Model 5514 advancing at constant mean forward speed while undergoing prescribed sinusoidal heave motion of frequency 1.1 rad/sec.	46
16.	Total, hydrostatic, and radiation pitch moment experienced by Models 5613 and 5514 at forward speed in prescribed pitch motion of frequency 1.1 rad/sec and amplitude 5°	47
17.	Minimum and maximum of total pitch moment experienced by Models 5613 and 5514 as they advance at constant mean forward speed while undergoing prescribed sinusoidal pitch motion of frequency 1.1 rad/sec.	49
18.	Ship-fixed vertical component of the total, hydrostatic, and radiation force experienced by Models 5613 and 5514 at zero forward speed in prescribed roll motion of frequency 0.3831 rad/sec and amplitude 45°	51
19.	Total, hydrostatic, and radiation roll moment experienced by Models 5613 and 5514 at zero forward speed in prescribed roll motion of frequency 0.3831 rad/sec and amplitude 45°	52

20.	Vertical component of the total, hydrostatic, Froude-Krylov, and diffraction force experienced by Models 5613 and 5514 at zero mean forward speed in stern quartering ($\beta = 45^\circ$) waves with $H/\lambda = 1/15$, and $\lambda = L$	53
21.	Vertical component of the total, hydrostatic, Froude-Krylov, and diffraction force experienced by Models 5613 and 5514 as they advance at constant mean forward speed in head waves with $H/\lambda = 1/15$, and $\lambda = L$	54
22.	Minimum and maximum vertical force experienced by Models 5613 and 5514 as they advance at 0-DOF steady mean forward speed in head waves of varying frequency.	55
23.	Total, Froude-Krylov, and diffraction yaw moment experienced by Models 5613 and 5514 in 0-DOF motion at zero mean forward speed in stern quartering ($\beta = 45^\circ$) waves with $H/\lambda = 1/15$ and $\lambda = L$	57
24.	Ship-fixed lateral component of the total, hydrostatic, Froude-Krylov, and hydrodynamic force experienced by Models 5613 and 5514 while contouring waves in beam seas at zero forward speed.	58
25.	Ship-fixed vertical component of the total, hydrostatic, Froude-Krylov, and hydrodynamic force experienced by Models 5613 and 5514 while contouring waves in beam seas at zero forward speed.	59
26.	Total, hydrostatic, Froude-Krylov, and hydrodynamic roll moment experienced by Models 5613 and 5514 while contouring waves in beam seas at zero forward speed.	60
27.	Vertical hydrostatic force and hydrostatic pitch moment acting on Models 5613 and 5514 advancing at forward speed in waves of steepness $H/\lambda = 1/15$ at the heading $\beta = 135^\circ$	63
28.	Ship-fixed vertical hydrostatic force acting on Model 5514 pitching at frequency 0.2079 rad/sec and amplitude 1.75° at zero forward speed.	65
29.	Ship-fixed vertical hydrostatic force acting on Model 5613 heaving at frequency 0.2079 rad/sec and amplitude 80% of draft at zero forward speed.	65
30.	Ship-fixed vertical component of the radiation force experienced by Model 5613 in prescribed pitch motion of amplitude 5° and frequencies 0.2079, 0.3831, and 1.1 rad/sec at zero forward speed.	67
31.	Ship-fixed vertical component of the radiation force experienced by Model 5514 at zero forward speed in prescribed pitch motion of frequency 0.2079 rad/sec at the pitch amplitudes 1.00° , 1.75° , 2.50° , 3.75° , and 5.00°	68
32.	Ship-fixed vertical component of the radiation force experienced by Model 5514 in prescribed roll motion of amplitude 45° and 65° at zero forward speed.	69
33.	Vertical diffraction force experienced by Model 5613 advancing in 0-DOF motion in head seas of wave steepness $H/\lambda = 1/15$ and $H/\lambda = 1/10$	70
34.	Vertical diffraction force experienced by Model 5613 advancing in 0-DOF motion in following seas of wave steepness $H/\lambda = 1/60$, $1/20$, $1/15$ and $1/10$ where $\lambda = L$	71
35.	Ship-fixed vertical component of radiation force experienced by Model 5613 advancing in calm water with 1-DOF pitch motion of frequency 0.2079 rad/sec and amplitudes 1.00° , 1.75° , 2.50° , 3.75° , and 5.00°	72

36. Ship-fixed vertical component of radiation force experienced by Model 5514 advancing in calm water with 1-DOF pitch motion of frequency 0.2079 rad/sec and amplitudes 1.00°, 1.75°, 2.50°, 3.75°, and 5.00°.	73
37. Ship-fixed vertical component of radiation force experienced by Model 5613 at zero forward speed in calm water with 1-DOF pitch motion of frequency 0.2079 rad/sec and amplitudes 1.00°, 1.75°, 2.50°, 3.75°, and 5.00°.	74
38. Ship-fixed vertical component of radiation force experienced by Model 5514 at zero forward speed in calm water with 1-DOF pitch motion of frequency 0.2079 rad/sec and amplitudes 1.00°, 1.75°, 2.50°, 3.75°, and 5.00°.	75
39. Ship-fixed vertical component of hydrodynamic force experienced by Models 5613 and 5514 as they contour a wave at forward speed in following seas.	76
40. Minimum and maximum of the ship-fixed vertical component of the radiation force experienced by Model 5613 in pitch motion at zero forward speed in otherwise undisturbed water at the frequency 1.1 rad/sec.	77
41. Time-history plots of the ship-fixed vertical component of the radiation force experienced by Model 5613 at zero forward speed in forced pitch motion of amplitudes 1.0°, 1.75°, 2.5°, 3.75°, and 5° and frequency 1.1 rad/sec.	79
42. Time-history plot of the vertical component of the total force experienced by Model 5613 in 0-DOF motion at zero forward speed in following seas with wavelength $\lambda/L = 1$ and amplitude $H/\lambda = 1/15$	81
43. Time-history plot of the vertical component of the total force experienced by Model 5613 in forced heave motion at frequency 1.1 rad/sec and amplitude 80 per cent of the draft for zero forward speed and forward speed corresponding to Froude number 0.3.	82
44. Time-history plot of the yaw component of the computed total moment experienced by Model 5514 in forced roll motion at frequency 0.672 rad/sec and amplitude 65° at forward speed corresponding to Froude number 0.3.	83

TABLES

	<i>Page</i>
1. Layout of the appendices.	3
2. Particulars of the ship hulls.	4
3. 1-DOF prescribed heave motion in task 1.	6
4. 1-DOF prescribed pitch motion in task 1.	6
5. 1-DOF prescribed roll motion in task 1.	6
6. Headings for task 2.	7
7. Waves for task 2.	7
8. Encounter period T_e in task 2.	8
9. Wave amplitude η_a for task 2.	8
10. Specifications for condition 1 of task 3.	9

11.	Specifications for condition 2 of task 3.	10
12.	Encounter period T_e in task 3.	10
13.	Computer codes involved in the force study.	11
14.	Time histories generally expected from code runners.	16
15.	Number of Periods of Data from Each Code for Forced Heave Motion in Task 1 .	20
16.	Number of Periods of Data from Each Code for Forced Roll Motion in Task 1 . .	22
17.	Number of Periods of Data from Each Code for Forced Pitch Motion in Task 1 . .	24
18.	Number of Periods of Data from Each Code for Task 2	26
19.	Number of Periods of Data from Each Code for Task 3	28
20.	Data received from NFA.	30
21.	Standard variables records for the various tasks.	33

NOMENCLATURE

$B(x)$	beam at the longitudinal distance x forward of the center of gravity
CG	center of gravity
C_{33}	hydrodynamic restoring coefficient in the vertical direction due to vertical motion
D/Dt	derivative following a grid point equal to $\partial/\partial t + \vec{V}_g \cdot \nabla$
F_n	Froude number = U/\sqrt{gL} where U is the mean forward speed of the ship, L is the length of the ship, and g is the acceleration of gravity [1]
\vec{F}^{dif}	diffraction force [kN]
$F_x^{\text{dif}}, F_y^{\text{dif}}, F_z^{\text{dif}}$	components of the diffraction force in the ship-fixed coordinate system [kN]
\vec{F}^{fk}	Froude-Krylov force [kN]
$F_x^{\text{fk}}, F_y^{\text{fk}}, F_z^{\text{fk}}$	components of the Froude-Krylov force in the ship-fixed coordinate system [kN]
\vec{F}^{hst}	hydrostatic force [kN]
$F_x^{\text{hst}}, F_y^{\text{hst}}, F_z^{\text{hst}}$	components of the hydrostatic force in the ship-fixed coordinate system [kN]
\vec{F}^{ptot}	total potential force [kN]
$F_x^{\text{ptot}}, F_y^{\text{ptot}}, F_z^{\text{ptot}}$	components of the total potential force in the ship-fixed coordinate system [kN]
\vec{F}^{rad}	radiation force [kN]
$F_x^{\text{rad}}, F_y^{\text{rad}}, F_z^{\text{rad}}$	components of the radiation force in the ship-fixed coordinate system [kN]
g	acceleration of gravity [m/s^2]
GM	metacentric height [m]
H	double wave amplitude of regular sinusoidal waves equal to twice η_a [m]
H/λ	wave steepness [1]
\hat{i}_e	unit vector along the horizontal x -axis of an earth-fixed coordinate system
\hat{j}_e	unit vector along the horizontal y -axis of an earth-fixed coordinate system
\hat{k}_e	unit vector along the vertical z -axis of an earth-fixed coordinate system
k	wavenumber equal to $2\pi/\lambda$ [m^{-1}]
KG	distance from the keel to the center of gravity [m]
L	ship length [m]
LCB	longitudinal center of buoyancy
\vec{M}^{dif}	diffraction moment about the center of gravity [kN-m]
$M_x^{\text{dif}}, M_y^{\text{dif}}, M_z^{\text{dif}}$	components of the diffraction moment about the center of gravity in the ship-fixed coordinate system [kN-m]
\vec{M}^{fk}	Froude-Krylov moment about the center of gravity [kN-m]
$M_x^{\text{fk}}, M_y^{\text{fk}}, M_z^{\text{fk}}$	components of the Froude-Krylov moment about the center of gravity in the ship-fixed coordinate system [kN-m]
\vec{M}^{hst}	hydrostatic moment about the center of gravity [kN-m]

$M_x^{\text{hst}}, M_y^{\text{hst}}, M_z^{\text{hst}}$	components of the hydrostatic moment about the center of gravity in the ship-fixed coordinate system [kN-m]
\vec{M}^{ptot}	total potential moment about the center of gravity [kN-m]
$M_x^{\text{ptot}}, M_y^{\text{ptot}}, M_z^{\text{ptot}}$	components of the total potential moment about the center of gravity in the ship-fixed coordinate system [kN-m]
\vec{M}^{rad}	radiation moment about the center of gravity [kN-m]
$M_x^{\text{rad}}, M_y^{\text{rad}}, M_z^{\text{rad}}$	components of the radiation moment about the center of gravity in the ship-fixed coordinate system [kN-m]
\vec{n}	unit normal vector pointing out of the fluid at a fluid boundary
(p, q, r)	rotational velocities
r	correlation function [variable dimension]
\vec{r}	position vector from the center of gravity
S_0	mean surface of the hull beneath the calm waterline
S_B	instantaneous wetted surface of the hull
t	time [s]
T	draft [m]
T_e	encounter period [s]
T_{mean}	mean draft [m]
U	mean forward speed of the ship [m/s]
VCG	vertical position of the center of gravity
\vec{V}_{CG}	velocity of the center of gravity
\vec{V}_g	grid velocity
$V(z)$	volume of the hull beneath the waterplane at z where z is the distance above the calm waterplane
w	the weight of the ship equal to the magnitude of the weight vector [kN]
x, y, z	coordinates of a rectangular ship-fixed coordinate system with the origin in the equilibrium calm waterplane, the positive x -axis forward, the y -axis positive to the starboard side of the hull, and the z -axis positive upward [m]
z_a	amplitude of sinusoidal heave motion [m]
z_e	vertical position of the center of gravity in an earth-fixed frame of reference with the origin at the mean free-surface level [m]
β	heading, the angle between the direction of wave propagation and the direction in which the ship advances [°]
ϵ	phase [1]
ζ_0	amplitude of the waves equal to η_a [m]
ζ_3	amplitude of heave motion [m]
ζ_4	amplitude of roll motion [°]
ζ_5	amplitude of pitch motion [°]
η	wave height [m]
η_a	amplitude of regular sinusoidal waves [m]

θ	pitch angle; the second Euler angle [°]
θ_a	amplitude of sinusoidal pitch motion [°]
λ	wavelength [m]
ρ	water density taken as 1025 kg/m ³
ϕ	roll angle; the third Euler angle [°]
φ	disturbance potential
ϕ_a	amplitude of roll motion [°]
Φ_T	total velocity potential
φ_w	velocity potential of the incident waves
ω	frequency [rad/s]
$\vec{\omega}$	rotational velocity
ω_0	absolute wave frequency [rad/s]
$\omega_1, \omega_2, \omega_3$	prescribed frequencies of oscillation [rad/s]
ω_e	encounter frequency [rad/s]
$\langle \cdot \rangle$	the mean value of a quantity obtained from a Fourier fit
$(\cdot)^*$	for any quantity f , $(f)^* = (f - \langle f \rangle) / a$ where a is z_a/T in the case of prescribed heave motion of amplitude z_a , ϕ_a in the case of prescribed roll motion of amplitude ϕ_a , θ_a in the case of prescribed pitch motion of amplitude θ_a , and wave steepness H/λ for 0-DOF motion in waves

THIS PAGE INTENTIONALLY LEFT BLANK

ABSTRACT

This report describes the tasks assigned to code runners in the potential flow force study, which is part of Task 1.4 (Computational Tools) of the Phase IV Hull Form Plan. It describes the computer codes selected to perform the tasks and the data received from the code runners. It highlights the work required to process the data so that force time histories from all the codes are in phase as well as other work required to obtain comparative time history plots of forces and moments during one full period of motion. The time history plots, which are provided in appendices, compare computed quantities from all codes in the force study during one period of motion. The report also presents plots of the minimum and maximum of forces and moments versus measures of nonlinearity for the radiation and diffraction problems in the study. The plots of the minimum and maximum are provided in appendices.

ADMINISTRATIVE INFORMATION

The work of collecting and analyzing data described in this report and the work involved in writing this report were performed at the Naval Surface Warfare Center Carderock Division (NSWCCD) by the Hydromechanics Department, Seakeeping Division, Code 5500. The work was sponsored by the Naval Sea System Command (NAVSEA) PMS 500 under work unit number 07-1-5500-765 as part of the FY07 Task 1.4 (Computational Tools) Phase IV Hull Form Plan (Program Element 0604300N).

INTRODUCTION

The Navy has a continuing need to determine the seakeeping and dynamic stability characteristics of ships. Especially with the advent of advanced hull forms that depart substantially from past practice and guidelines, the Navy must rely on increased experimentation and simulation. Both are needed but the number of conditions that must be considered demand increased reliance on simulation since experimentation is relatively more expensive. Furthermore, model testing has its limitations because a model basin limits run time and distance, random testing is impractical for the required range of conditions, wind effects are not easily modeled, and scale effects cannot be overcome. Model testing remains important because it is required to validate predictions from software or to augment numerical simulation where theoretical predictions are inaccurate or insufficient.

In view of such heavy reliance on computer software, it is wise to assess the capability of current computer programs for predicting forces and moments in situations that approach capsizes and even for seakeeping where obtaining predictions is perhaps less demanding. All computer codes suitable for the number of simulations required are built on potential flow theory with viscous effects added in models. The potential flow force study was designed to compare existing computer codes in their ability to calculate potential flow forces and moments acting on hulls in motions that range from small to large.

Several potential flow programs were selected to compute the forces and moments exerted on bodies undergoing various prescribed motions. The flow configurations ranged from a regime where linearity might be sufficient to regimes where nonlinearities are expected to be important.

Code runners, in most cases the code developers, were assigned well-defined tasks of three types: one where the ship undergoes 1-DOF prescribed oscillations in calm water (task 1, the radiation problem), one where the ship advances with zero degrees of freedom at a fixed forward speed in waves (task 2, the diffraction problem), and one where the ship undergoes hybrid 2-DOF prescribed motion in waves (task 3, the nominal wave contouring problem). Each task assigned to a code runner required the computation to be done for two speeds and two models scaled to full size.

The two sections after this introductory section describe the tasks assigned in the potential flow force study (Task Descriptions) and the computer codes selected to perform the tasks (The Computer Codes). The code runners were requested to provide their data in text files that could be read by the plotting program TECPLOT, and the section entitled Data Received describes the format. The section also lists the data received as of the time this report was written. Another section (Standardization) describes the work required to manipulate the data received so that the force time histories from the codes are in phase, the forces and moments are referred to the same frame of reference, and the dimensions match. A section (Processing) describes what was done to obtain comparative time-history plots of forces and moments for one full period of motion and plots of the minimum and maximum of each variable. In the next section (Observations), selected results from the force study are presented and discussed. There is a final concluding section.

This report presents plots of results in 18 appendices which have been placed in bookmarked PDF files to facilitate navigation through them. Appendices A through J contain time history plots. Appendices K through R contain plots of the minimum and maximum of each variable as a function of a measure of nonlinearity in the problem. As the appendices are traversed in order from A to R, the results contained in them alternate between those for Model 5613 and Model 5514. The results depicted in the time history plots of Appendix A are from the same set of computations as those depicted in the minimum and maximum plots of Appendix K; Appendices A through H correspond to Appendices K through R, respectively. Due to the nature of task 3, the time-history plots of Appendices I and J do not have corresponding plots of the minimum and maximum. The layout of the appendices is depicted in Table 1.

This report is intended for readers interested in how forces and moments computed by “state-of-the-art” free-surface potential flow programs compare when the codes are used in situations with significant geometric nonlinearities and steep waves. Time history plots of forces and moments presented in the appendices to this report can be compared for varying frequencies, ships, speeds, amplitudes, wave steepnesses, and so forth. The time history plots can be compared with the corresponding plots of the minimum and maximum of computed forces and moments versus the the amplitude of the motion or the wave steepness.

When this task was started, no experimental data were available with which to compare computational results. Experiments have now been completed for the case of forced roll for one of the models, but no comparisons with the data are presented in this report since the data were still being processed at the time of writing.

TASK DESCRIPTIONS

Two ships were chosen for the simulations. The first corresponds to Model 5514 scaled to the length 142 m (with ship to model scale ratio equal to 46.6). The ship is the pre-contract DDG-51

Table 1. Layout of the appendices.

Model	Task	(Problem) Motion	Time History Plots	Minimum and Maximum Plots
5613	1	(Radiation) 1-DOF Heave	Appendix A	Appendix K
5514	1	(Radiation) 1-DOF Heave	Appendix B	Appendix L
5613	1	(Radiation) 1-DOF Roll	Appendix C	Appendix M
5514	1	(Radiation) 1-DOF Roll	Appendix D	Appendix N
5613	1	(Radiation) 1-DOF Pitch	Appendix E	Appendix O
5514	1	(Radiation) 1-DOF Pitch	Appendix F	Appendix P
5613	2	(Diffraction) 0-DOF	Appendix G	Appendix Q
5514	2	(Diffraction) 0-DOF	Appendix H	Appendix R
5613	3	(Hybrid) 2-DOF	Appendix I	—
5514	3	(Hybrid) 2-DOF	Appendix J	—

Table 2. Particulars of the ship hulls.

Ship Model	M5514	M5613 (ONRTH)
Length (m)	142	154
Displacement	V-Line	—
Volume (m ³)	9146	8543
Weight (kN)	9.20×10^4	8.59×10^4
Forward Draft (m)	6.51	5.5
Aft Draft (m)	6.51	5.5
VCG (m ABL)	6.51	5.5
LCB (m aft of FP)	72.1	79.6
GM (m)	3.016	4.248
KM (m)	9.526	9.748

hull with a 6.51 m draft at the V-line service limit load condition. It has flare and is representative of many current naval ships.^{1, 2*} The second ship is the tumblehome variant of the ONR 3-Topsides Series referred to as ONRTH with length 154 m and draft 5.5 m. The corresponding model is the 1/32-scale Model 5613-1. The ship is representative of a ship that might be in the future Navy. The hull is described by Bishop et al.³ Figure 1 shows the body plans and Fig. 2 shows isometric views of the two hulls. For either hull, the geometry at the waterline changes significantly with small changes in draft. Other particulars of the hulls are summarized in Table 2. The ship speeds correspond to Froude numbers 0.0 and 0.3 for each hull. Since each simulation was to be repeated for both hulls and both Froude numbers, there are four sets of runs classified solely according to the speed and ship. The simulations can be arranged into three tasks that test the ability of codes to compute the solution of 1-DOF radiation problems (task 1), 1-DOF diffraction problems (task 2), and hybrid 2-DOF wave contouring problems (task 3).

In each simulation of task 1, the ship oscillates in one of the modes heave, roll, and pitch. The frequencies and amplitudes of the oscillations are listed in Tables 3–5 for the three modes of motion. In each mode there are three frequencies and five amplitudes. The amplitudes range from relatively small where linear theory is presumed to be adequate to large where significant nonlinearities are important. In fact, the bow and stern move vertically with an amplitude greater than the draft of the ship in pitch motion of the highest amplitude, and the deck edge is periodically submerged in roll motion of the highest roll amplitude. The frequencies were chosen because they are representative of typical capsizing encounter frequencies.[†] The number of runs is 180, which can be obtained by multiplication since there are 3 modes, 5 amplitudes, 3 frequencies, 2 speeds, and 2 ships for which computations are to be performed.

*A complete listing of references is given on pages 85–86.

[†]They were determined from three SS8 modal periods (13.9 sec, 16.4 sec, and 20 sec) for a ship advancing in bow quartering, beam, and stern quartering seas at speeds corresponding to Froude numbers 0.2, 0.3, and 0.4. The minimum, average, and maximum encounter frequencies were obtained for each modal period. The average minimum, average, and maximum frequencies thus obtained were 0.208 rad/sec, 0.383 rad/sec and 0.672 rad/sec. For the prescribed heave and pitch motions, the highest frequency was replaced with the frequency 1.1 rad/sec, a frequency close to estimated natural frequencies.

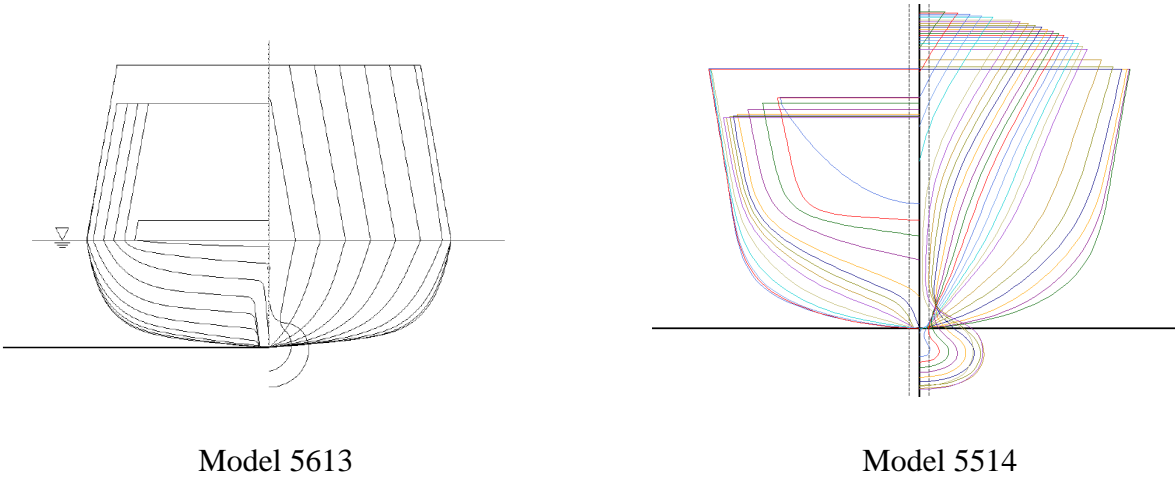


Fig. 1. Body plans for Models 5613 and 5514.

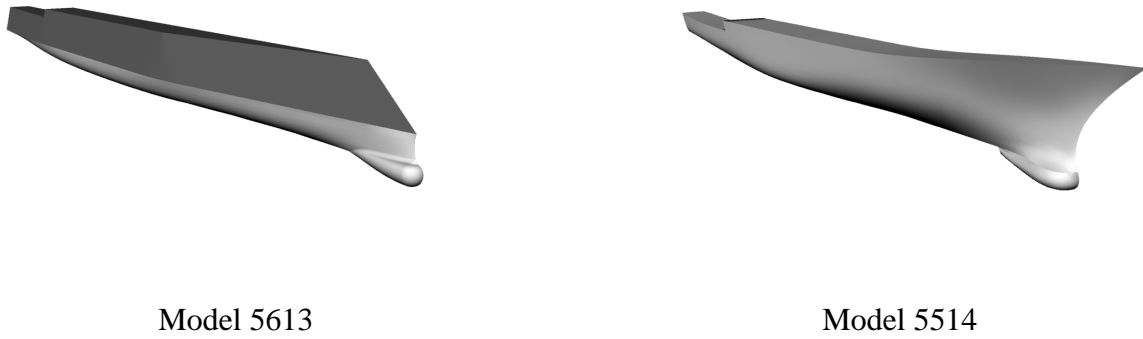


Fig. 2. Isometric views of Models 5613 and 5514.

Table 3. 1-DOF prescribed heave motion in task 1.

Heave Motion $z_e = z_a \sin(\omega t)$					
Heave Amplitudes z_a					
% of T_{mean}	5	10	20	40	80
M5514 (m)	0.326	0.651	1.302	2.604	5.208
M5613 (m)	0.275	0.550	1.100	2.200	4.400
Heave Frequencies ω					
ω_1 (rad/s)	0.2079	0.2079	0.2079	0.2079	0.2079
ω_2 (rad/s)	0.3831	0.3831	0.3831	0.3831	0.3831
ω_3 (rad/s)	1.1	1.1	1.1	1.1	1.1

Table 4. 1-DOF prescribed pitch motion in task 1.

Pitch Motion $\theta = \theta_a \sin(\omega t)$					
Rotation Point about LCG					
Pitch Amplitudes θ_a					
θ_a (°)	1	1.75	2.5	3.75	5
Pitch Frequencies ω					
ω_1 (rad/s)	0.2079	0.2079	0.2079	0.2079	0.2079
ω_2 (rad/s)	0.3831	0.3831	0.3831	0.3831	0.3831
ω_3 (rad/s)	1.1	1.1	1.1	1.1	1.1

Table 5. 1-DOF prescribed roll motion in task 1.

Roll Motion $\phi = \phi_a \sin(\omega t)$					
Rotation Point about VCG					
Roll Amplitudes ϕ_a					
ϕ_a (°)	5	15	30	45	65
Roll Frequencies ω					
ω_1 (rad/s)	0.2079	0.2079	0.2079	0.2079	0.2079
ω_2 (rad/s)	0.3831	0.3831	0.3831	0.3831	0.3831
ω_3 (rad/s)	0.672	0.672	0.672	0.672	0.672

Table 6. Headings for task 2.

β ($^{\circ}$)	Seas
0	Following
45	Stern quartering
90	Beam
135	Bow quartering
180	Head

Table 7. Waves for task 2.

Wavelength λ/L	Wave Steepness H/λ
1	1/60
1	1/20
1	1/15
1	1/10

Task 2 was designed to test the behavior of the codes in varying degrees of wave steepness ranging from the relatively small steepness $1/60$ to the steepness $1/10$ where nonlinearity is very likely to be important. Since the ship has no degrees of freedom, the ship does not oscillate in any mode. The ship is either fixed at zero forward speed ($F_n = 0.0$) or advances at a constant forward speed ($F_n = 0.3$). The wave heights and wave steepnesses are specified in terms of the ship length L . It should be noted that the wave amplitude exceeds the draft for both ships at the highest wave steepness. The code runners were given the five equally spaced headings β between head and following seas listed in Table 6. For easy reference the wavelengths and wave steepnesses are given in Table 7, the encounter periods for this task are listed in Table 8, and the wave amplitudes are given in Table 9. Based on linear wave theory, one can calculate approximations to the encounter period from the equations

$$\begin{aligned}
 U &= F_n \sqrt{gL}, \\
 \omega &= \sqrt{2\pi g/\lambda}, \\
 \omega_e &= \omega - (\omega^2 U/g) \cos \beta,
 \end{aligned}$$

and

$$T_e = 2\pi/\omega_e.$$

If all the assigned computations have been completed for this task, each code runner will have performed 80 computer runs for the 5 headings, 4 waves, 2 speeds, and 2 ships.

Task 3 involves 2-DOF hybrid forced oscillations in waves for which the ship nominally encounters a wave in following or beam seas. In condition 1, the ship heaves and pitches in following

Table 8. Encounter period T_e in task 2.

β (°)	Model 5514		Model 5613	
	$T_e(F_n = 0.0)$ (sec)	$T_e(F_n = 0.3)$ (sec)	$T_e(F_n = 0.0)$ (sec)	$T_e(F_n = 0.3)$ (sec)
0	9.54	38.5	9.93	40.0
45	9.54	20.4	9.93	21.2
90	9.54	9.54	9.93	9.93
135	9.54	6.23	9.93	6.48
180	9.54	5.44	9.93	5.67

Table 9. Wave amplitude η_a for task 2.

λ/L	H/λ	Model 5514 η_a (m)	Model 5613 η_a (m)
1	1/60	1.18	1.28
1	1/20	3.55	3.85
1	1/15	4.73	5.13
1	1/10	7.10	7.70

seas. The heave motion is such that the center of gravity is coincident with the free surface. The pitch motion is such that the longitudinal slope of the hull matches the slope of the wave at the center of gravity. The wavelength λ is twice the length L of the ship and the wave steepness H/λ is given by the equation $H/\lambda = 1/20$. The description of this computational problem is summarized in Table 10. In condition 2, the ship heaves and rolls in beam seas. The center of gravity is coincident with the free surface. The roll motion is such that the transverse slope of the hull is the same as the wave slope at the center of gravity. The wavelength in this case is the length of the ship and the wave steepness H/λ satisfies $H/\lambda = 1/10$. The details of condition 2 in task 3 are summarized in Table 11. Specifying beam seas could mean that the waves come from either the port or the starboard side of the hull, and the results from the code runners indicate that the choice has not been made consistently. Rotations are about the center of gravity and the center of gravity is located in the equilibrium waterplane. Eight runs were expected from the code runners from task 3 for 2 speeds, 2 ships, and 2 conditions. The encounter periods for this task are given in Table 12.

For condition 1 of task 3, where the ship travels in following seas, one can assume that CG is always at $x = Ut$ in an earth-fixed coordinate system. Then the wave height η at CG and pitch angle θ satisfy the equations

$$\eta \equiv z_e = \eta_a \sin(\omega t - kx)|_{x=Ut} = \eta_a \sin(\omega_e t)$$

and

$$\theta = -\tan^{-1} \left(\frac{\partial \eta}{\partial x} \bigg|_{x=Ut} \right) \approx \eta_a k \cos(\omega t - kUt) \equiv \eta_a k \cos(\omega_e t),$$

Table 10. Specifications for condition 1 of task 3.

Following Seas with Heave and Pitch	
Wavelength	$\lambda/L = 2$
Wave steepness	$H/\lambda = 1/20$
Amplitude of heave motion	$\zeta_3 = \zeta_0 = H/2$
Frequency of heave motion	ω_e
Phase of heave motion	CG coincident with η
Amplitude of pitch motion	$\zeta_5 = k\zeta_0 = kH/2$
Frequency of pitch motion	ω_e
Phase of pitch motion	Coincident slopes

which is valid if $\eta_a k = 2\pi\eta_a/\lambda$ is small. The motion is therefore nearly sinusoidal.

For condition 2 of task 3, where the ship travels forward in beam seas, the direction into which the waves propagate has been chosen as the port side: Waves travel from the starboard to the port side of the hull.[‡] If the waves propagate in the direction of the positive earth-fixed x -axis, the ship travels in the direction of the negative earth-fixed y -axis. The roll angle ϕ is the rotation angle about a ship-fixed longitudinal line through the center of gravity. Thus the wave height at the center of gravity and the roll angle are given by the equations

$$\eta \equiv z_e = \eta_a \sin(\omega t - kx)|_{x=0}$$

and

$$\phi = \tan^{-1} \left(\frac{\partial \eta}{\partial x} \bigg|_{x=0} \right) = \tan^{-1} [-k\eta_a \cos(\omega t)] \approx -k\eta_a \cos(\omega t) ,$$

which is valid if $\eta_a k = 2\pi\eta_a/\lambda$ is small. As was the case for condition 1, the motion is approximately sinusoidal.

[‡]This requires a transformation of the results from AEGIR-1 and AEGIR-2.

Table 11. Specifications for condition 2 of task 3.

Beam Seas with Heave and Roll	
Wavelength	$\lambda/L = 1$
Wave steepness	$H/\lambda = 1/10$
Amplitude of heave motion	$\zeta_3 = \zeta_0 = H/2$
Frequency of heave motion	ω_e
Phase of heave motion	CG coincident with η
Amplitude of pitch motion	$\zeta_4 = k\zeta_0 = kH/2$
Frequency of pitch motion	ω_e
Phase of pitch motion	Coincident slopes

Table 12. Encounter period T_e in task 3.

F_n	Condition	Model	λ/L	β ($^\circ$)	T_e (sec)
0.0	1	5514	2	0	13.5
0.3	1	5514	2	0	28.8
0.0	1	5613	2	0	14.0
0.3	1	5613	2	0	30.0
0.0	2	5514	1	90	9.54
0.3	2	5514	1	90	9.54
0.0	2	5613	1	90	9.93
0.3	2	5613	1	90	9.93

Table 13. Computer codes involved in the force study.

2-Letter Code	Program Name	Where Developed
A1	AEGIR-1	Applied Physical Sciences and Flight Safety Technology
A2	AEGIR-2	Applied Physical Sciences and Flight Safety Technology
FD	FREDYN	MARIN
L1	LAMP-1	SAIC-Annapolis
L3	LAMP-3	SAIC-Annapolis
L4	LAMP-4	SAIC-Annapolis
NF	NFA	SAIC-La Jolla
NS	NSHIPMO	University of Michigan

THE COMPUTER PROGRAMS

The codes selected for the force study are listed in Table 13 together with their provenance. The table also gives a two-letter code that is used later in figures showing plots of time histories and plots of the minimum and maximum of forces versus measures of nonlinearity.

The two AEGIR codes embody further development of the techniques found in the computer program SWAN2 developed at MIT during the late 1980s and the 1990s.⁴ The velocity potential is expressed as linear combinations of B-spline functions whose coefficients are sought in the solution process. AEGIR-1 is strictly linear whereas AEGIR-2 computes nonlinear Froude-Krylov and hydrostatic forces and moments. The AEGIR codes are representative of higher order 3D panel methods.

The LAMP codes have been under development since about 1990. These codes are distinguished from one another in their boundary conditions, which are described as body linear, approximate body nonlinear, and body nonlinear respectively in the LAMP-1, LAMP-3, and LAMP-4 versions used in the force study.⁵ The differences among the codes cannot be explained clearly without the aid of equations and the equations that follow are based on documents supplied by SAIC as part of the potential flow force study. If the total velocity potential Φ_T is written as the sum of the incident wave potential φ_w and a disturbance potential φ , then the pressure p is obtained from Bernoulli's equation as follows:

$$\begin{aligned}
 \frac{p}{\rho} &= -\frac{\partial \Phi_T}{\partial t} - \frac{1}{2} |\nabla \Phi_T|^2 - gz \\
 &= \left[\left(-\frac{\partial \varphi}{\partial t} - \vec{V}_g \cdot \nabla \varphi \right) + \vec{V}_g \cdot \nabla \varphi \right] - \frac{1}{2} |\nabla \varphi + \nabla \varphi_w|^2 - gz - \frac{\partial \varphi_w}{\partial t} \\
 &\equiv -\frac{D\varphi}{Dt} + \vec{V}_g \cdot \nabla \varphi - \frac{1}{2} |\nabla \varphi + \nabla \varphi_w|^2 - gz - \frac{\partial \varphi_w}{\partial t}.
 \end{aligned}$$

Here \vec{V}_g is a grid velocity that is required because the only convenient way to approximate the time derivative of the velocity potential numerically is from a finite difference formula following a grid

point. Surface integrals of the terms in this equation are treated differently by the various versions of the LAMP codes.

LAMP-1 satisfies a boundary condition on S_0 , the mean wetted surface of the hull. Hydrostatic forces and moments are calculated from waterplane quantities. Froude-Krylov forces and moments are calculated from integrals over the mean position of the hull up to the mean free-surface level as given by the equation

$$\vec{F}^{\text{fk}} = -\rho \int_{S_0} \frac{\partial \varphi_w}{\partial t} \vec{n} dS$$

where \vec{n} is the unit normal vector pointing into the body. A hydrodynamic force \vec{F}^{hydr1} is calculated in LAMP-1 from another integral over the mean hull surface S_0 up to the calm waterplane as given by the equation

$$\vec{F}^{\text{hydr1}} = -\rho \int_{S_0} \left(\frac{D\varphi}{Dt} - \vec{V}_g \cdot \nabla \varphi \right) \vec{n} dS.$$

In LAMP-1, the grid velocity vector \vec{V}_g is given by the equation

$$\vec{V}_g = U \hat{i}_e + \left[\left(\vec{V}_{\text{CG}} + \vec{\omega} \times \vec{r} \right) \cdot \hat{k}_e \right] \hat{k}_e \quad (\text{only in LAMP-1}),$$

which is an approximation to $\vec{V}_{\text{CG}} + \vec{\omega} \times \vec{r}$. Here $\vec{\omega}$ is the angular velocity of the body and \vec{r} is the position vector from the center of gravity. Even when the grid does not move, extra grid velocity terms beyond the usual terms included in a linear code are included for consistency among the codes of the LAMP suite and are expected to be small. SAIC created a special temporary version of LAMP-1 to verify that certain forces and moments are near those calculated by other linear codes when \vec{V}_g is $\vec{0}$ (in a case of zero forward speed). The special version was used for only a few simulations when the deviation from the results of linear codes became particularly noticeable. Results from the temporary version are not presented in this report. In any case, the linear force and moment computed by LAMP-1 are not the same as the forces and moments computed by other linear codes due to the grid velocity terms. The hydrodynamic force includes contributions from the steady Kelvin wave, radiation, and diffraction potentials. LAMP-1 computes second order hydrodynamic forces according to the equation

$$\vec{F}^{\text{hydr2}} = -\frac{\rho}{2} \int_{S_0} |\nabla \varphi + \nabla \varphi_w|^2 \vec{n} dS.$$

The moments are calculated from analogous integrals. Forces and moments are transformed to a ship-fixed coordinate system and applied at the actual position of the body.

In the approximate body nonlinear approach of LAMP-3, the body-linear solution of the disturbance potential is combined with integration of the hydrostatic and Froude-Krylov force com-

ponents over the wetted surface of the hull as given in the equations

$$\begin{aligned}\vec{F}^{\text{hs}} &= -\rho g \int_{S_B} z \vec{n} dS \\ \vec{F}^{\text{fk}} &= -\rho \int_{S_B} \frac{\partial \varphi_w}{\partial t} \vec{n} dS \\ \vec{F}^{\text{hydr1}} &= -\rho \int_{S_0} \left(\frac{D\varphi}{Dt} - \vec{V}_g \cdot \nabla \varphi \right) \vec{n} dS\end{aligned}$$

and

$$\vec{F}^{\text{hydr2}} = -\frac{\rho}{2} \int_{S_0} |\nabla \varphi + \nabla \varphi_w|^2 \vec{n} dS$$

where S_B is the instantaneous wetted surface of the hull. For LAMP-3, the grid velocity vector \vec{V}_g is given by the equation

$$\vec{V}_g = \vec{V}_{\text{CG}} + \vec{\omega} \times \left[\vec{r} - \left(\vec{r} \cdot \hat{k}_e \right) \hat{k}_e \right] \quad (\text{only in LAMP-3}),$$

which is an approximation to $\vec{V}_{\text{CG}} + \vec{\omega} \times \vec{r}$. Forces and moments calculated from integrals over S_0 are transformed to a ship-fixed coordinate system and applied at the actual position of the body.

In the approach taken in LAMP-4, the boundary-value problem is linearized with respect to the incident waves. The velocity potential is obtained from a boundary-value problem that incorporates the forward speed of the ship, the radiation potential, and the diffraction potential in the hull boundary condition. All the forces and moments are obtained by integrating the pressure on the hull up to the incident wave height:

$$\begin{aligned}\vec{F}^{\text{hs}} &= -\rho g \int_{S_B} z \vec{n} dS \\ \vec{F}^{\text{fk}} &= -\rho \int_{S_B} \frac{\partial \varphi_w}{\partial t} \vec{n} dS \\ \vec{F}^{\text{hydr1}} &= -\rho \int_{S_B} \left(\frac{D\varphi}{Dt} - \vec{V}_g \cdot \nabla \varphi \right) \vec{n} dS\end{aligned}$$

and

$$\vec{F}^{\text{hydr2}} = -\frac{\rho}{2} \int_{S_B} |\nabla \varphi + \nabla \varphi_w|^2 \vec{n} dS.$$

In LAMP-4, the grid velocity vector \vec{V}_g is obtained from a backward difference in time of the position of a grid point. SAIC used approximately 6000 panels for the simulations in the force study. Initial test runs required several days for a single simulation of 6000 time steps. To reduce computational time, SAIC then implemented a recently developed precorrected Fast Fourier Transform (pFFT) method that reduces the computational time by a factor of five. Since the original version of LAMP-4 required 19.5 CPU hours to complete 2000 time steps with 6000 panels, it appears that

the 6000 time steps and 6000 panels for each simulation required about 11 hours of CPU time with the new pFFT method.[§]

SAIC has been calling these programs collectively the LAMP “system” or “suite.” All versions of LAMP are time-domain codes. The LAMP codes were chosen for the potential flow force study to represent 3D constant panel methods.

NFA is still under development. It is based on a volume of fluid technique and uses Cartesian grids. A consequence of using such grids is that the hull boundary does not necessarily intersect the grids at grid points. NFA requires huge computational resources in the form of clusters of high-performance computers.^{6, 7} In view of the heavy computational resources required by this code, results were not expected from all of the runs assigned to the code runners.

NSHIPMO is under development and is based on nonlinear two-dimensional strip theory where the hull is paneled and singularities are placed above the free surface. An outer domain is used to reduce wave reflections from the edges of the computational free surface. NSHIPMO uses a slender body approach where plane sections remain plane. Consequently, when a body pitches and yaws, the sections heave and sway. The number of panels on the hull remains the same for all time and change their shape to account for the moving hull/free-surface intersection, which must be calculated at each time step. At each time step, mixed two-dimensional boundary-value problems are solved to obtain the velocity potential section by section. The problem is well posed since the normal derivative of the velocity potential is known on the wetted hull surface of the hull (Neumann boundary condition), the velocity potential is known on the free surface (Dirichlet boundary condition), and radiation conditions require the velocity potential to die away infinitely far from the hull. A third-order Adams-Bashforth method is used to update the free surface from time step to time step. Longitudinal x -derivatives of the velocity potential are obtained with the aid of radial basis functions. Forces and moments are computed from pressure integrals up to the surface of the incident waves. For the prescribed heave and pitch motions of task 1, the body was extended vertically upward (in the ship-fixed frame of reference) from the shear line to create a wall-sided body for which no part of a deck ever submerged below the free surface. For the prescribed roll motion of task 1, a deck was created to close the body. The pressure integrals extended over the wetted surface of the body thus modified. By definition, NSHIPMO calculates nonlinear hydrostatic and Froude-Krylov forces.[¶]

FREDYN started as a maneuvering code and has been developed into its current state that still includes parts originating from the 1970s.^{8, 9, 10} It is based on a blended technique where nonlinear computations are used for the Froude-Krylov and hydrostatics parts of the total force acting on the hull.¹ These quantities are obtained from integrals over the parts of the hull beneath the incident waves. FREDYN computes the Froude-Krylov and hydrostatic forces and moments together; i.e. it does not calculate the Froude-Krylov force and the hydrostatic force first before they are added together. FREDYN incorporates nonlinear viscous effects in maneuvering coefficients and its roll damping models. Other parts, such as the parts of the forces attributed to wave radiation and diffraction, are purely linear. These force and moment components are obtained from

[§]Source: Documents supplied by SAIC as part of the potential flow force study. The numbers cited appear to be for a simulation that does not possess port-starboard symmetry. Presumably, the number of panels would be halved for simulations possessing such symmetry.

[¶]Source: Private communication.

data precomputed in the frequency domain and applied in the time domain at each time step after they have been transformed to a ship-fixed coordinate system. The computations in the frequency domain are based on two-dimensional strip theory with STF (Salvesen-Tuck-Faltinsen) forward speed corrections.¹¹

The version of FREDYN used for this force study is a modification to 9.59N. Modifications were required to write out forces and moments not normally written out by FREDYN and to obtain motions not available by entering data into an input file.

DATA RECEIVED

The code runners were expected to supply time histories of ship-fixed components of all available moments about the center of gravity as well as the forces. Here the force and moment are defined as the force and moment exerted by the fluid on the hull and therefore exclude the weight vector. The origin of the ship-fixed coordinate system is at the center of gravity, the x -axis is positive forward, the y -axis is positive to the port side of the hull, and the z -axis points upward.

The data were to be supplied in text files that could be read directly by the plotting program TECPLOT. The code runners were asked to merge their data into ten files, one file for each ship and subtask of a task as follows:

- Task 1, forced heave motion, Model 5514
- Task 1, forced heave motion, Model 5613
- Task 1, forced roll motion, Model 5514
- Task 1, forced roll motion, Model 5613
- Task 1, forced pitch motion, Model 5514
- Task 1, forced pitch motion, Model 5613
- Task 2, Model 5514
- Task 2, Model 5613
- Task 3, Model 5514
- Task 3, Model 5613

Since TECPLOT considers lines that begin with the character # a comment, the code runners were free to put comments within the data files to ensure that the files do not become confused by improper renaming.

Ideally the time histories given in Table 14 would be received, but it was realized that not all codes divide up the force and moment into the components listed there. Templates were supplied so that the differences in form of the data files received could be minimized. The template suggested variable names as given in Table 14.

Table 14. Time histories generally expected from code runners.

Variable	Description	Suggested Name within Data Files
t	time	time
η	wave height at CG	eta
z_e	vertical position of CG	heave
ϕ	roll angle	phi
θ	pitch angle	theta
β	heading	beta
F_n	Froude number	fn
\vec{F}^{hst}	hydrostatic force	fhst_x, fhst_y, fhst_z
\vec{M}^{hst}	hydrostatic moment about CG	fhst_mx, fhst_my, fhst_mz
\vec{F}^{rad}	radiation force	frad_x, frad_y, frad_z
\vec{M}^{rad}	radiation moment about CG	frad_mx, frad_my, frad_mz
\vec{F}^{dif}	diffraction force	fdif_x, fdif_y, fdif_z
\vec{M}^{dif}	diffraction moment about CG	fdif_mx, fdif_my, fdif_mz
\vec{F}^{fk}	Froude-Krylov force	ffk_x, ffk_y, ffk_z
\vec{M}^{fk}	Froude-Krylov moment about CG	ffk_mx, ffk_my, ffk_mz
\vec{F}^{ptot}	total potential force	fptot_x, fptot_y, fptot_z
\vec{M}^{ptot}	total potential moment about CG	fptot_mx, fptot_my, fptot_mz

A variables record is supplied within a TECPLOT file to give names to variables appearing in columns of numbers. Figure 3 shows the multi-line variables record in a data file received for task 1, forced heave, Model 5514, for AEGIR-1. The record has been reformatted slightly to fit inside the margins. The variables record varied from code to code since codes sometimes do not compute exactly the forces and moments requested. The code runners were requested to provide all forces and moments that they had available and additional forces and moments contributed to variations in the variables record.

Data for individual cases within the TECPLOT files follow a corresponding zone record. Figure 4 shows an edited list of zone records that appear in the same AEGIR-1 data file from which the variables record was extracted. Figures 5 and 6 contain edited lists of zone records for the other subtasks of task 1 received for AEGIR-1. Figures 7 and 8 contain edited lists of zone records for tasks 2 and 3. The zone records in the data files showed little variation from code to code.

Tables 15–19 list every simulation assigned in the potential flow force study and the number of periods of data received for the simulation from each code. Except for NFA, data for each simulation were contained in a single zone of a TECPLOT file. The number of periods given in the table is the number of periods in that zone. For NFA the number of periods refers to the number of periods in the results from each simulation. When no data were received, it is indicated by a dash.

Data from AEGIR-2 were received for all the assigned simulations. However, very short time histories were provided for task 2 with Model 5514 for the case $H/\lambda = 1/10$ at the three oblique headings. No results were provided for NFA at zero forward speed. At forward speed, results were

```

variables = "time", "eta", "heave", "phi", "theta",
"beta", "fn", "fptot_x", "fptot_y", "fptot_z", "fptot_mx",
"fptot_my", "fptot_mz", "fhst_x", "fhst_y", "fhst_z",
"fhst_mx", "fhst_my", "fhst_mz", "ffk_x", "ffk_y", "ffk_z",
"ffk_mx", "ffk_my", "ffk_mz", "frad_x", "frad_y", "frad_z",
"frad_mx", "frad_my", "frad_mz", "fdif_x", "fdif_y",
"fdif_z", "fdif_mx", "fdif_my", "fdif_mz", "fvisc_x",
"fvisc_y", "fvisc_z", "fvisc_mx", "fvisc_my", "fvisc_mz",
"frad1_x", "frad1_y", "frad1_z", "frad1_mx", "frad1_my",
"frad1_mz", "frad2_x", "frad2_y", "frad2_z", "frad2_mx",
"frad2_my", "frad2_mz", "fdif1_x", "fdif1_y", "fdif1_z",
"fdif1_mx", "fdif1_my", "fdif1_mz", "fdif2_x", "fdif2_y",
"fdif2_z", "fdif2_mx", "fdif2_my", "fdif2_mz"

```

Fig. 3. Variables record for task 1, forced heave, Model 5514, obtained from a data file received for AEGIR-1.

provided for only the higher amplitudes of motion in task 1 and for the higher wave steepnesses of task 2. SAIC provided results from NFA only for head seas in task 2. No results were provided from NSHIPMO at the highest wave steepness in task 2. In all cases, only three periods of data were provided from NSHIPMO.

The results have not been examined quantitatively for how well the initial transients have died out by the last period of data provided.

```

zone t="A1 ampltd=0.05 omega=0.2079 fn=0.0"
zone t="A1 ampltd=0.10 omega=0.2079 fn=0.0"
zone t="A1 ampltd=0.20 omega=0.2079 fn=0.0"
zone t="A1 ampltd=0.40 omega=0.2079 fn=0.0"
zone t="A1 ampltd=0.80 omega=0.2079 fn=0.0"
zone t="A1 ampltd=0.05 omega=0.3831 fn=0.0"
...
zone t="A1 ampltd=0.80 omega=1.1000 fn=0.0"
zone t="A1 ampltd=0.05 omega=0.2079 fn=0.3"
...
zone t="A1 ampltd=0.80 omega=1.1000 fn=0.3"

```

Fig. 4. Edited list of zone records in a data file containing data from AEGIR-1 for forced heave motions of task 1 for one of the ships.

```

zone t="A1 ampltd=5.00 omega=0.2079 fn=0.0"
zone t="A1 ampltd=15.0 omega=0.2079 fn=0.0"
zone t="A1 ampltd=30.0 omega=0.2079 fn=0.0"
zone t="A1 ampltd=45.0 omega=0.2079 fn=0.0"
zone t="A1 ampltd=65.0 omega=0.2079 fn=0.0"
zone t="A1 ampltd=5.00 omega=0.3831 fn=0.0"
...
zone t="A1 ampltd=65.0 omega=0.6720 fn=0.0"
zone t="A1 ampltd=5.00 omega=0.2079 fn=0.3"
...
zone t="A1 ampltd=65.0 omega=0.6720 fn=0.3"

```

Fig. 5. Edited list of zone records in a data file containing data from AEGIR-1 for forced roll motions of task 1 for one of the ships.


```

zone t="A1  amplt=1.00  omega=0.2079  fn=0.0"
zone t="A1  amplt=1.75  omega=0.2079  fn=0.0"
zone t="A1  amplt=2.50  omega=0.2079  fn=0.0"
zone t="A1  amplt=3.75  omega=0.2079  fn=0.0"
zone t="A1  amplt=5.00  omega=0.2079  fn=0.0"
zone t="A1  amplt=1.00  omega=0.3831  fn=0.0"
...
zone t="A1  amplt=5.00  omega=0.3831  fn=0.0"
zone t="A1  amplt=1.00  omega=1.1000  fn=0.0"
...
zone t="A1  amplt=5.00  omega=1.1000  fn=0.3"

```

Fig. 6. Edited list of zone records in a data file containing data from AEGIR-1 for forced pitch motions of task 1 for one of the ships.

```

zone t="A1  loh=60  beta=000  fn=0.0"
zone t="A1  loh=20  beta=000  fn=0.0"
zone t="A1  loh=15  beta=000  fn=0.0"
zone t="A1  loh=10  beta=000  fn=0.0"
zone t="A1  loh=60  beta=045  fn=0.0"
...
zone t="A1  loh=10  beta=180  fn=0.0"
zone t="A1  loh=60  beta=000  fn=0.3"
zone t="A1  loh=20  beta=000  fn=0.3"
...
zone t="A1  loh=10  beta=180  fn=0.3"

```

Fig. 7. Edited list of zone records in a data file containing data from AEGIR-1 for task 2 for one of the ships.

```

zone t="A1  condition 1  fn=0.0"
zone t="A1  condition 2  fn=0.0"
zone t="A1  condition 1  fn=0.3"
zone t="A1  condition 2  fn=0.3"

```

Fig. 8. Edited list of zone records in a data file containing data from AEGIR-1 for task 3 for one of the ships.

Table 15. Number of Periods of Data from Each Code for Forced Heave Motion in Task 1

Model	Mode	z_a/T (1)	ω (rad/s)	F_n	A1	A2	FD	L1	L3	L4	NF	NS
5514	3	0.05	0.2079	0.0	10.0	10.0	13.2	11.9	11.9	11.9	—	3.0
5514	3	0.05	0.3831	0.0	10.0	10.0	24.4	14.6	14.6	14.6	—	3.0
5514	3	0.05	1.1	0.0	10.0	9.9	70.0	21.0	21.0	21.0	—	3.0
5514	3	0.1	0.2079	0.0	10.0	10.0	13.2	11.9	11.9	11.9	—	3.0
5514	3	0.1	0.3831	0.0	10.0	10.0	24.4	14.6	14.6	14.6	—	3.0
5514	3	0.1	1.1	0.0	10.0	9.9	70.0	21.0	21.0	21.0	—	3.0
5514	3	0.2	0.2079	0.0	10.0	10.0	13.2	11.9	11.9	11.9	—	3.0
5514	3	0.2	0.3831	0.0	10.0	10.0	24.4	14.6	14.6	14.6	—	3.0
5514	3	0.2	1.1	0.0	10.0	9.9	70.0	21.0	21.0	21.0	—	3.0
5514	3	0.4	0.2079	0.0	10.0	10.0	13.2	11.9	11.9	11.9	—	3.0
5514	3	0.4	0.3831	0.0	10.0	10.0	24.4	14.6	14.6	14.6	—	3.0
5514	3	0.4	1.1	0.0	10.0	9.9	70.0	21.0	21.0	21.0	—	3.0
5514	3	0.8	0.2079	0.0	10.0	10.0	13.2	11.9	11.9	11.9	—	3.0
5514	3	0.8	0.3831	0.0	10.0	10.0	24.4	14.6	14.6	14.6	—	3.0
5514	3	0.8	1.1	0.0	10.0	9.9	70.0	21.0	21.0	21.0	—	3.0
5514	3	0.05	0.2079	0.3	10.0	10.0	13.2	11.9	11.9	11.9	—	3.0
5514	3	0.05	0.3831	0.3	10.0	10.0	24.4	14.6	14.6	14.6	—	3.0
5514	3	0.05	1.1	0.3	10.0	9.9	70.0	21.0	21.0	21.0	—	3.0
5514	3	0.1	0.2079	0.3	10.0	10.0	13.2	11.9	11.9	11.9	—	3.0
5514	3	0.1	0.3831	0.3	10.0	10.0	24.4	14.6	14.6	14.6	—	3.0
5514	3	0.1	1.1	0.3	10.0	9.9	70.0	21.0	21.0	21.0	—	3.0
5514	3	0.2	0.2079	0.3	10.0	10.0	13.2	11.9	11.9	11.9	—	3.0
5514	3	0.2	0.3831	0.3	10.0	10.0	24.4	14.6	14.6	14.6	3.9	3.0
5514	3	0.2	1.1	0.3	10.0	9.9	70.0	21.0	21.0	21.0	4.4	3.0
5514	3	0.4	0.2079	0.3	10.0	10.0	13.2	11.9	11.9	11.9	—	3.0
5514	3	0.4	0.3831	0.3	10.0	10.0	24.4	14.6	14.6	14.6	3.9	3.0
5514	3	0.4	1.1	0.3	10.0	9.9	70.0	21.0	21.0	21.0	4.2	3.0
5514	3	0.8	0.2079	0.3	10.0	10.0	13.2	11.9	11.9	11.9	—	3.0
5514	3	0.8	0.3831	0.3	10.0	10.0	24.4	14.6	14.6	14.6	3.9	3.0
5514	3	0.8	1.1	0.3	10.0	9.9	70.0	21.0	21.0	21.0	4.4	3.0
5613	3	0.05	0.2079	0.0	10.0	10.0	13.2	11.9	11.9	11.9	—	3.0
5613	3	0.05	0.3831	0.0	10.0	10.0	24.4	7.3	7.3	7.3	—	3.0
5613	3	0.05	1.1	0.0	10.0	9.9	70.0	21.0	21.0	21.0	—	3.0
5613	3	0.1	0.2079	0.0	10.0	10.0	13.2	11.9	11.9	11.9	—	3.0
5613	3	0.1	0.3831	0.0	10.0	10.0	24.4	7.3	7.3	7.3	—	3.0
5613	3	0.1	1.1	0.0	10.0	9.9	70.0	21.0	21.0	21.0	—	3.0

(Continued)

Table 15. Number of Periods of Data from Each Code for Forced Heave Motion in Task 1
(Continued)

Model	Mode	z_a/T (1)	ω (rad/s)	F_n	A1	A2	FD	L1	L3	L4	NF	NS
5613	3	0.2	0.2079	0.0	10.0	10.0	13.2	11.9	11.9	11.9	—	3.0
5613	3	0.2	0.3831	0.0	10.0	10.0	24.4	7.3	7.3	7.3	—	3.0
5613	3	0.2	1.1	0.0	10.0	9.9	70.0	21.0	21.0	21.0	—	3.0
5613	3	0.4	0.2079	0.0	10.0	10.0	13.2	11.9	11.9	11.9	—	3.0
5613	3	0.4	0.3831	0.0	10.0	10.0	24.4	7.3	7.3	7.3	—	3.0
5613	3	0.4	1.1	0.0	10.0	9.9	70.0	21.0	21.0	21.0	—	3.0
5613	3	0.8	0.2079	0.0	10.0	10.0	13.2	11.9	11.9	11.9	—	3.0
5613	3	0.8	0.3831	0.0	10.0	10.0	24.4	7.3	7.3	7.3	—	3.0
5613	3	0.8	1.1	0.0	10.0	9.9	70.0	21.0	21.0	21.0	—	3.0
5613	3	0.05	0.2079	0.3	10.0	10.0	13.2	11.9	11.9	11.9	—	3.0
5613	3	0.05	0.3831	0.3	10.0	10.0	24.4	7.3	7.3	7.3	—	3.0
5613	3	0.05	1.1	0.3	10.0	9.9	70.0	21.0	21.0	21.0	—	3.0
5613	3	0.1	0.2079	0.3	10.0	10.0	13.2	11.9	11.9	11.9	—	3.0
5613	3	0.1	0.3831	0.3	10.0	10.0	24.4	7.3	7.3	7.3	—	3.0
5613	3	0.1	1.1	0.3	10.0	9.9	70.0	21.0	21.0	21.0	—	3.0
5613	3	0.2	0.2079	0.3	10.0	10.0	13.2	11.9	11.9	11.9	—	3.0
5613	3	0.2	0.3831	0.3	10.0	10.0	24.4	7.3	7.3	7.3	4.0	3.0
5613	3	0.2	1.1	0.3	10.0	9.9	70.0	21.0	21.0	21.0	4.6	3.0
5613	3	0.4	0.2079	0.3	10.0	10.0	13.2	11.9	11.9	11.9	—	3.0
5613	3	0.4	0.3831	0.3	10.0	10.0	24.4	7.3	7.3	7.3	4.0	3.0
5613	3	0.4	1.1	0.3	10.0	9.9	70.0	21.0	21.0	21.0	4.6	3.0
5613	3	0.8	0.2079	0.3	10.0	10.0	13.2	11.9	11.9	11.9	—	3.0
5613	3	0.8	0.3831	0.3	10.0	10.0	24.4	7.3	7.3	7.3	4.0	3.0
5613	3	0.8	1.1	0.3	10.0	9.9	70.0	21.0	21.0	21.0	5.8	3.0

Table 16. Number of Periods of Data from Each Code for Forced Roll Motion in Task 1

Model	Mode	ϕ_a ($^\circ$)	ω (rad/s)	F_n	A1	A2	FD	L1	L3	L4	NF	NS
5514	4	5	0.2079	0.0	10.0	10.0	13.2	7.9	7.9	7.9	—	3.0
5514	4	5	0.3831	0.0	10.0	10.0	24.4	14.6	14.6	14.6	—	3.0
5514	4	5	0.672	0.0	9.9	9.9	42.8	25.7	25.7	25.7	—	3.0
5514	4	15	0.2079	0.0	10.0	10.0	13.2	7.9	7.9	7.9	—	3.0
5514	4	15	0.3831	0.0	10.0	10.0	24.4	14.6	14.6	14.6	—	3.0
5514	4	15	0.672	0.0	9.9	9.9	42.8	25.7	25.7	25.7	—	3.0
5514	4	30	0.2079	0.0	10.0	10.0	13.2	7.9	7.9	7.9	—	3.0
5514	4	30	0.3831	0.0	10.0	10.0	24.4	14.6	14.6	14.6	—	3.0
5514	4	30	0.672	0.0	9.9	9.9	42.8	25.7	25.7	25.7	—	3.0
5514	4	45	0.2079	0.0	10.0	10.0	13.2	7.9	7.9	7.9	—	3.0
5514	4	45	0.3831	0.0	10.0	10.0	24.4	14.6	14.6	14.6	—	3.0
5514	4	45	0.672	0.0	9.9	9.9	42.8	25.7	25.7	25.7	—	3.0
5613	4	65	0.2079	0.3	10.0	10.0	13.2	7.9	7.9	7.9	—	3.0
5613	4	65	0.3831	0.3	10.0	8.6	24.4	7.3	7.3	7.3	3.2	3.0
5613	4	65	0.672	0.3	9.9	9.9	42.8	12.8	12.8	12.8	2.8	3.0
5514	4	5	0.2079	0.3	10.0	10.0	13.2	7.9	7.9	7.9	—	3.0
5514	4	5	0.3831	0.3	10.0	10.0	24.4	14.6	14.6	14.6	—	3.0
5514	4	5	0.672	0.3	9.9	9.9	42.8	25.7	25.7	25.7	—	3.0
5514	4	15	0.2079	0.3	10.0	10.0	13.2	7.9	7.9	7.9	—	3.0
5514	4	15	0.3831	0.3	10.0	10.0	24.4	14.6	14.6	14.6	—	3.0
5514	4	15	0.672	0.3	9.9	9.9	42.8	25.7	25.7	25.7	—	3.0
5514	4	30	0.2079	0.3	10.0	10.0	13.2	7.9	7.9	7.9	—	3.0
5514	4	30	0.3831	0.3	10.0	10.0	24.4	14.6	14.6	14.6	3.1	3.0
5514	4	30	0.672	0.3	9.9	9.9	42.8	25.7	25.7	25.7	2.7	3.0
5514	4	45	0.2079	0.3	10.0	10.0	13.2	7.9	7.9	7.9	—	3.0
5514	4	45	0.3831	0.3	10.0	10.0	24.4	14.6	14.6	14.6	3.1	3.0
5514	4	45	0.672	0.3	9.9	9.9	42.8	25.7	25.7	25.7	2.7	3.0
5514	4	65	0.2079	0.3	10.0	10.0	13.2	7.9	7.9	7.9	—	3.0
5514	4	65	0.3831	0.3	10.0	10.0	24.4	14.6	14.6	14.6	3.1	3.0
5514	4	65	0.672	0.3	9.9	9.9	42.8	25.7	25.7	25.7	2.7	3.0
5613	4	5	0.2079	0.0	10.0	10.0	13.2	7.9	7.9	7.9	—	3.0
5613	4	5	0.3831	0.0	10.0	10.0	24.4	7.3	7.3	7.3	—	3.0
5613	4	5	0.672	0.0	9.9	9.9	42.8	12.8	12.8	12.8	—	3.0
5613	4	15	0.2079	0.0	10.0	10.0	13.2	7.9	7.9	7.9	—	3.0
5613	4	15	0.3831	0.0	10.0	10.0	24.4	7.3	7.3	7.3	—	3.0
5613	4	15	0.672	0.0	9.9	9.9	42.8	12.8	12.8	12.8	—	3.0
5613	4	30	0.2079	0.0	10.0	10.0	13.2	7.9	7.9	7.9	—	3.0

(Continued)

Table 16. Number of Periods of Data from Each Code for Forced Roll Motion in Task 1
(Continued)

Model	Mode	ϕ_a ($^{\circ}$)	ω (rad/s)	F_n	A1	A2	FD	L1	L3	L4	NF	NS
5613	4	30	0.3831	0.0	10.0	10.0	24.4	7.3	7.3	7.3	—	3.0
5613	4	30	0.672	0.0	9.9	9.9	42.8	12.8	12.8	12.8	—	3.0
5613	4	45	0.2079	0.0	10.0	10.0	13.2	7.9	7.9	7.9	—	3.0
5613	4	45	0.3831	0.0	10.0	10.0	24.4	7.3	7.3	7.3	—	3.0
5613	4	45	0.672	0.0	9.9	9.9	42.8	12.8	12.8	12.8	—	3.0
5613	4	65	0.2079	0.0	10.0	10.0	13.2	7.9	7.9	7.9	—	3.0
5613	4	65	0.3831	0.0	10.0	8.6	24.4	7.3	7.3	7.3	—	3.0
5613	4	65	0.672	0.0	9.9	9.9	42.8	12.8	12.8	12.8	—	3.0
5613	4	5	0.2079	0.3	10.0	10.0	13.2	7.9	7.9	7.9	—	3.0
5613	4	5	0.3831	0.3	10.0	10.0	24.4	7.3	7.3	7.3	—	3.0
5613	4	5	0.672	0.3	9.9	9.9	42.8	12.8	12.8	12.8	—	3.0
5613	4	15	0.2079	0.3	10.0	10.0	13.2	7.9	7.9	7.9	—	3.0
5613	4	15	0.3831	0.3	10.0	10.0	24.4	7.3	7.3	7.3	—	3.0
5613	4	15	0.672	0.3	9.9	9.9	42.8	12.8	12.8	12.8	—	3.0
5613	4	30	0.2079	0.3	10.0	10.0	13.2	7.9	7.9	7.9	—	3.0
5613	4	30	0.3831	0.3	10.0	10.0	24.4	7.3	7.3	7.3	3.2	3.0
5613	4	30	0.672	0.3	9.9	9.9	42.8	12.8	12.8	12.8	2.8	3.0
5613	4	45	0.2079	0.3	10.0	10.0	13.2	7.9	7.9	7.9	—	3.0
5613	4	45	0.3831	0.3	10.0	10.0	24.4	7.3	7.3	7.3	3.2	3.0
5613	4	45	0.672	0.3	9.9	9.9	42.8	12.8	12.8	12.8	2.8	3.0
5613	4	65	0.2079	0.0	10.0	10.0	13.2	7.9	7.9	7.9	—	3.0
5613	4	65	0.3831	0.0	10.0	8.6	24.4	7.3	7.3	7.3	—	3.0
5613	4	65	0.672	0.0	9.9	9.9	42.8	12.8	12.8	12.8	—	3.0

Table 17. Number of Periods of Data from Each Code for Forced Pitch Motion in Task 1

Model	Mode	θ_a ($^\circ$)	ω (rad/s)	F_n	A1	A2	FD	L1	L3	L4	NF	NS
5514	5	1	0.2079	0.0	10.0	10.0	13.2	7.9	7.9	7.9	—	3.0
5514	5	1	0.3831	0.0	10.0	10.0	24.4	14.6	14.6	14.6	—	3.0
5514	5	1	1.1	0.0	10.0	9.9	70.0	21.0	21.0	21.0	—	3.0
5514	5	1.75	0.2079	0.0	10.0	10.0	13.2	7.9	7.9	7.9	—	3.0
5514	5	1.75	0.3831	0.0	10.0	10.0	24.4	14.6	14.6	14.6	—	3.0
5514	5	1.75	1.1	0.0	10.0	9.9	70.0	21.0	21.0	21.0	—	3.0
5514	5	2.5	0.2079	0.0	10.0	10.0	13.2	7.9	7.9	7.9	—	3.0
5514	5	2.5	0.3831	0.0	10.0	10.0	24.4	14.6	14.6	14.6	—	3.0
5514	5	2.5	1.1	0.0	10.0	9.9	70.0	21.0	21.0	21.0	—	3.0
5514	5	3.75	0.2079	0.0	10.0	10.0	13.2	7.9	7.9	7.9	—	3.0
5514	5	3.75	0.3831	0.0	10.0	10.0	24.4	14.6	14.6	14.6	—	3.0
5514	5	3.75	1.1	0.0	10.0	9.9	70.0	21.0	21.0	21.0	—	3.0
5514	5	5	0.2079	0.0	10.0	10.0	13.2	7.9	7.9	7.9	—	3.0
5514	5	5	0.3831	0.0	10.0	10.0	24.4	14.6	14.6	14.6	—	3.0
5514	5	5	1.1	0.0	10.0	9.9	70.0	21.0	21.0	21.0	—	3.0
5514	5	1	0.2079	0.3	10.0	10.0	13.2	7.9	7.9	7.9	—	3.0
5514	5	1	0.3831	0.3	10.0	10.0	24.4	14.6	14.6	14.6	—	3.0
5514	5	1	1.1	0.3	10.0	9.9	70.0	21.0	21.0	21.0	—	3.0
5514	5	1.75	0.2079	0.3	10.0	10.0	13.2	7.9	7.9	7.9	—	3.0
5514	5	1.75	0.3831	0.3	10.0	10.0	24.4	14.6	14.6	14.6	—	3.0
5514	5	1.75	1.1	0.3	10.0	9.9	70.0	21.0	21.0	21.0	—	3.0
5514	5	2.5	0.2079	0.3	10.0	10.0	13.2	7.9	7.9	7.9	—	3.0
5514	5	2.5	0.3831	0.3	10.0	10.0	24.4	14.6	14.6	14.6	3.9	3.0
5514	5	2.5	1.1	0.3	10.0	9.9	70.0	21.0	21.0	21.0	4.4	3.0
5514	5	3.75	0.2079	0.3	10.0	10.0	13.2	7.9	7.9	7.9	—	3.0
5514	5	3.75	0.3831	0.3	10.0	10.0	24.4	14.6	14.6	14.6	3.9	3.0
5514	5	3.75	1.1	0.3	10.0	9.9	70.0	21.0	21.0	21.0	4.4	3.0
5514	5	5	0.2079	0.3	10.0	10.0	13.2	7.9	7.9	7.9	—	3.0
5514	5	5	0.3831	0.3	10.0	10.0	24.4	14.6	14.6	14.6	3.9	3.0
5514	5	5	1.1	0.3	10.0	9.9	70.0	21.0	21.0	21.0	4.4	3.0
5613	5	1	0.2079	0.0	10.0	10.0	13.2	7.9	7.9	7.9	—	3.0
5613	5	1	0.3831	0.0	10.0	10.0	24.4	7.3	7.3	7.3	—	3.0
5613	5	1	1.1	0.0	10.0	9.9	70.0	21.0	21.0	21.0	—	3.0
5613	5	1.75	0.2079	0.0	10.0	10.0	13.2	7.9	7.9	7.9	—	3.0
5613	5	1.75	0.3831	0.0	10.0	10.0	24.4	7.3	7.3	7.3	—	3.0
5613	5	1.75	1.1	0.0	10.0	9.9	70.0	21.0	21.0	21.0	—	3.0

(Continued)

Table 17. Number of Periods of Data from Each Code for Forced Pitch Motion in Task 1
(Continued)

Model	Mode	θ_a ($^\circ$)	ω (rad/s)	F_n	A1	A2	FD	L1	L3	L4	NF	NS
5613	5	2.5	0.2079	0.0	10.0	10.0	13.2	7.9	7.9	7.9	—	3.0
5613	5	2.5	0.3831	0.0	10.0	10.0	24.4	7.3	7.3	7.3	—	3.0
5613	5	2.5	1.1	0.0	10.0	9.9	70.0	21.0	21.0	21.0	—	3.0
5613	5	3.75	0.2079	0.0	10.0	10.0	13.2	7.9	7.9	7.9	—	3.0
5613	5	3.75	0.3831	0.0	10.0	10.0	24.4	7.3	7.3	7.3	—	3.0
5613	5	3.75	1.1	0.0	10.0	9.9	70.0	21.0	21.0	21.0	—	3.0
5613	5	5	0.2079	0.0	10.0	10.0	13.2	7.9	7.9	7.9	—	3.0
5613	5	5	0.3831	0.0	10.0	10.0	24.4	7.3	7.3	7.3	—	3.0
5613	5	5	1.1	0.0	10.0	9.9	70.0	21.0	21.0	21.0	—	3.0
5613	5	1	0.2079	0.3	10.0	10.0	13.2	7.9	7.9	7.9	—	3.0
5613	5	1	0.3831	0.3	10.0	10.0	24.4	7.3	7.3	7.3	—	3.0
5613	5	1	1.1	0.3	10.0	9.9	70.0	21.0	21.0	21.0	—	3.0
5613	5	1.75	0.2079	0.3	10.0	10.0	13.2	7.9	7.9	7.9	—	3.0
5613	5	1.75	0.3831	0.3	10.0	10.0	24.4	7.3	7.3	7.3	—	3.0
5613	5	1.75	1.1	0.3	10.0	9.9	70.0	21.0	21.0	21.0	—	3.0
5613	5	2.5	0.2079	0.3	10.0	10.0	13.2	7.9	7.9	7.9	—	3.0
5613	5	2.5	0.3831	0.3	10.0	10.0	24.4	7.3	7.3	7.3	4.0	3.0
5613	5	2.5	1.1	0.3	10.0	9.9	70.0	21.0	21.0	21.0	4.6	3.0
5613	5	3.75	0.2079	0.3	10.0	10.0	13.2	7.9	7.9	7.9	—	3.0
5613	5	3.75	0.3831	0.3	10.0	10.0	24.4	7.3	7.3	7.3	4.0	3.0
5613	5	3.75	1.1	0.3	10.0	9.9	70.0	21.0	21.0	21.0	4.6	3.0
5613	5	5	0.2079	0.3	10.0	10.0	13.2	7.9	7.9	7.9	—	3.0
5613	5	5	0.3831	0.3	10.0	10.0	24.4	7.3	7.3	7.3	4.0	3.0
5613	5	5	1.1	0.3	10.0	9.9	70.0	21.0	21.0	21.0	4.6	3.0

Table 18. Number of Periods of Data from Each Code for Task 2

Model	H/λ	$\beta(^{\circ})$	F_n	A1	A2	FD	L1	L3	L4	NF	NS
5514	1/10	0	0.0	10.0	9.9	42.0	12.6	12.6	12.6	—	—
5514	1/15	0	0.0	10.0	9.9	42.0	12.6	12.6	12.6	—	3.0
5514	1/20	0	0.0	10.0	9.9	42.0	12.6	12.6	12.6	—	3.0
5514	1/60	0	0.0	10.0	10.0	42.0	12.6	12.6	12.6	—	3.0
5514	1/10	45	0.0	10.0	2.3	42.0	12.6	12.6	12.6	—	—
5514	1/15	45	0.0	10.0	9.9	42.0	12.6	12.6	12.6	—	3.0
5514	1/20	45	0.0	10.0	9.9	42.0	12.6	12.6	12.6	—	3.0
5514	1/60	45	0.0	10.0	9.9	42.0	12.6	12.6	12.6	—	3.0
5514	1/10	90	0.0	10.0	1.0	42.0	12.6	12.6	12.6	—	—
5514	1/15	90	0.0	10.0	9.9	42.0	12.6	12.6	12.6	—	3.0
5514	1/20	90	0.0	10.0	9.9	42.0	12.6	12.6	12.6	—	3.0
5514	1/60	90	0.0	10.0	9.9	42.0	12.6	12.6	12.6	—	3.0
5514	1/10	135	0.0	10.0	1.6	42.0	12.6	12.6	12.6	—	—
5514	1/15	135	0.0	10.0	9.9	42.0	12.6	12.6	12.6	—	3.0
5514	1/20	135	0.0	10.0	9.9	42.0	12.6	12.6	12.6	—	3.0
5514	1/60	135	0.0	10.0	9.9	42.0	12.6	12.6	12.6	—	3.0
5514	1/10	180	0.0	10.0	9.9	42.0	12.6	12.6	12.6	—	—
5514	1/15	180	0.0	10.0	9.9	42.0	12.6	12.6	12.6	—	3.0
5514	1/20	180	0.0	10.0	9.9	42.0	12.6	12.6	12.6	—	3.0
5514	1/60	180	0.0	10.0	9.9	42.0	12.6	12.6	12.6	—	3.0
5514	1/10	0	0.3	10.0	10.0	10.4	6.2	6.2	6.2	—	—
5514	1/15	0	0.3	10.0	10.0	10.4	6.2	6.2	6.2	—	3.0
5514	1/20	0	0.3	10.0	10.0	10.4	6.2	6.2	6.2	—	3.0
5514	1/60	0	0.3	10.0	10.0	10.4	6.2	6.2	6.2	—	3.0
5514	1/10	45	0.3	10.0	0.4	19.6	5.9	5.9	5.9	—	—
5514	1/15	45	0.3	10.0	6.7	19.6	5.9	5.9	5.9	—	3.0
5514	1/20	45	0.3	10.0	10.0	19.6	5.9	5.9	5.9	—	3.0
5514	1/60	45	0.3	10.0	10.0	19.6	5.9	5.9	5.9	—	3.0
5514	1/10	90	0.3	10.0	1.0	42.0	12.6	12.6	12.6	—	—
5514	1/15	90	0.3	10.0	9.9	42.0	12.6	12.6	12.6	—	3.0
5514	1/20	90	0.3	10.0	9.9	42.0	12.6	12.6	12.6	—	3.0
5514	1/60	90	0.3	10.0	9.9	42.0	12.6	12.6	12.6	—	3.0
5514	1/10	135	0.3	9.9	1.6	64.2	19.3	19.3	19.3	—	—

(Continued)

Table 18. Number of Periods of Data from Each Code for Task 2

(Continued)

Model	H/λ	$\beta(^{\circ})$	F_n	A1	A2	FD	L1	L3	L4	NF	NS
5514	1/15	135	0.3	9.9	9.9	64.2	19.3	19.3	19.3	—	3.0
5514	1/20	135	0.3	9.9	9.9	64.2	19.3	19.3	19.3	—	3.0
5514	1/60	135	0.3	9.9	9.9	64.2	19.3	19.3	19.3	—	3.0
5514	1/10	180	0.3	9.9	9.9	73.5	22.0	22.0	22.0	5.6	—
5514	1/15	180	0.3	9.9	9.9	73.5	22.0	22.0	22.0	8.8	3.0
5514	1/20	180	0.3	9.9	9.9	73.5	22.0	22.0	22.0	8.8	3.0
5514	1/60	180	0.3	9.9	9.9	73.5	22.0	22.0	22.0	—	3.0
5613	1/10	0	0.0	10.0	10.0	40.3	12.1	12.1	12.1	—	—
5613	1/15	0	0.0	10.0	10.0	40.3	12.1	12.1	12.1	—	3.0
5613	1/20	0	0.0	10.0	10.0	40.3	12.1	12.1	12.1	—	3.0
5613	1/60	0	0.0	10.0	10.0	40.3	12.1	12.1	12.1	—	3.0
5613	1/10	45	0.0	10.0	10.0	40.3	12.1	12.1	12.1	—	—
5613	1/15	45	0.0	10.0	10.0	40.3	12.1	12.1	12.1	—	3.0
5613	1/20	45	0.0	10.0	10.0	40.3	12.1	12.1	12.1	—	3.0
5613	1/60	45	0.0	10.0	10.0	40.3	12.1	12.1	12.1	—	3.0
5613	1/10	90	0.0	10.0	10.0	40.3	12.1	12.1	12.1	—	—
5613	1/15	90	0.0	10.0	10.0	40.3	12.1	12.1	12.1	—	3.0
5613	1/20	90	0.0	10.0	10.0	40.3	12.1	12.1	12.1	—	3.0
5613	1/60	90	0.0	10.0	10.0	40.3	12.1	12.1	12.1	—	3.0
5613	1/10	135	0.0	10.0	10.0	40.3	12.1	12.1	12.1	—	—
5613	1/15	135	0.0	10.0	10.0	40.3	12.1	12.1	12.1	—	3.0
5613	1/20	135	0.0	10.0	10.0	40.3	12.1	12.1	12.1	—	3.0
5613	1/60	135	0.0	10.0	10.0	40.3	12.1	12.1	12.1	—	3.0
5613	1/10	180	0.0	10.0	10.0	40.3	12.1	12.1	12.1	—	—
5613	1/15	180	0.0	10.0	10.0	40.3	12.1	12.1	12.1	—	3.0
5613	1/20	180	0.0	10.0	10.0	40.3	12.1	12.1	12.1	—	3.0
5613	1/60	180	0.0	10.0	10.0	40.3	12.1	12.1	12.1	—	3.0
5613	1/10	0	0.3	10.0	10.0	10.0	6.0	6.0	6.0	—	—
5613	1/15	0	0.3	10.0	10.0	10.0	6.0	6.0	6.0	—	3.0
5613	1/20	0	0.3	10.0	10.0	10.0	6.0	6.0	6.0	—	3.0
5613	1/60	0	0.3	10.0	10.0	10.0	6.0	6.0	6.0	—	3.0
5613	1/10	45	0.3	10.0	10.0	18.8	5.7	5.7	5.7	—	—
5613	1/15	45	0.3	10.0	10.0	18.8	5.7	5.7	5.7	—	3.0
5613	1/20	45	0.3	10.0	10.0	18.8	5.7	5.7	5.7	—	3.0
5613	1/60	45	0.3	10.0	10.0	18.8	5.7	5.7	5.7	—	3.0
5613	1/10	90	0.3	10.0	10.0	40.3	12.1	12.1	12.1	—	—
5613	1/15	90	0.3	10.0	10.0	40.3	12.1	12.1	12.1	—	3.0

(Continued)

Table 18. Number of Periods of Data from Each Code for Task 2

(Continued)

Model	H/λ	$\beta(^{\circ})$	F_n	A1	A2	FD	L1	L3	L4	NF	NS
5613	1/20	90	0.3	10.0	10.0	40.3	12.1	12.1	12.1	—	3.0
5613	1/60	90	0.3	10.0	10.0	40.3	12.1	12.1	12.1	—	3.0
5613	1/10	135	0.3	10.0	10.0	61.8	18.5	18.5	18.5	—	—
5613	1/15	135	0.3	10.0	10.0	61.8	18.5	18.5	18.5	—	3.0
5613	1/20	135	0.3	10.0	10.0	61.8	18.5	18.5	18.5	—	3.0
5613	1/60	135	0.3	10.0	10.0	61.8	18.5	18.5	18.5	—	3.0
5613	1/10	180	0.3	10.0	10.0	70.5	21.2	21.2	21.2	5.6	—
5613	1/15	180	0.3	10.0	10.0	70.5	21.2	21.2	21.2	8.8	3.0
5613	1/20	180	0.3	10.0	10.0	70.5	21.2	21.2	21.2	8.8	3.0
5613	1/60	180	0.3	10.0	10.0	70.5	21.2	21.2	21.2	—	3.0

Table 19. Number of Periods of Data from Each Code for Task 3

Model	$\beta(^{\circ})$	F_n	A1	A2	FD	L1	L3	L4	NF	NS
5514	0	0.0	9.6	9.6	28.6	17.2	17.2	17.2	—	2.9
5514	90	0.0	9.6	9.6	40.4	24.3	24.3	24.3	—	2.9
5514	0	0.3	9.5	9.5	13.2	7.9	7.9	7.9	—	2.8
5514	90	0.3	9.6	9.6	40.4	24.3	24.3	24.3	—	2.9
5613	0	0.0	9.8	9.8	28.1	8.4	8.4	8.4	—	2.9
5613	90	0.0	9.8	9.8	39.8	11.9	11.9	11.9	—	2.9
5613	0	0.3	10.0	10.0	13.3	8.0	8.0	8.0	—	3.0
5613	90	0.3	9.8	9.8	39.8	11.9	11.9	11.9	—	2.9

STANDARDIZATION

For each code for which data were received, ten “standard” data files were created that enforce absolute uniformity in the variables records and zone records for each task. The files are named `std-*.dat` where `*` is a wildcard standing for strings of characters providing the task number, subtask, model number, etc. Extra information such as components of viscous forces is no longer present in the standard files. The files also enforce uniformity of phase for all the codes.

If necessary, time was shifted so that the displacement always obeys the equation $a \sin(\omega t)$ for some amplitude a and frequency ω . The displacement for task 1 is the prescribed one. The displacement for task 2 is taken as the wave height at the center of gravity. For task 3, the displacement is the heave, the distance of the center of gravity above the mean free-surface level. In general, the first two time steps were found where the displacement crossed from a negative to a positive value. Then inverse interpolation based on Aitken’s iterative linear interpolation¹² was used to obtain the time of the zero upcrossing more precisely. The value thus obtained was subtracted from the time supplied by the code runners. The procedure assumes that the displacement is symmetric about zero. For the nonlinear waves in task 2, the assumption is only an approximation.

For task 3, the components of the radiation and diffraction forces received from the codes were added together, called the hydrodynamic force, and stored in the place reserved for the diffraction force. At the same time, all components of the radiation force were set to zero:

$$\begin{aligned}\vec{F}^{\text{dif}} + \vec{F}^{\text{rad}} &\rightarrow \vec{F}^{\text{hyd}} \\ \vec{M}^{\text{dif}} + \vec{M}^{\text{rad}} &\rightarrow \vec{M}^{\text{hyd}} \\ \vec{0} &\rightarrow \vec{F}^{\text{rad}} \\ \vec{0} &\rightarrow \vec{M}^{\text{rad}}\end{aligned}$$

NSHIPMO. No time shift was required for task 1 as the displacements appear to satisfy $a \sin(\omega t)$. For task 2, the wave elevation provided in the data files was at its maximum at $t = 0$. Therefore the time of the first zero upcrossing of η was found and this time was subtracted from all times provided in the data files. The components of the force and moment vectors had dimensions of N and N-m instead of kN and kN-m. The weight vector had to be subtracted from the force components to obtain the hydrostatic force and the total potential force exerted by the fluid on the hull.

NFA. Data received from NFA were not contained in TECPLOT files. Instead, 20 columns of nondimensional data in text files were provided. The first column contained the time; the second column contained the displacement. The components of the total potential (normal) force and moment were provided in columns 3, 6, 9, 12, 15, and 18. Other columns contained data for the total tangential force and the sum of the normal and tangential force. Since this study is concerned with the potential force, only the columns containing the time, displacement, and the components of the normal forces and moments are considered here. The files had been placed in directories that keep the frequencies separate as given in Table 20.

For NFA, data for the plots appearing in the appendices were taken from files with names `process_*.dat` where `*` is a wildcard that stands for any string of characters. These files had undergone postprocessing by SAIC to convert vector components to a body-fixed frame of reference. In addition, data had undergone smoothing of the form

$$u'_j = (u_{j-1} + 2u_j + u_{j+1}) / 4$$

for $j = 2, \dots, N-1$ where N is the number of data points. The original data files, the files containing the data used in the appendices, and the programs required to do the necessary transformations were supplied by SAIC. For example, in the case of forced heave motion at an amplitude equal to 80% of the draft, SAIC supplied the original data file `5514_heave80.dat`, a processed data file `process_5514_heave80.dat`, a Fortran program `heave.f`, a shell script `heave.sh`, and input files to `heave.f`. The postprocessed files contained data still in nondimensional form.

To obtain data consistent with data from other codes, nondimensional time was multiplied by L/U , force components were multiplied by $\rho U^2 L^2 / (1000 N / kN)$, and moment components were multiplied by $\rho U^2 L^3 / (1000 N / kN)$. The components of the force and moment vectors then have dimensions kN and kN-m. Here ρ is the density of water taken to be 1025 kg/m^3 , U is the speed of the ship, and L is the length of the ship.

For task 2, the displacement that was provided is the wave height at the forward perpendicular, not at the center of gravity. In addition, the wave elevation is not linear; it was computed from the

Table 20. Data received from NFA.

Directory	Simulations in the Directory
./process_heave_run1	Task 1: prescribed heave of amplitude $z_a/T = 0.2$, 0.4, and 0.8 and frequency $\omega = 1.1$ rad/s, $F_n = 0.3$
./process_heave_run2	Task 1: prescribed heave of amplitude $z_a/T = 0.2$, 0.4, and 0.8 and frequency $\omega = 0.3831$ rad/s, $F_n = 0.3$
./process_pitch_run1	Task 1: prescribed pitch of amplitude $\theta_a = 2.5^\circ$, 3.75° , and 5° and frequency $\omega = 1.1$ rad/s, $F_n = 0.3$
./process_pitch_run2	Task 1: prescribed pitch of amplitude $\theta_a = 2.5^\circ$, 3.75° , and 5° and frequency $\omega = 0.3831$ rad/s, $F_n = 0.3$
./process_roll_run1	Task 1: prescribed roll of amplitude $\phi_a = 15^\circ$, 30° , 45° , and 65° and frequency $\omega = 0.672$ rad/s, $F_n = 0.3$
./process_roll_run2	Task 1: prescribed roll of amplitude $\phi_a = 30^\circ$, 45° , and 65° and frequency $\omega = 0.3831$ rad/s, $F_n = 0.3$
./process_wave	Task 2: $H/\lambda = 1/10$, $1/15$, and $1/20$ in head seas, $F_n = 0.3$

Airy function by SAIC as part of their postprocessing. To align time histories, the wave height at the center of gravity was approximated from linear theory. If the waves are monochromatic and travel in the direction of a negative earth-fixed x_e -axis, then the wave height is given by

$$\eta = \eta_a \sin(\omega_0 t + kx_e + \epsilon)$$

where $\omega_0 = \sqrt{2\pi g/\lambda}$ is the absolute wave frequency. In the case of head seas, the ship travels in the direction of the positive x_e -axis at the speed U . The center of gravity of the ship is assumed to be at $x_e = 0$ when $t = 0$ so that

$$\eta_{CG} = \eta_a \sin(\omega_0 t + kUt + \epsilon) = \eta_a \sin(\omega_e t + \epsilon)$$

for some phase ϵ . If x_{FP} is the distance of the forward perpendicular from the center of gravity, then the wave height at the forward perpendicular is

$$\begin{aligned} \eta_{FP} &= \eta_a \sin[\omega_0 t + k(x_{FP} + Ut) + \epsilon] = \eta_a \sin\left(\omega_e t + k\lambda \frac{x_{FP}}{\lambda} + \epsilon\right) \\ &= \eta_a \sin\left[\omega_e \left(t + \frac{x_{FP}}{\lambda} T_e\right) + \epsilon\right] \end{aligned}$$

since $k\lambda = \omega_e T_e = 2\pi$. The distance x_{FP} is $0.508L$ for Model 5514 and $0.517L$ for Model 5613 where $\lambda = L$. As a first approximation, the wave height at the center of gravity at time t is taken as the wave height at the forward perpendicular at time $t - x_{FP}T_e/\lambda$ that was supplied in the data files. Inverse interpolation based on Aitken's iterative linear interpolation¹² is used to obtain this wave

height. Data from approximately the last half period are discarded since the wave height cannot be obtained from interpolation.

The peaks are much higher than the troughs are deep in the case of $H/\lambda = 1/10$. Even so, time was shifted so that $\eta = 0$ at $t = 0$ for consistency with the procedure undertaken with the results of other codes.

LAMP. Components of the diffraction and radiation force were not provided for the LAMP codes. Instead, forces and moments \vec{F}^{hyd1} , \vec{M}^{hyd1} , \vec{F}^{hyd2} , \vec{M}^{hyd2} , \vec{F}^{hyd} , and \vec{M}^{hyd} were provided. This hydrodynamic force contained components of the hydrodynamic force and moment due to radiation, diffraction, and Kelvin components. The Kelvin component vanishes only at zero forward speed. Since there is no diffraction force in task 1, the pure radiation force can be extracted from the results only when the ship has no forward speed. In task 2 there is no radiation force and the pure diffraction force can be extracted from the results only when the ship has no forward speed. For task 3, the radiation and diffraction components are added together into a hydrodynamic component in the plots and tables that appear in the appendices. For nonzero forward speed, the Kelvin component is present in the hydrodynamic force and moment provided for the LAMP codes. At forward speed, there is a steady sinkage force and steady nonzero trim moment in the hydrodynamic force and moment.

FREDYN. FREDYN uses right-handed earth-fixed and ship-fixed coordinate systems with z positive downward. The coordinate systems are rotated through 180° about a longitudinal axis through the center of gravity from the standard coordinate systems where z is positive upward. Consequently, components of vectors obtained from FREDYN must be transformed. In addition, the pitch angle θ and the yaw angle ψ must be transformed to retain their right-handed sense about the y - and z -axes. Specifically, the following substitutions were made:

$$\begin{aligned}\eta &\rightarrow -\eta \\ z_e &\rightarrow -z_e \\ \theta &\rightarrow -\theta \\ F_y &\rightarrow -F_y \\ F_z &\rightarrow -F_z \\ M_y &\rightarrow -M_y \\ M_z &\rightarrow -M_z\end{aligned}$$

where η is the wave elevation at the center of gravity, z_e is the distance of the center of gravity above the mean free-surface level, F stands for any of the forces, and M stands for any of the moments.

AEGIR-1 and AEGIR-2. In the data received, the weight of the ship had been added to the force. The weight was therefore removed from the hydrostatic and total potential forces by subtracting the components of the weight vector. The negative of the components of the weight vector are given by the matrix equation

$$\begin{bmatrix} \cos \psi \cos \theta & \sin \psi \cos \theta & -\sin \theta \\ \cos \psi \sin \theta \sin \phi - \sin \psi \cos \phi & \sin \psi \sin \theta \sin \phi + \cos \psi \cos \phi & \cos \psi \sin \phi \\ \cos \psi \sin \theta \cos \phi + \sin \psi \sin \phi & \sin \psi \sin \theta \cos \phi - \cos \psi \sin \phi & \cos \theta \cos \phi \end{bmatrix} \begin{bmatrix} 0 \\ 0 \\ w \end{bmatrix}$$

where w is the weight, the magnitude of the weight vector. The earth-fixed components of the weight vector are $(0, 0, -w)$ and the matrix multiplication obtains the ship-fixed components of the negative of the weight vector. The angles $\psi(= \beta)$, θ , and ϕ are the Euler angles defined in the order yaw, pitch, and roll.

For task 3, condition 2, where the ship heaves and rolls in beam seas, the waves come from the direction opposite to that of all the other codes. The data supplied for AEGIR-1 can be compared to the data from other codes after multiplying the roll angle ϕ , the y -component of all force vectors, and the x - and z -components of all moment vectors by -1. The following Fortran do-loop accomplishes the task for AEGIR:

```

phi = -phi
do i = 2, 6, 2
  fptot(i) = -fptot(i)
  fhst(i) = -fhst(i)
  ffk(i) = -ffk(i)
  frad(i) = -frad(i)
  fdif(i) = -fdif(i)
  fvisc(i) = -fvisc(i)
  frad1(i) = -frad1(i)
  frad2(i) = -frad2(i)
  fdif1(i) = -fdif1(i)
  fdif2(i) = -fdif2(i)
end do

```

All six components of the vectors \vec{F}^{dif1} , \vec{F}^{dif} , \vec{F}^{rad1} , \vec{F}^{rad2} , and \vec{F}^{rad} were identically zero for all time steps.

Except for NFA, files with names like the following for LAMP-1 were provided by the code runners:

```

L1-task1-heave-m5514.dat
L1-task1-pitch-m5514.dat
L1-task1-roll-m5514.dat
L1-task2-m5514.dat
L1-task3-m5514.dat

```

Corresponding standard files whose names have the characters 'std-' appended to the front were made for all codes. They are TECPLOT files with data formatted as uniform as possible to facilitate processing. Thus, for the case of forced heave of Model 5514 in task 1, the correspondence

$$\text{L1-heave-m5514.dat} \rightarrow \text{std-L1-heave-m5514.dat}$$

provides the name of the file containing standardized data. A similar file naming convention was followed for other codes. The standard files contain data from the original files unless the time has been shifted, a coordinate system transformation has been applied, columns of data have been modified to correspond to the same variable for all codes, or columns of data have been deleted

Table 21. Standard variables records for the various tasks.

Motion	Variables Record
1-DOF Forced Heave	variables = "time", "heave", "fptot_x", "fptot_y", "fptot_z", "fptot_mx", "fptot_my", "fptot_mz", "fhst_x", "fhst_y", "fhst_z", "fhst_mx", "fhst_my", "fhst_mz", "frad_x", "frad_y", "frad_z", "frad_mx", "frad_my", "frad_mz"
1-DOF Forced Roll	variables = "time", "phi", "fptot_x", "fptot_y", "fptot_z", "fptot_mx", "fptot_my", "fptot_mz", "fhst_x", "fhst_y", "fhst_z", "fhst_mx", "fhst_my", "fhst_mz", "frad_x", "frad_y", "frad_z", "frad_mx", "frad_my", "frad_mz"
1-DOF Forced Pitch	variables = "time", "theta", "fptot_x", "fptot_y", "fptot_z", "fptot_mx", "fptot_my", "fptot_mz", "fhst_x", "fhst_y", "fhst_z", "fhst_mx", "fhst_my", "fhst_mz", "frad_x", "frad_y", "frad_z", "frad_mx", "frad_my", "frad_mz"
0-DOF In Waves	variables = "time", "eta", "fptot_x", "fptot_y", "fptot_z", "fptot_mx", "fptot_my", "fptot_mz", "fhst_x", "fhst_y", "fhst_z", "fhst_mx", "fhst_my", "fhst_mz", "ffk_x", "ffk_y", "ffk_z", "ffk_mx", "ffk_my", "ffk_mz", "fdif_x", "fdif_y", "fdif_z", "fdif_mx", "fdif_my", "fdif_mz"
2-DOF Wave Contouring	variables = "time", "eta", "fptot_x", "fptot_y", "fptot_z", "fptot_mx", "fptot_my", "fptot_mz", "fhst_x", "fhst_y", "fhst_z", "fhst_mx", "fhst_my", "fhst_mz", "ffk_x", "ffk_y", "ffk_z", "ffk_mx", "ffk_my", "ffk_mz", "frad_x", "frad_y", "frad_z", "frad_mx", "frad_my", "frad_mz", "fdif_x", "fdif_y", "fdif_z", "fdif_mx", "fdif_my", "fdif_mz", "phi", "theta"

because of irrelevance to this potential flow force study. The TECPLOT variables records in the standard files are listed in Table 21.

PROCESSING

Data were extracted from each of the newly created standard files for the last full period of motion and placed in another new file with the file extension `.tec` in place of `.dat`. The time t in the new file was changed so that $t = 0$ corresponds to the beginning of the period according to the formula

$$t \bmod T_e \rightarrow t.$$

Here T_e may be an absolute or an encounter period according to the context. Another new file with the extension `csv` (standing for comma separated value), was created for each of the standard files. For each zone of the standard file, there is a table within the csv file giving the zone name, the period, and the variable names in the task. For each variable, the tables contain a row for the mean, the magnitudes and phases of the first few harmonics, the unfiltered minimum and maximum, and the smoothed minimum and maximum. The file can be read with a spreadsheet program.

Dominant Periodicity

For the tasks in the force study, the dominant periodicity T_e can be calculated with paper and pencil if it isn't explicitly prescribed. Automatic detection of the periodicity was found to be a useful check of the results provided by the code runners. For automatic detection of the dominant periodicity, several methods are available. One can calculate the mean and count the number of times the displacement crosses the mean. The period is obtained from the average time between crossings with attention paid to whether the number of crossings is odd or even. Since only a few periods of data were provided by the code runners, a second method was employed to check the value thus obtained. Assuming data u_k are provided at uniformly spaced discrete times, one can calculate a correlation coefficient r between the sequence

$$u_0, u_1, \dots,$$

and

$$1, \cos\left(\frac{2\pi}{p}\right), \sin\left(\frac{2\pi}{p}\right), \cos\left(\frac{4\pi}{p}\right), \sin\left(\frac{4\pi}{p}\right), \dots$$

where $p\Delta t$ is a presumed trial period:

$$r = \frac{\Delta t}{N} \left\{ \left[\sum_{j=0}^N u_j \cos\left(j \frac{2\pi}{p}\right) \right]^2 + \left[\sum_{j=0}^N u_j \sin\left(j \frac{2\pi}{p}\right) \right]^2 \right\}$$

The formula is found in a book by Whittaker and Robinson.^{13||} Other formulas can be obtained from spectral techniques. Using the extended trapezoidal rule for a continuous function $u(t)$, we

^{||}Whittaker and Robinson refer the reader to four papers authored between 1898 and 1906 by Schuster who introduced the concept of periodogram analysis for determining periodicities.

find that

$$\begin{aligned} \frac{1}{\Delta t} \int_0^{N\Delta t} u(t) \sin(\omega t) dt &= \sum_{j=0}^N u_j \sin\left(j\Delta t \frac{2\pi}{p\Delta t}\right) \\ &\quad - \frac{u_N \sin(\omega N\Delta t)}{2} + O(N\Delta t^3) \\ \frac{1}{\Delta t} \int_0^{N\Delta t} u(t) \cos(\omega t) dt &= \sum_{j=0}^N u_j \cos\left(j\Delta t \frac{2\pi}{p\Delta t}\right) \\ &\quad - \frac{u_0 + u_N \cos(\omega N\Delta t)}{2} + O(N\Delta t^3) \end{aligned}$$

where $u_j = u(j\Delta t)$ and $\omega = 2\pi/(p\Delta t)$. Therefore, for large N and small Δt , the approximation

$$r \approx N\Delta t \left| \int_0^{N\Delta t} u(t) e^{i\omega t} dt \right|^2$$

relates r to the continuous function $u(t)$. Essentially, the method seeks the angular frequency $\omega = 2\pi/p$ at which the power is a maximum.¹⁴ The integer k was found for which $p = k$ produces a maximum correlation coefficient. Then trial periods for fractional values of p were checked to obtain the maximum correlation within 0.01 of a time step. The values returned by both methods were noted. Unfortunately, neither automatic method was reliable due to the limited number of cycles of data. In the end, it was decided to rely heavily on the pencil-and-paper method.

If the period T_e is known, one can obtain coefficients of a Fourier fit of the form

$$a_0 + a_1 \cos(\omega_e t) + b_1 \sin(\omega_e t) + a_2 \cos(2\omega_e t) + b_2 \sin(2\omega_e t) + \dots$$

to data u_k at $t = k\Delta t$.^{**} An easy way is to calculate the least-squares solution of

$$u_k = a_0 + \sum_{j=1}^M [a_j \cos(\omega_e j k \Delta t) + b_j \sin(\omega_e j k \Delta t)]$$

where M is the number of harmonics and the number of equations (data points) is at least $2M + 1$. To avoid the initial transients, only the last half of the data supplied by the code runners was used in this analysis. The normal equations were solved by LU decomposition; in this case it is not necessary to use the methods based on singular value decomposition advocated by the authors of *Numerical Recipes*.¹⁴ Only a few harmonics were calculated. The information through the second harmonic is sometimes useful when comparing time histories of the data supplied from the various codes. The analysis was done for all variables.

Data Smoothing

The minimum and maximum for one period of motion were calculated for each variable supplied by a code runner. Unfortunately, there are spikes in the data which are probably of a purely

^{**}After the mean and the first harmonic have been subtracted from the data, it is not necessarily the case that the dominant frequency of the residual is $2\omega_e$ or any other integral multiple of ω_e as is assumed here. Nevertheless, the information obtained from this Fourier fit is useful.

numerical nature. Although spikes frequently arise when linear filtering is introduced to enhance numerical stability, it is not claimed here that all the spikes are due to filtering. Data from all codes were smoothed by a filtering technique discussed in the first edition of *Numerical Recipes*.¹⁴ The technique is based on the use of Fourier transforms and was implemented in a subroutine similar to subroutine SMOOFT given in *Numerical Recipes*. Ten points on each side of a data point were used to obtain smoothed data. The minimum and maximum of the smoothed data also appears in the csv files.

Before proceeding, numerical experimentation was done to compare data smoothing techniques. The diffraction force component F_x^{dif} computed by LAMP-4 is considered in the following. This force component was chosen because it exhibited a time history with typical spikes that ought to be smoothed before the minimum and maximum values are computed. In this case the maximum is nearly equal to the value at the spike. Other cases exist for which the maximum is attained at a spike. Such spikes make it difficult to conclude anything about nonlinear behavior as a function of the amplitude of the motion or the steepness of waves in a wave train. The diffraction problem for the test data corresponds to a simulation in task 2 for which $H/\lambda = 1/10$, $\lambda/L = 1$, $\beta = 45^\circ$, and $F_n = 0.0$ for Model 5514 scaled to $L = 142$ m. The time step for the LAMP-4 data is 0.06 sec, the period is 9.52 sec, and the number of points per period is 159.

Figure 9 compares the original data with the data after smoothing by two techniques. The original data are plotted in red. The black curve depicts smoothed data from the Fourier transform technique outlined in the first edition of *Numerical Recipes* when $n = 10$ points on either side of a data point (21 points altogether) enter into the determination of a smoothed value. The blue curve shows smoothed data from a technique found in the older book by Whittaker and Robinson¹³ which again uses 21 points. Whittaker and Robinson obtained their formula from a least squares fit of a parabola to the 21 points. The two smoothing techniques produce similar results.

Whittaker and Robinson have a whole chapter on data smoothing. They obtained formulas from least squares fits of polynomials of degree $2k$ and $2k + 1$ to discrete data — the formula obtained from using $2k$ is identical to the formula obtained using $2k + 1$. Formulas for $k = 0, 1, 2$ and $n \leq 10$, where $2n + 1$ is the total number of points in the formula, are given in section 146 entitled “Tables of these Formulae.” After comparing 20 formulas given by Whittaker and Robinson, the “best formula” seemed to be their formula for Case II when $k = 1$ and $n = 10$ (obtained by fitting a parabola and cubic to $2n + 1 = 21$ points):

$$\begin{aligned} u'_0 = \frac{1}{3059} [& 329u_0 + 324(u_1 + u_{-1}) + 309(u_2 + u_{-2}) \\ & + 284(u_3 + u_{-3}) + 249(u_4 + u_{-4}) + 204(u_5 + u_{-5}) \\ & + 149(u_6 + u_{-6}) + 84(u_7 + u_{-7}) + 9(u_8 + u_{-8}) \\ & - 76(u_9 + u_{-9}) - 171(u_{10} + u_{-10})] \end{aligned}$$

The formula obtained by fitting a parabola and cubic to $2n + 1 = 11$ points ($n = 5$ points to each side) when $k = 1$ is

$$\begin{aligned} u'_0 = \frac{1}{429} [& 89u_0 + 84(u_1 + u_{-1}) + 69(u_2 + u_{-2}) \\ & + 44(u_3 + u_{-3}) + 9(u_4 + u_{-4}) - 36(u_5 + u_{-5})] \end{aligned}$$

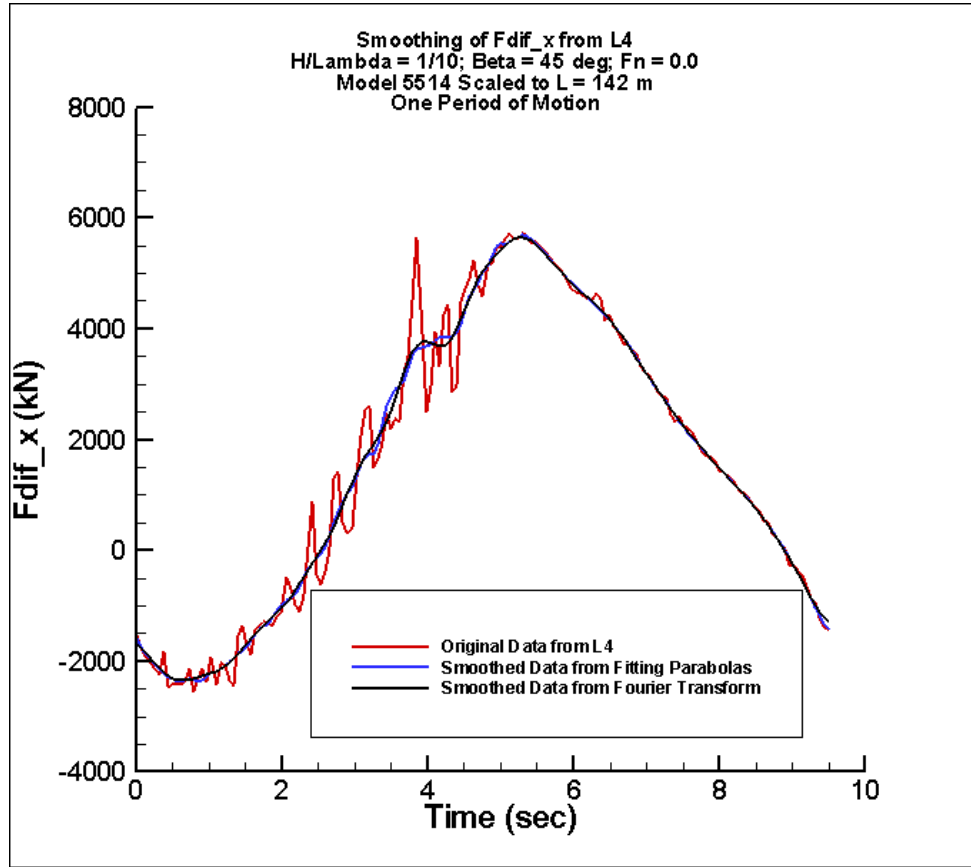


Fig. 9. Time history of F_x^{dif} for the last period of motion as predicted by LAMP-4 together with smoothed time histories from two techniques; 21 data points used in the smoothing; $H/\lambda = 1/10$; $\lambda/L = 1$; $\beta = 45^\circ$; $F_n = 0.0$; Model 5514 scaled to $L = 142$ m.

Figure 10 shows a plot similar to that of Fig. 9 except that $n = 5$ so that 11, instead of 21, points were used to obtain smoothed values from both the Fourier transform technique and the technique of Whittaker and Robinson. Traces of the original spike near 4 seconds are more obvious when fewer points are used. The ideal number of points used for smoothing depends on the data. Limited comparison suggests that using the same number of points in the smoothing technique based on Fourier transforms and the technique based on fitting parabolas produces smoothed data that are qualitatively similar.

Figures 11 and 12 show selected portions of the time history of the roll moment computed by LAMP-4 for forced roll motion of Model 5514 at $F_n = 0$, frequency 0.2079 rad/s, and roll amplitude 65° . They also show the smoothed data that results from the Fourier transform smoothing technique with 10 points used to either side. As one might expect, the smoothing lowers the maximum and raises the minimum of the roll moment. In Fig. 12 a peak in Fig. 11 has been magnified to show more detail of how the smoothing affects the data in this case.

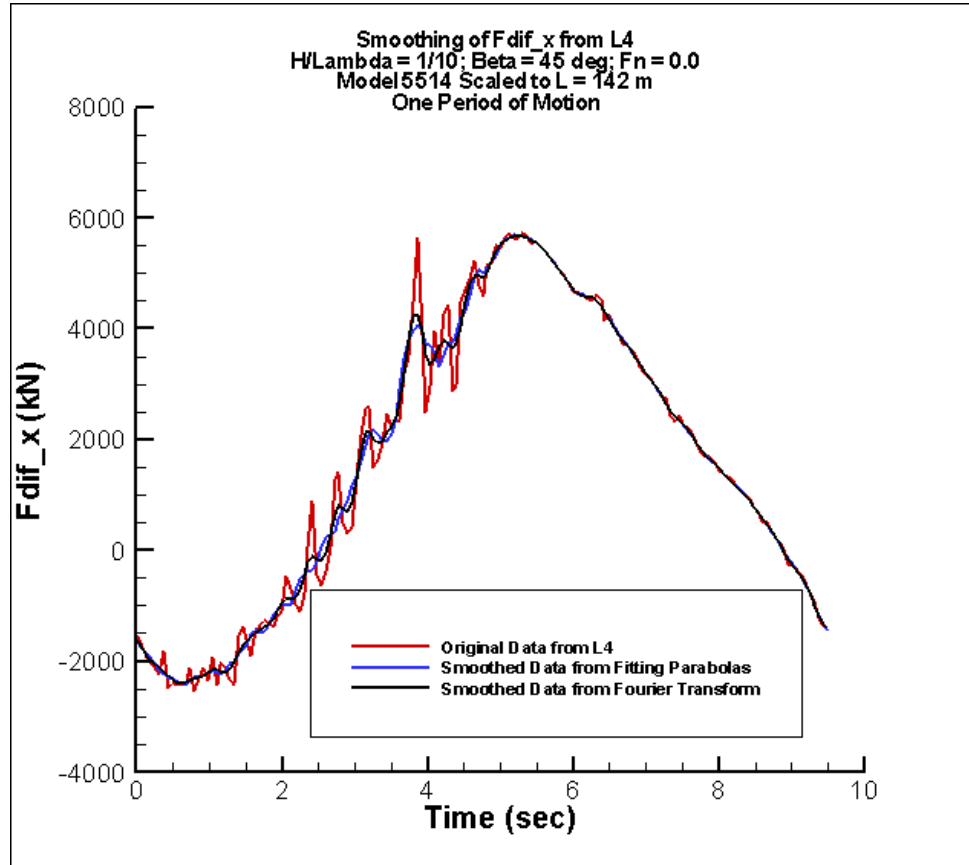


Fig. 10. Time history of F_x^{dif} for the last period of motion as predicted by LAMP-4 together with smoothed time histories from two techniques; 11 data points used in the smoothing; $H/\lambda = 1/10$; $\lambda/L = 1$; $\beta = 45^\circ$; $F_n = 0.0$; Model 5514 scaled to $L = 142$ m.

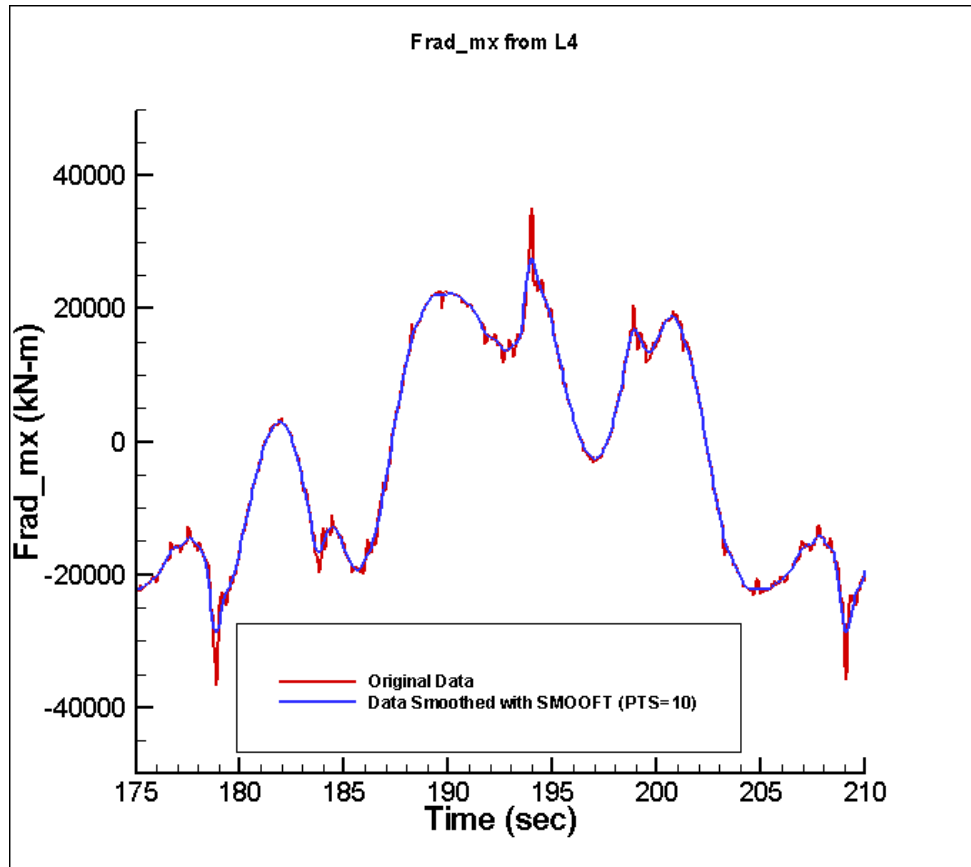


Fig. 11. Part of the time history of M_x^{rad} as predicted by LAMP-4 together with the smoothed time history from a Fourier transform technique; 21 data points used in the smoothing; frequency = 0.2079 rad/s; roll amplitude = 65° ; $F_n = 0.0$; Model 5514 scaled to $L = 142$ m.

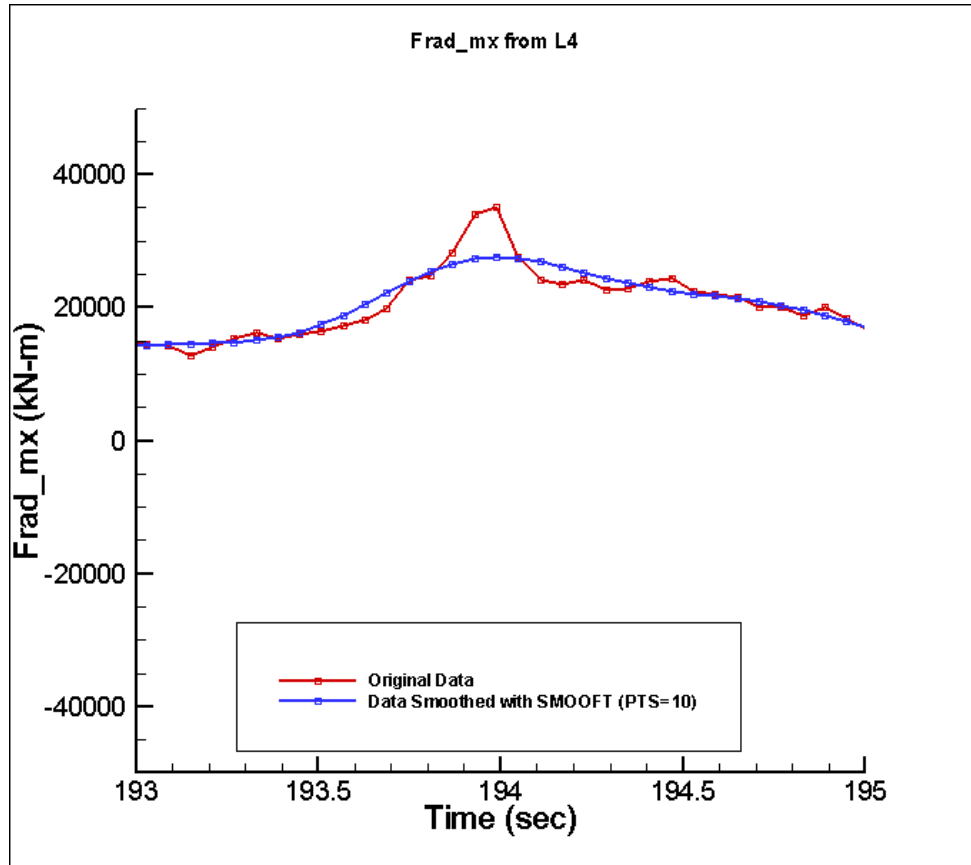


Fig. 12. Closeup of a peak in the previous figure showing part of the time history of M_x^{rad} as predicted by LAMP-4 together with smoothed time histories from a Fourier transform technique. 21 data points used in the smoothing; frequency = 0.2079 rad/s; roll amplitude = 65° ; $F_n = 0.0$; Model 5514 scaled to $L = 142$ m.

Time Histories

For comparative plots of the time histories of the components of the force and moment vectors during the last full period of motion, the reader is referred to Appendices A–J. The appendices contain thousands of figures and tables and have been placed in bookmarked PDF’s to ease navigation through them.

A plot of the time history of each variable is provided except that variables are excluded when they should be identically zero based solely on consideration of symmetry. In the plots, time was shifted so that the displacement is of the form $a \sin \omega t$ for some amplitude a and some frequency ω . The displacement is the prescribed displacement in task 1 and the wave height at the center of gravity in tasks 2 and 3. When the data provided were insufficient to span one full period of motion or were identically zero, the data were not plotted and a note at the bottom of the plot informs the reader of the omission.

There are two tables following each time-history plot. The first table gives the coefficients a_n for $n = 0, 1, 2$ and the phases Φ_n for $n = 1, 2$ of a Fourier fit of the form

$$a_0 + a_1 \sin(\omega_e t + \Phi_1) + a_2 \sin(2\omega_e t + \Phi_2)$$

to the data in the plot. The coefficients were obtained from a least-squares fit. A lack of data is indicated by a dash in the table. The second table provides the minimum and the maximum of the variable that is plotted. The minimum and maximum is provided for both smoothed and unsmoothed data. Again a lack of data is indicated by a dash in the table.

The time-history plots in Appendices A–H should be compared with the plots of the minimum and maximum of each variable in Appendices K–R. The correspondence between the appendices containing the time-history plots with the appendices containing the plots of the minimum and maximum was given in Table 1.

Data plotted in the time-history plots have not been smoothed.

Minima and Maxima

To show how computed quantities vary with nonlinearity, the measure of nonlinearity chosen for task 1 is the amplitude of the prescribed oscillation. It is z_a/T for prescribed heave motion, θ_a for prescribed pitch motion, and ϕ_a for prescribed roll motion. For task 2, the wave steepness H/λ is chosen as the measure. Since task 3 involves only eight runs, no such measure was deemed appropriate.

For plots and associated tables of the minimum and maximum of each force component provided by the code runners, the reader is referred to Appendices K–R. The figures and tables in each appendix can be compared with time-history plots and tables of data in a corresponding appendix among Appendices A–H as given in Table 1. All data plotted are obtained from smoothed time

histories. For each variable f in task 1, the quantity

$$\begin{array}{ll} \frac{f - \langle f \rangle}{z_a/T} & \text{in the case of forced heave motion} \\ \frac{f - \langle f \rangle}{\phi_a} & \text{in the case of forced roll motion} \\ \frac{f - \langle f \rangle}{\theta_a} & \text{in the case of forced pitch motion} \end{array}$$

is plotted. The quantity $\langle f \rangle$ is the mean value of the variable f , which may be obtained from a Fourier fit. The quantities (z_a/T) , ϕ_a , and θ_a are plotted along the horizontal axis and are taken as the measure of nonlinearity in the problem. For task 1, each plot depicts data for all codes at one frequency and one speed. For each variable f of task 2, the quantity

$$\frac{f - \langle f \rangle}{H/\lambda}$$

is plotted; each plot depicts data from all codes at one heading and one speed.

Linear variation with respect to the measure of nonlinearity appears as a horizontal line whereas quadratic variation appears as a straight line with nonzero slope. Quadratic variation of some variables is seen even in linear codes. An example of such variation is found in the results for the ship-fixed vertical force in the case of prescribed sinusoidal roll motion. The data depicted in the plot were obtained from the maximum and the minimum of the filtered time history data. An examination of the amplitude a_2 of the second harmonic for this force component found in tables in this report shows that a_2/ϕ_a is indeed approximately linear in ϕ_a .

For each variable, tables containing the mean value and the minimum and maximum of the unfiltered and filtered variable follow the plot of the minimum and maximum. Missing data are indicated by dashes.

OBSERVATIONS

Nonlinearity

For forced heave motion the greatest evidence of nonlinearity is at the highest frequency and highest amplitudes. Figure 13 provides a comparison of the computed vertical component of the total, hydrostatic, and radiation force obtained from the codes when they simulate prescribed heave motion of frequency 1.1 rad/sec and amplitude 80 percent of the draft for Models 5613 and 5514 advancing at constant mean forward speed into otherwise undisturbed water. Since SAIC provided only the total force from NFA, the hydrostatic and radiation components of the force from NFA are missing from the plots. The spike between 2.6 and 2.8 sec occurs in the cycle near the time that the center of gravity is forced down through the mean free-surface level. The spike is due to a spike in the vertical radiation force. Here is a case where nonlinearity makes a difference and that nonlinearity lies in both the computed radiation force and the computed hydrostatic force. Figure 14 shows the corresponding pitch moment. There is a spike in the computed radiation moment in

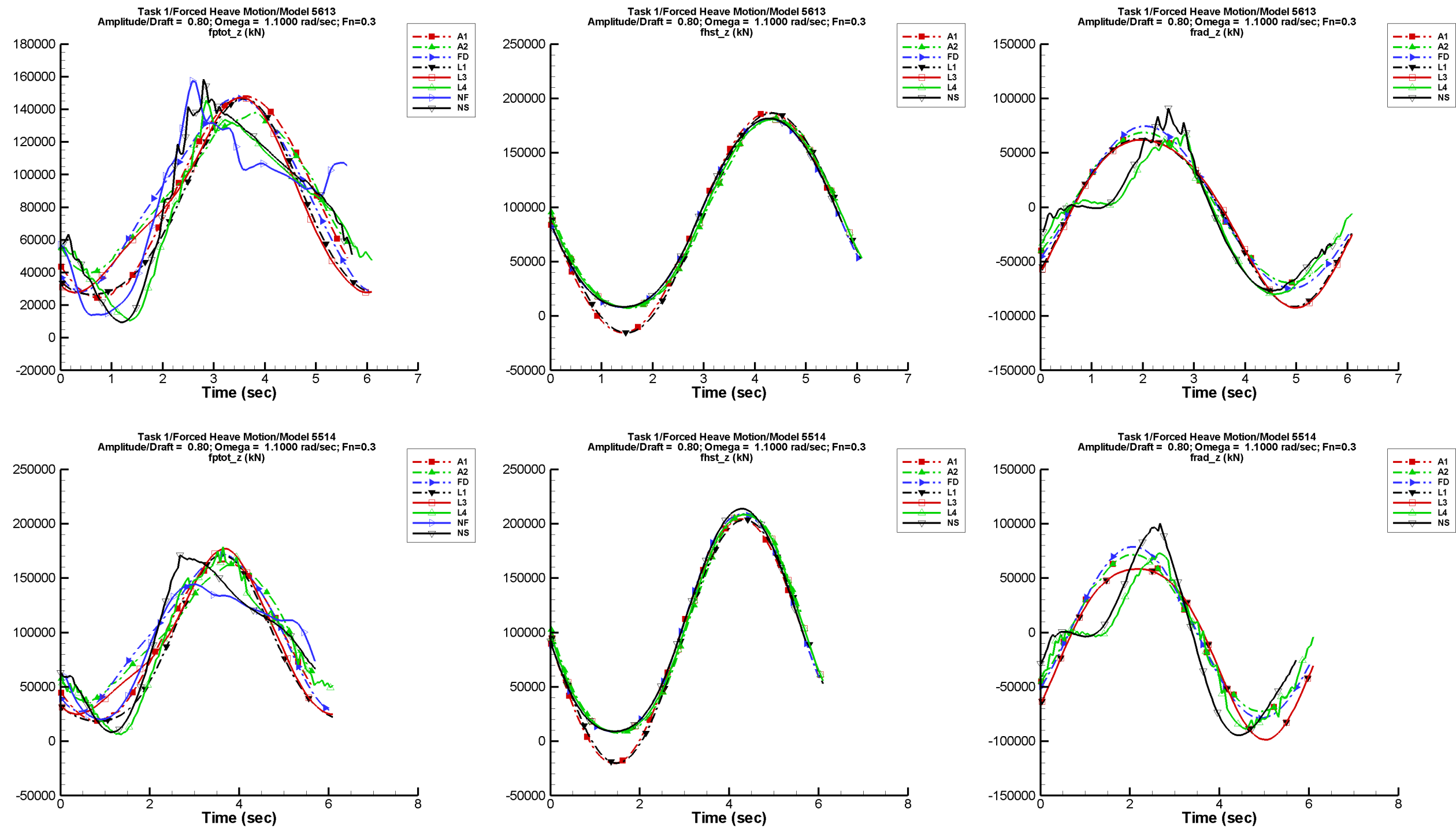


Fig. 13. Vertical component of the total (left), hydrostatic (center), and radiation (right) force experienced by Models 5613 (top) and 5514 (bottom) at forward speed ($F_n = 0.3$) in prescribed heave motion of frequency 1.1 rad/sec and amplitude 80% of the draft.

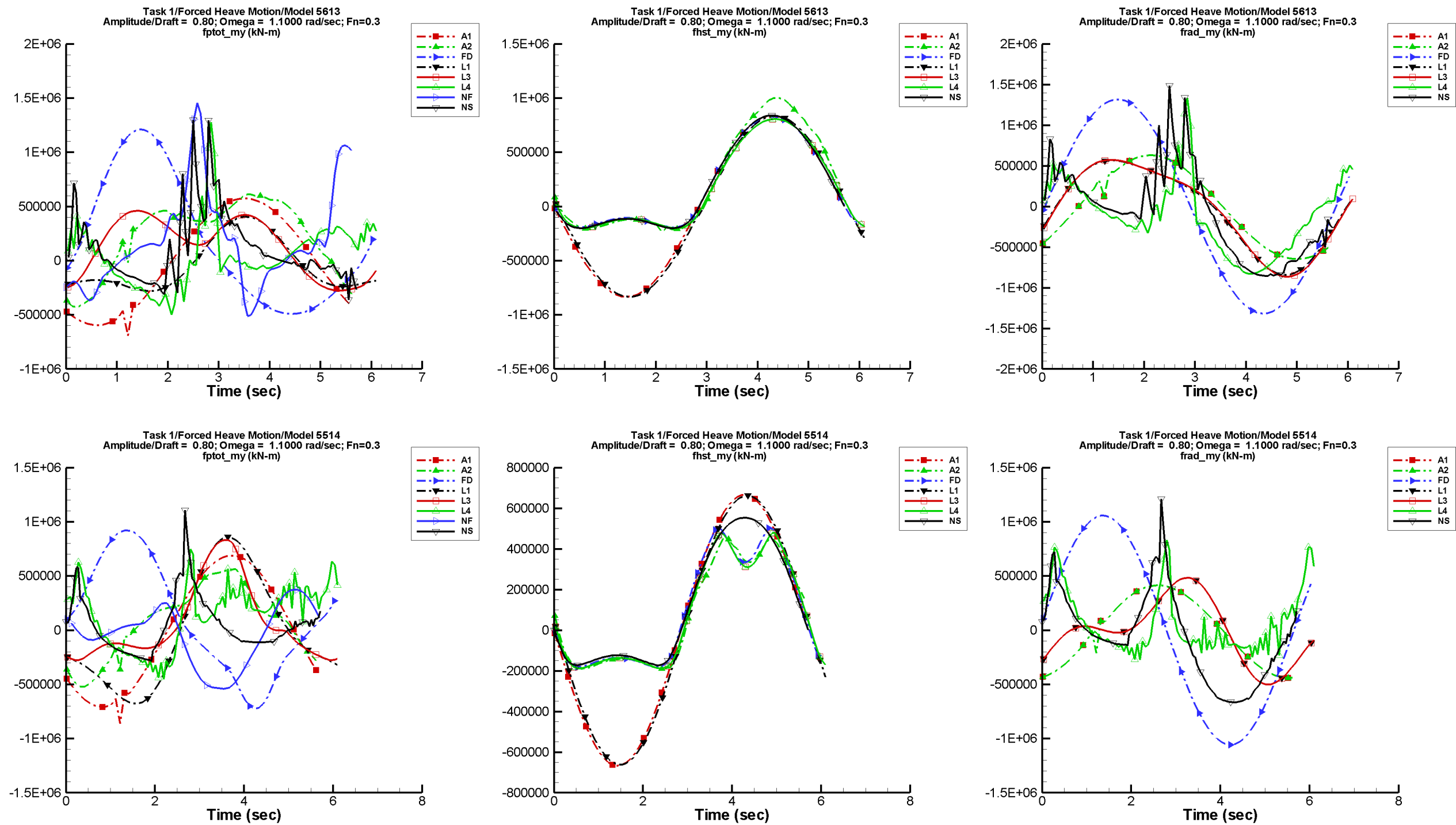


Fig. 14. Total (left), hydrostatic (center), and radiation (right) pitch moment experienced by Models 5613 (top) and 5514 (bottom) as they advance at forward speed ($F_n = 0.3$) in prescribed heave motion of frequency 1.1 rad/sec and amplitude 80% of the draft.

the middle of the cycle from the two nonlinear codes for which the radiation moment was separated out. The spike is evident in the plots of the total pitch moment computed by the three nonlinear codes LAMP-4, NFA, and NSHIPMO except that the spike is absent from the total vertical force and pitch moment computed by NFA for Model 5415 (or only faintly visible). Figure 15 shows how the minimum and maximum of the vertical force and pitch moment depend on the amplitude of the heave motion. Flat horizontal lines would indicate complete linearity. As the amplitude of the heave motion approaches zero, the curves ought to have zero slope if linear theory has increasing validity with decreasing amplitude. The amplitude of the motion might never be small enough to see zero slope. The curves for LAMP-4 do not behave in the expected manner due to relatively large noise in the computed results for small amplitudes of motion. The extrema of the moment are less linear, but the nonlinearity appears erratic and may be contaminated by “noise” at the low amplitudes. This is consistent with Figs. 13 and 14, which show more noise in the pitch moment than in the vertical force.

Generally, the codes fall into two classes according to how they compute the hydrostatic force and moment. One class contains those codes that compute hydrostatics from waterplane quantities and the other class contains those codes that compute hydrostatics from pressure integrals. Results from the two classes are visible in the plots of Figs. 13 and 14. The components of the hydrostatic force and moment that have been plotted depict the effect of geometric nonlinearity on hydrostatics.

Figure 16 contains plots of the computed total, hydrostatic, and radiation pitch moment experienced by Models 5613 and 5514 undergoing prescribed sinusoidal pitch motion of frequency 1.1 rad/sec and amplitude 5° at forward speed. Comments analogous to the observations made for the results from prescribed heave motion depicted in Figs. 13 and 14 apply here. Spikes are present in the total pitch moment computed by LAMP-4 and NSHIPMO. However, they are absent from the moment computed by NFA for both hulls in these simulations. The minimum and maximum of the total pitch moment as functions of the amplitude of the pitch motion at this frequency for Models 5613 and 5514 are plotted in Fig. 17. The variation with respect to the amplitude of the motion is fairly smooth.

Figure 18 contains plots of the ship-fixed vertical component of the total, hydrostatic, and radiation force computed by various codes for Models 5613 and 5514 at zero mean forward speed in prescribed roll motion of frequency 0.3831 rad/sec and amplitude 45° . While the earth-fixed vertical component of the radiation force vanishes for truly linear codes, the ship-fixed vertical component plotted here does not vanish even for those codes due to the transformation of the components of the force vector. Nonlinearity appears to make a big difference in the radiation force, but it does not affect the total force significantly. Noise is clearly visible in the total force computed by NSHIPMO and is much greater for Model 5613 than it is for Model 5514. A plausible explanation is that the tumblehome geometry of Model 5613 presents more of a computational challenge for NSHIPMO than does the flared geometry of Model 5514. The computed hydrostatic force falls into one group if it is computed from waterplane quantities or a second group if it is computed from pressure integrals. The spikes in the hydrostatic and total force from Model 5514 are in the results of AEGIR-2. Figure 19 contains plots of the computed roll moment due to the same prescribed roll motion of Models 5613 and 5514 at zero forward speed. Again, there are nonlinear effects in the radiation roll moment, but they are very small compared to the total roll moment.

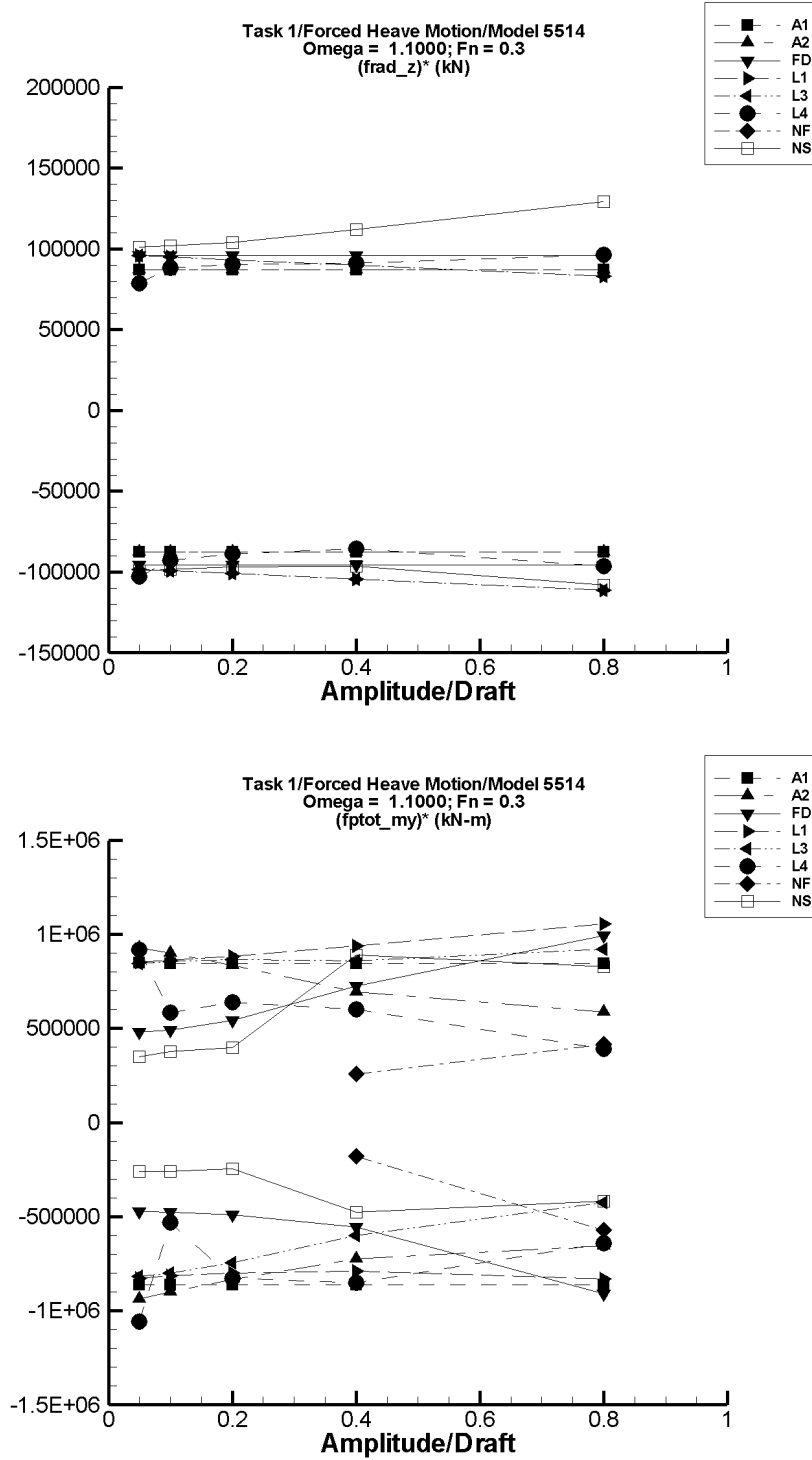


Fig. 15. Minimum and maximum of total vertical radiation force (top) and total pitch moment (bottom) versus amplitude of motion experienced by Model 5514 advancing at constant mean forward speed ($F_n = 0.3$) while undergoing prescribed sinusoidal heave motion of frequency 1.1 rad/sec.

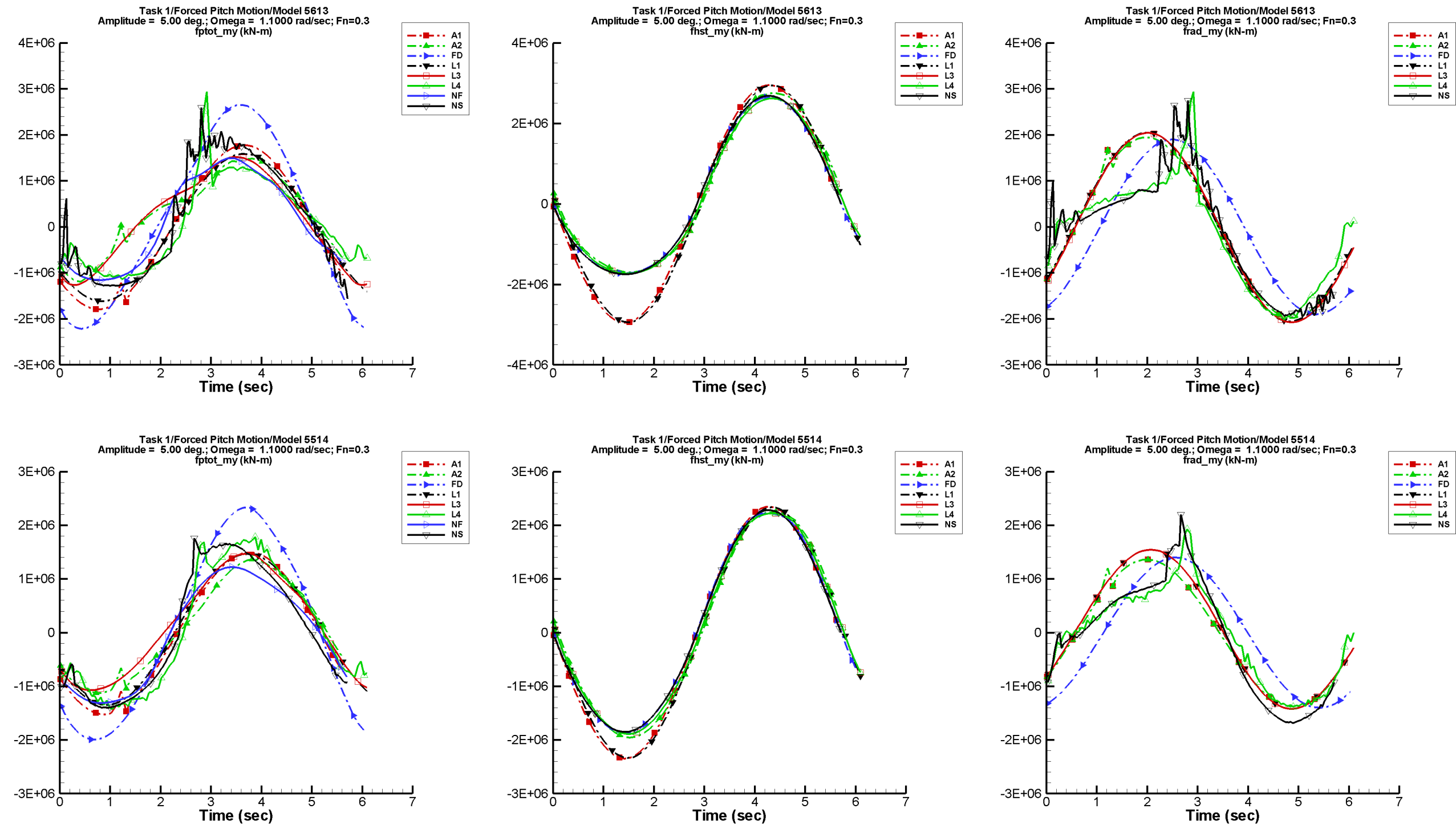


Fig. 16. Total (left), hydrostatic (center), and radiation (right) pitch moment experienced by Models 5613 (top) and 5514 (bottom) at forward speed ($F_n = 0.3$) in prescribed pitch motion of frequency 1.1 rad/sec and amplitude 5° .

THIS PAGE INTENTIONALLY LEFT BLANK.

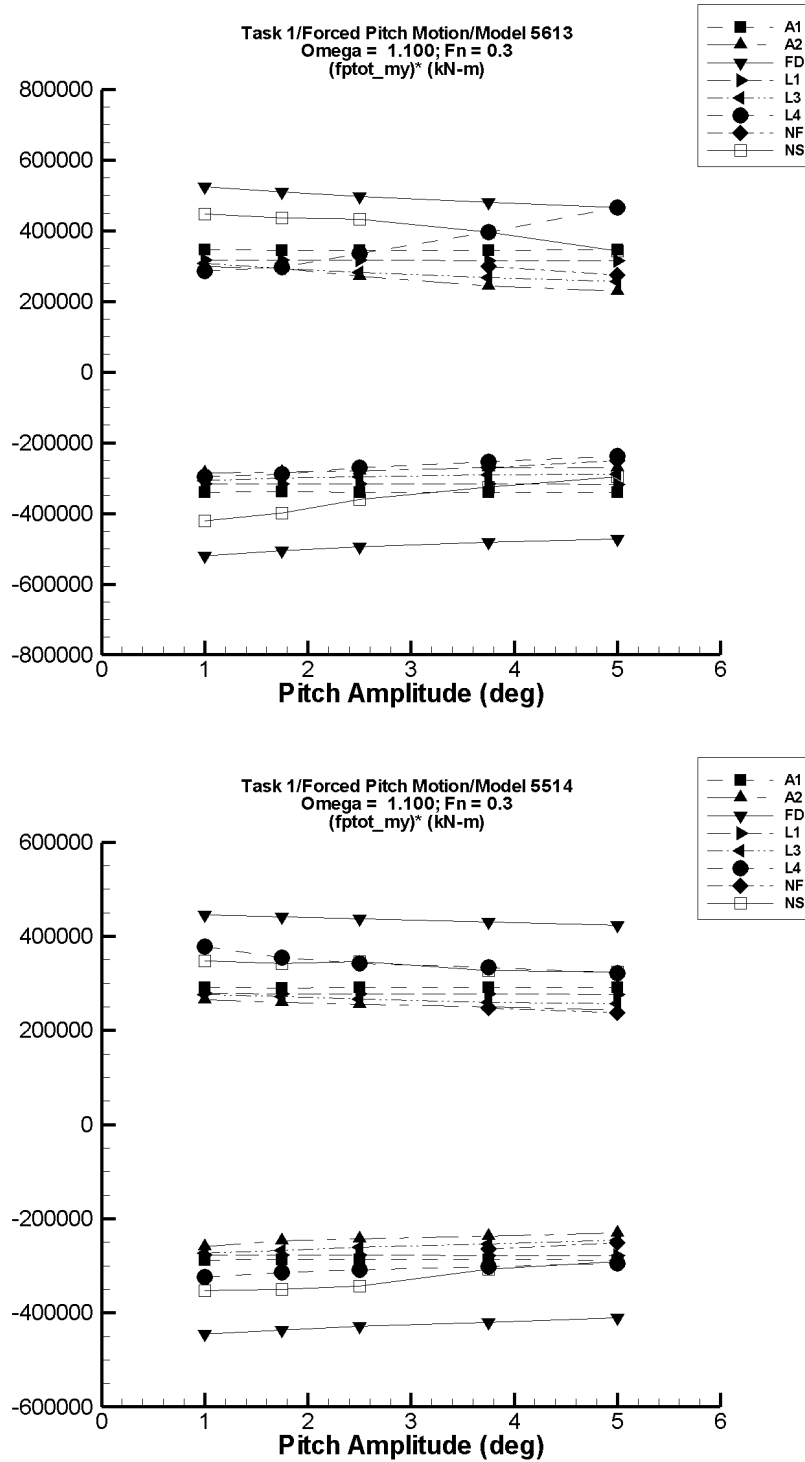


Fig. 17. Minimum and maximum of total pitch moment experienced by Models 5613 (top) and 5514 (bottom) as they advance at constant mean forward speed ($F_n = 0.3$) while undergoing prescribed sinusoidal pitch motion of frequency 1.1 rad/sec.

Figure 20 contains plots of the vertical component of the computed total, hydrostatic, Froude-Krylov, and diffraction forces experienced by Models 5613 and 5514 for 0-DOF motion at zero forward speed in waves of steepness $H/\lambda = 1/15$, wavelength $\lambda = L$, and heading $\beta = 45^\circ$. Since no transformation from earth-fixed to ship-fixed components was necessary for any of the results depicted in the figure, departure from linearity is indicated by departure from simple trigonometric form. Thus every plot in the figure shows evidence of nonlinearity. The spike in the diffraction force component computed by NSHIPMO for Model 5613 occurs in the cycle near the minimum in the wave height at the center of gravity. The spike is visible in the plot of the total vertical force component. Since it is not present in the results from LAMP-4, the spike may be due to difficulties in handling the geometry. For Model 5514, NSHIPMO has missed the peak in the hydrostatic force computed by AEGIR-2, FREDYN, LAMP-3, and LAMP-4. Since the time t has been shifted so that the free-surface wave height at the center of gravity is of the form $a \sin \omega t$ for some a and some ω , the peak occurs when the water level rises from the mean free-surface level. Perhaps the difference is due to how the geometry of Model 5514 above the waterline is handled. The effect is visible in the total computed vertical force for Model 5514.

Results from task 2 are available from NFA only for mean forward speed in head seas. In addition, only the total forces and moments were provided. The plots in Fig. 21 compare the vertical component of the total, hydrostatic, Froude-Krylov, and diffraction forces computed by NFA with that computed by other codes for Models 5514 and 5613 at forward speed in head waves of steepness $H/\lambda = 1/15$ and wavelength $\lambda = L$. The peak in the hydrostatic force is missed by NSHIPMO also in this simulation for Model 5514, but in a part of the cycle different from the corresponding discrepancy noted in Fig. 20. Here it occurs when the wave height at the center of gravity is dropping below the mean free-surface level. The speeds and headings for which data are plotted in the two figures are different, however. The vertical diffraction force computed by the codes is plotted to the right in Fig. 21. Except that the results from NFA are zero because they were not provided, the results from the nonlinear codes are indeed nonlinear but the differences among them do not appear to be easy to interpret. The difference between LAMP-1 and LAMP-3 on the one hand and AEGIR-1 and AEGIR-2 on the other hand is partly due to the steady sinkage force, the Kelvin force, that is included with the hydrodynamic force by the LAMP codes. The difference is not present in the plots of Fig. 20 for the case of zero forward speed. How the vertical force behaves as a function of the wave steepness can be seen in Fig. 22 which contains plots of the total vertical force for both ships.

Figure 23 contains plots of the computed yaw moment for the same simulations as those for which data are plotted in Fig. 20. If the codes have computed the diffraction moment accurately, then there is obvious nonlinearity in the computed diffraction moment which can be detected in the total yaw moment.

Figures 24–26 contain plots of forces and moments experienced by Models 5613 and 5514 while contouring waves in beam seas at zero forward speed. The plots correspond to simulations in condition 2 of task 3 for which a description of the waves is given in Table 11. The wavelength is the length of the hull ($\lambda = L$) and the wave steepness H/λ is $1/10$. The results depicted in these figures are for simple harmonic waves. (NFA can compute forces and moments for nonlinear waves, but there are no results from NFA for task 3.) As was shown earlier in the report, the

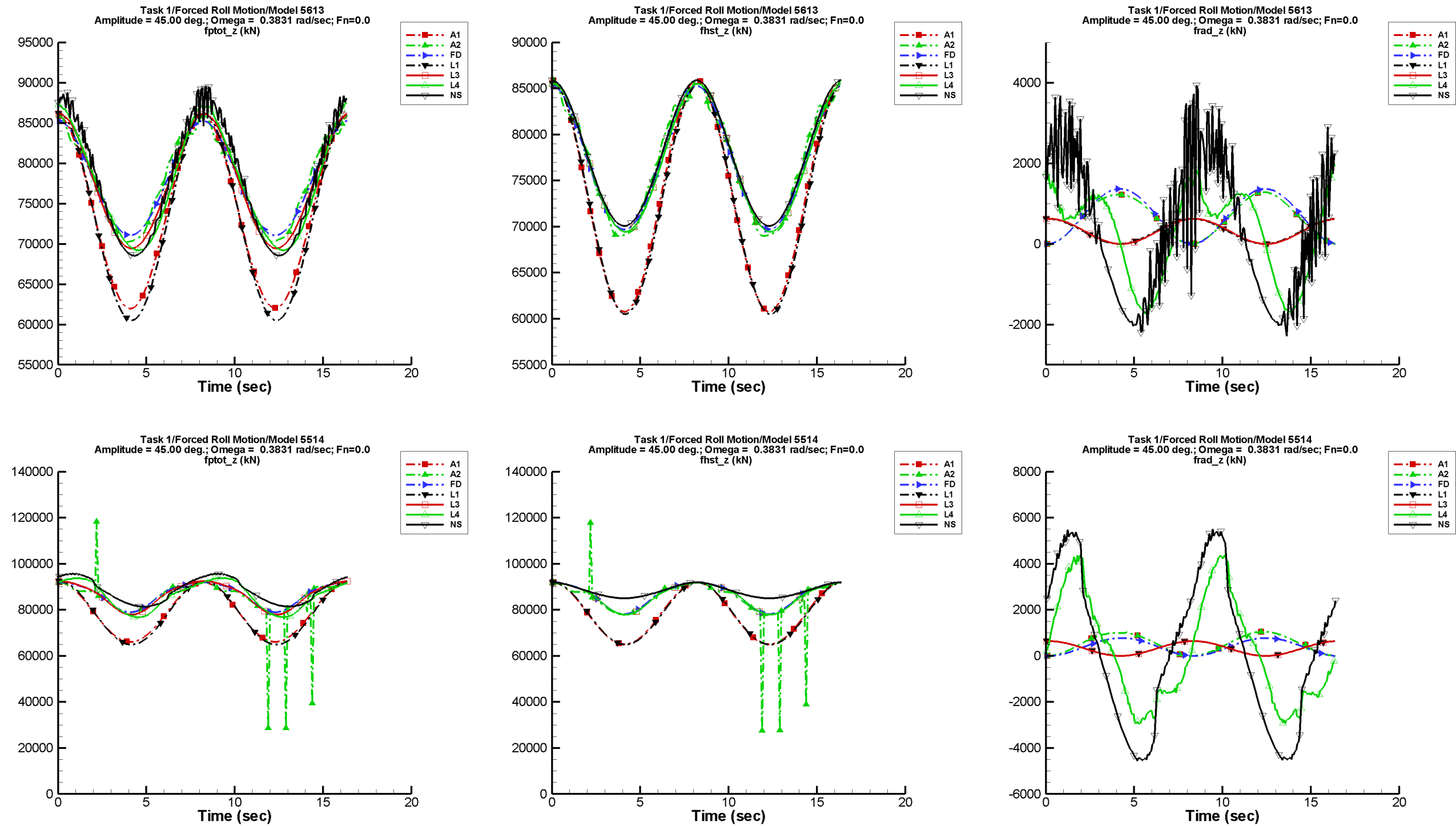


Fig. 18. Ship-fixed vertical component of the total (left), hydrostatic (center), and radiation (right) force experienced by Models 5613 (top) and 5514 (bottom) at zero forward speed in prescribed roll motion of frequency 0.3831 rad/sec and amplitude 45° .

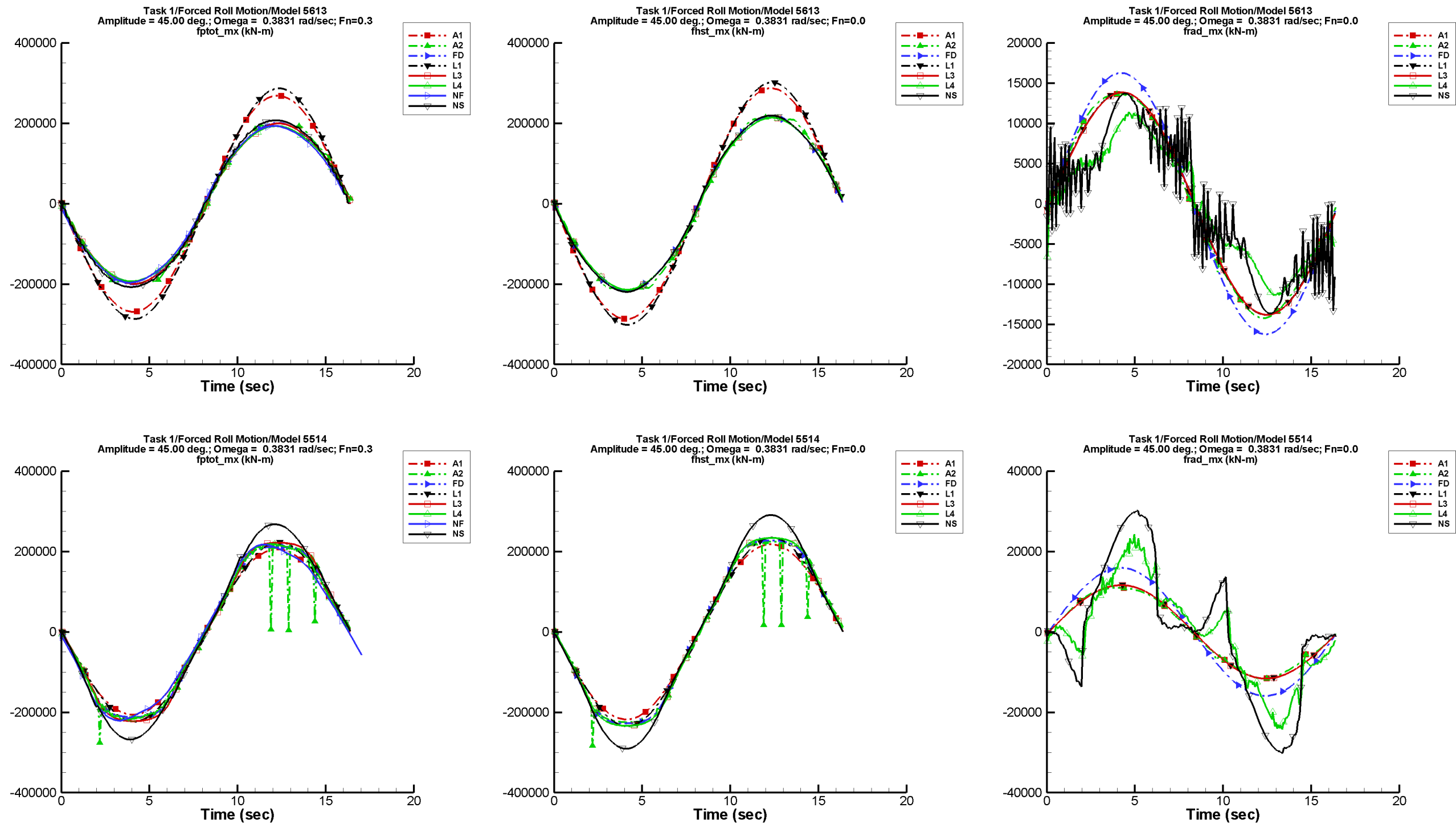


Fig. 19. Total (left), hydrostatic (center), and radiation (right) roll moment experienced by Models 5613 (top) and 5514 (bottom) at zero forward speed in prescribed roll motion of frequency 0.3831 rad/sec and amplitude 45°.

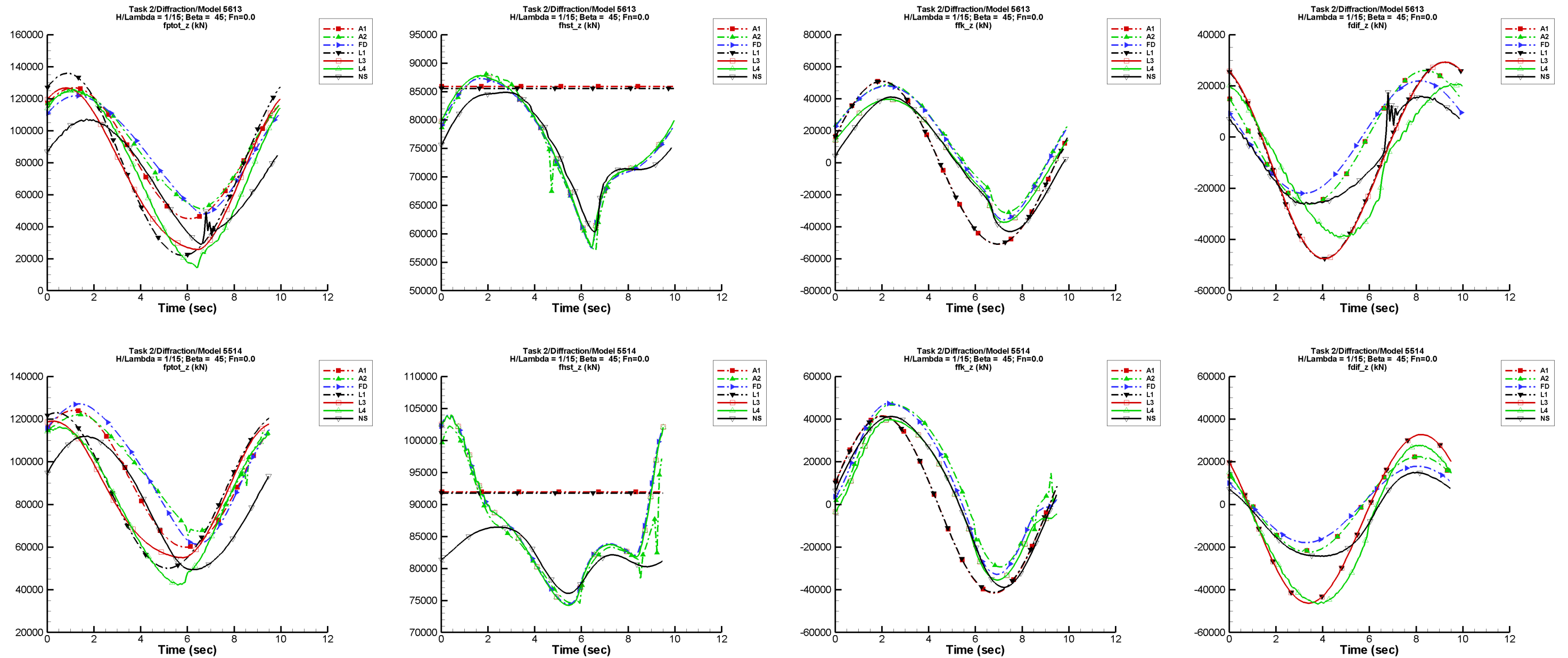


Fig. 20. Vertical component of the total (left), hydrostatic (center left), Froude-Krylov (center right), and diffraction (right) force experienced by Models 5613 (top) and 5514 (bottom) at zero mean forward speed in stern quartering ($\beta = 45^\circ$) waves with $H/\lambda = 1/15$, and $\lambda = L$.

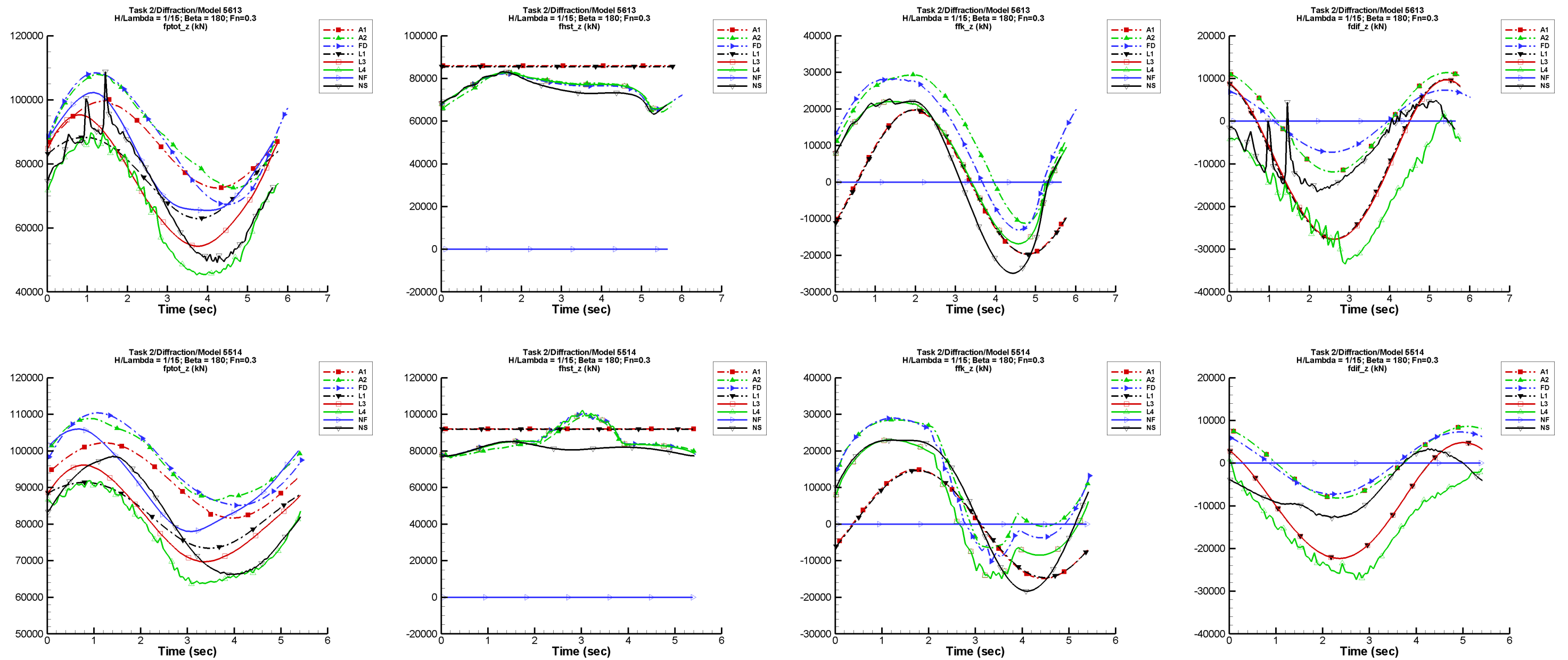


Fig. 21. Vertical component of the total (left), hydrostatic (center left), Froude-Krylov (center right), and diffraction (right) force experienced by Models 5613 (top) and 5514 (bottom) as they advance at constant mean forward speed ($F_n = 0.3$) in head waves with $H/\lambda = 1/15$ and $\lambda = L$.

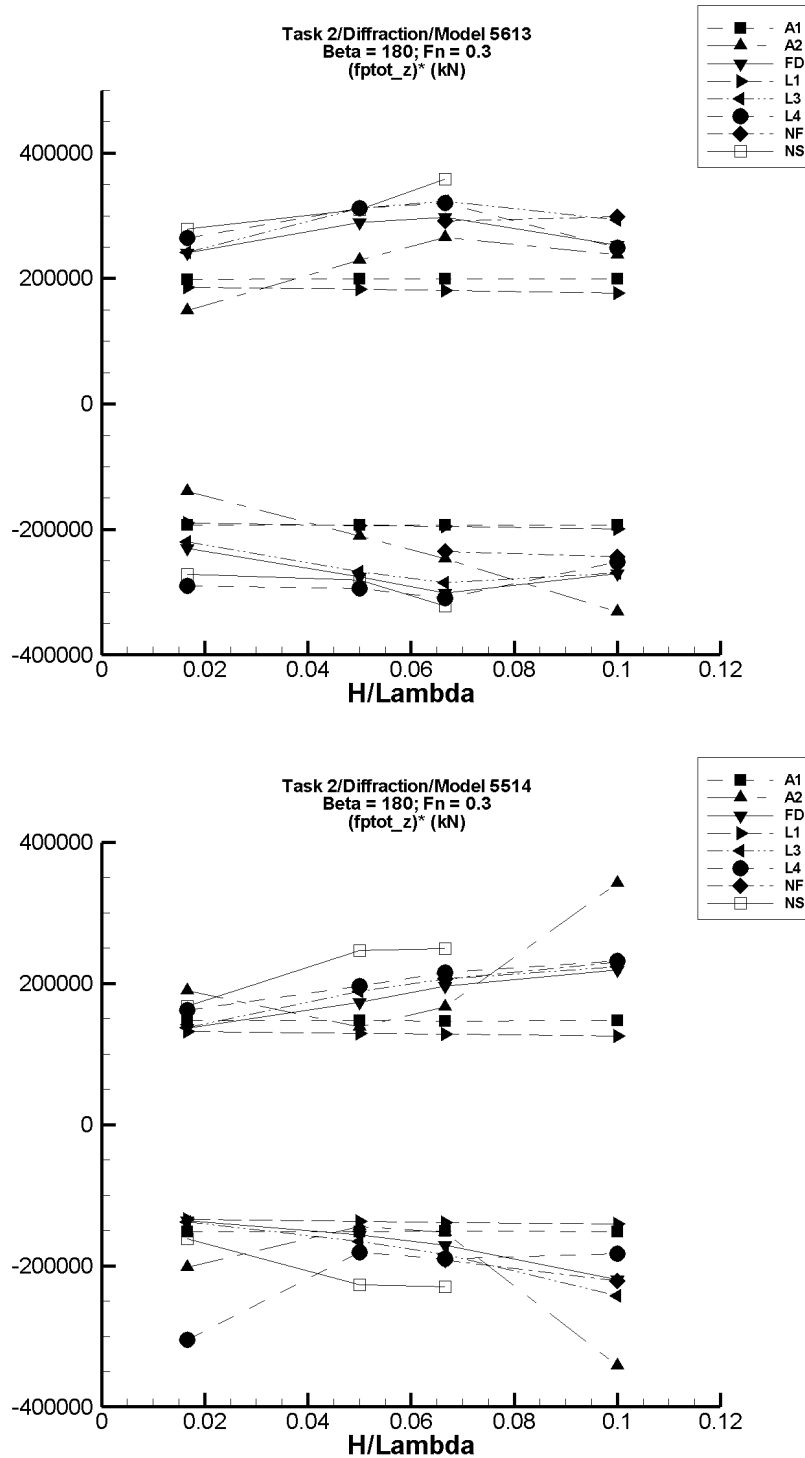


Fig. 22. Minimum and maximum vertical force experienced by Models 5613 and 5514 as they advance at 0-DOF steady mean forward speed in head waves of varying frequency.

motion resulting from the wave contouring is nearly sinusoidal. For either ship, the amplitude of the roll motion is approximately 17° . The amplitude of the heave motion is about 7.7 m for Model 5613 and 7.2 m for Model 5514. The time on the horizontal axis has been shifted so that the earth-fixed vertical position of the hull obeys an equation of the form $a \sin(\omega t)$ for some amplitude a and some frequency ω ; i.e. at the *shifted* time $t = 0$, the center of gravity is rising through the mean free-surface level. The ship-fixed lateral forces are small compared to the ship-fixed vertical forces. The differences are partly due to transformation of vector components from an earth-fixed to a ship-fixed coordinate system. The differences in the plots of the components of total computed ship-fixed vertical force and roll moment are mostly due to differences in the computed hydrodynamic force and moment. The codes may have used “pressure stretching” in an inconsistent manner. In addition, the contribution from $|\nabla\Phi_T|^2/2$ appears to be very large in task 3 and may overwhelm the computed force and moment. In any case, the plots at the right in Fig. 25 show that the three LAMP codes compute ship-fixed vertical components of the hydrodynamic force that are close to one another but different from that computed by the linear code AEGIR-1. One difference between AEGIR-1 and LAMP-1 is that LAMP-1 includes the $|\nabla\Phi_T|^2$ term whereas AEGIR-1 does not. In the plots of Fig. 24–26 cancellation among the components of the force and moment has contributed to the oscillation in the total force and moment. If the components are computed separately, this implies that each component must be computed more accurately to minimize the loss of significance in the total force or moment.

Lack of Agreement Among the Codes

In general, the extent of the divergence of the results from the various codes from one another is unexpected. Some of the discrepancies arise because codes compute quantities of the same name that have different definitions. Some code runners could not compute forces and moments requested of them or could not separate some forces and moments from the total force and moment. Even when the results for which such issues make a difference are discounted, an unexpected disagreement is still present.

Hydrostatic Force and Moment

In this report, the hydrostatic force is defined as the integral of the hydrostatic pressure over a surface and therefore excludes any contribution from the weight vector. Some components of the hydrostatic force and moment vectors are orders of magnitude larger than the corresponding components of other forces and moments such as those arising from wave radiation. Consequently, inaccuracies in computing components of a force like the radiation force may seem unimportant for the total picture. However, a small force or moment can make the difference in whether a ship capsizes especially if there is cancellation among the components as appears to be the case in task 3.

If a code computes the hydrostatic force and moment from hull integrals, it should be able to calculate them without any difficulty no matter whether the integral of the hydrostatic pressure is over S_0 or S_B . Nevertheless, the computed hydrostatic force varies substantially among the codes as can be seen in the plots of Fig. 27 which depicts computed results for simulations of task 2 (0-DOF diffraction) with wave steepness $H/\lambda = 1/15$ and heading $\beta = 135^\circ$. For Model

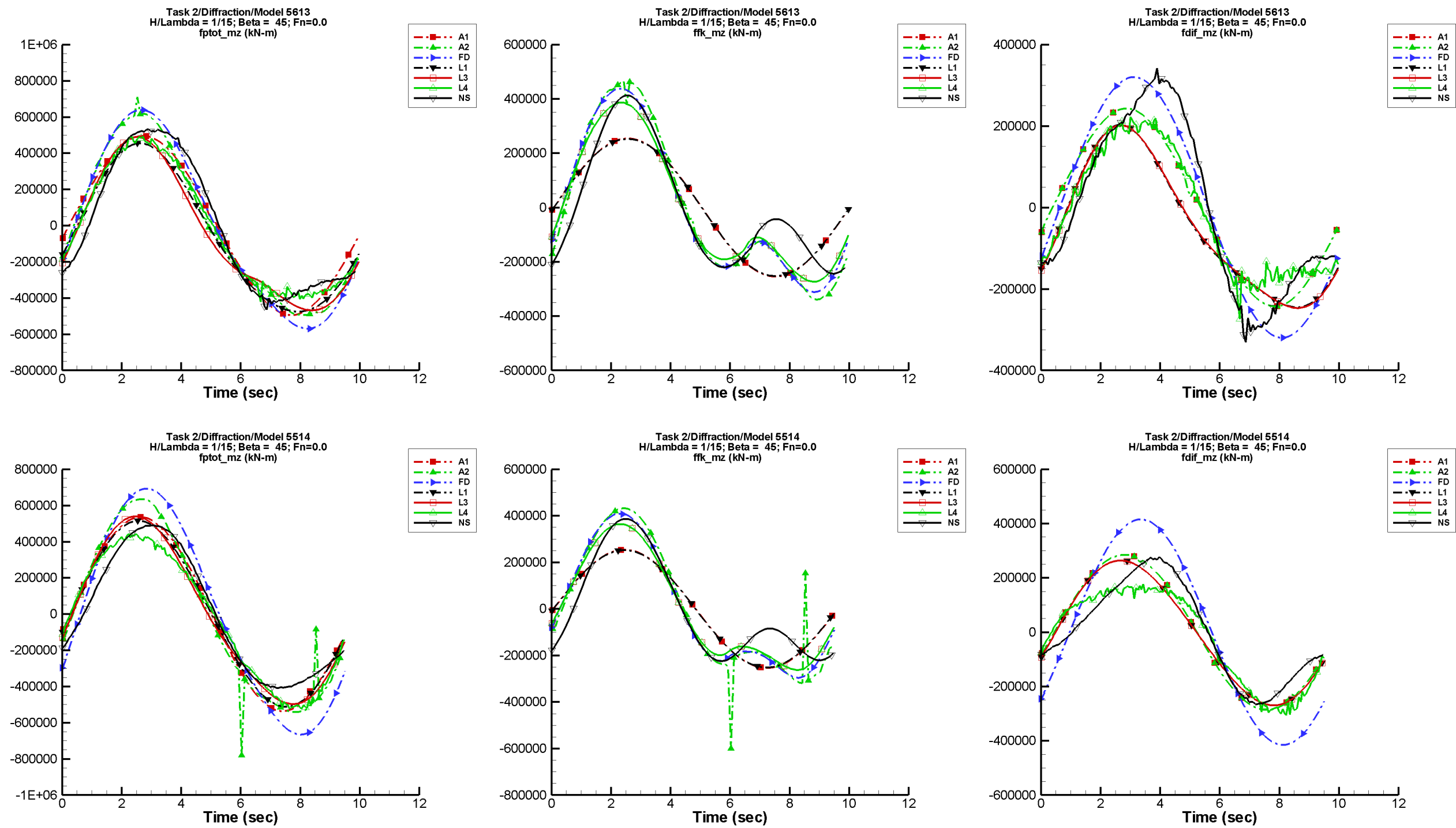


Fig. 23. Total (left), Froude-Krylov (center), and diffraction (right) yaw moment experienced by Models 5613 (top) and 5514 (bottom) in 0-DOF motion at zero mean forward speed in stern quartering ($\beta = 45^\circ$) waves with $H/\lambda = 1/15$ and $\lambda = L$.

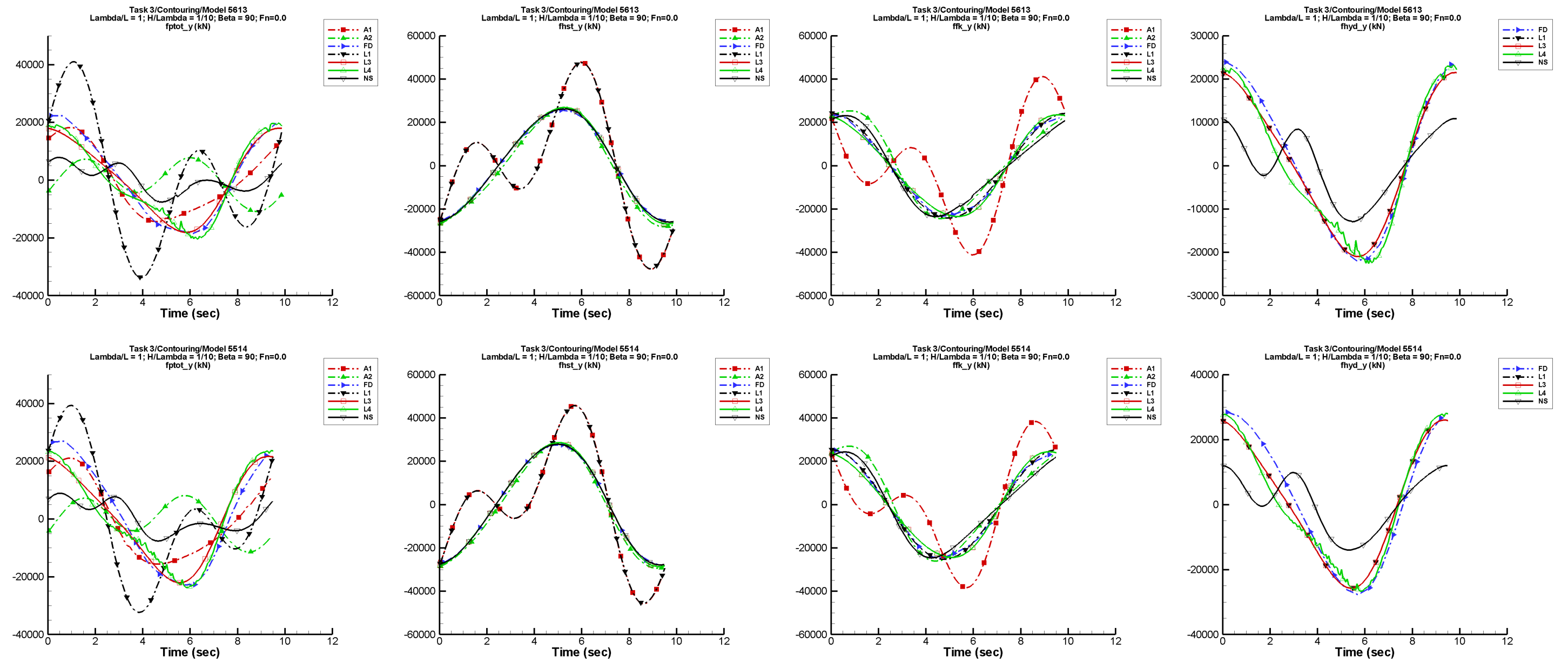


Fig. 24. Ship-fixed lateral component of the total (left), hydrostatic (center left), Froude-Krylov (center right), and hydrodynamic (right) force experienced by Models 5613 (top) and 5514 (bottom) while contouring waves in beam seas at zero forward speed.

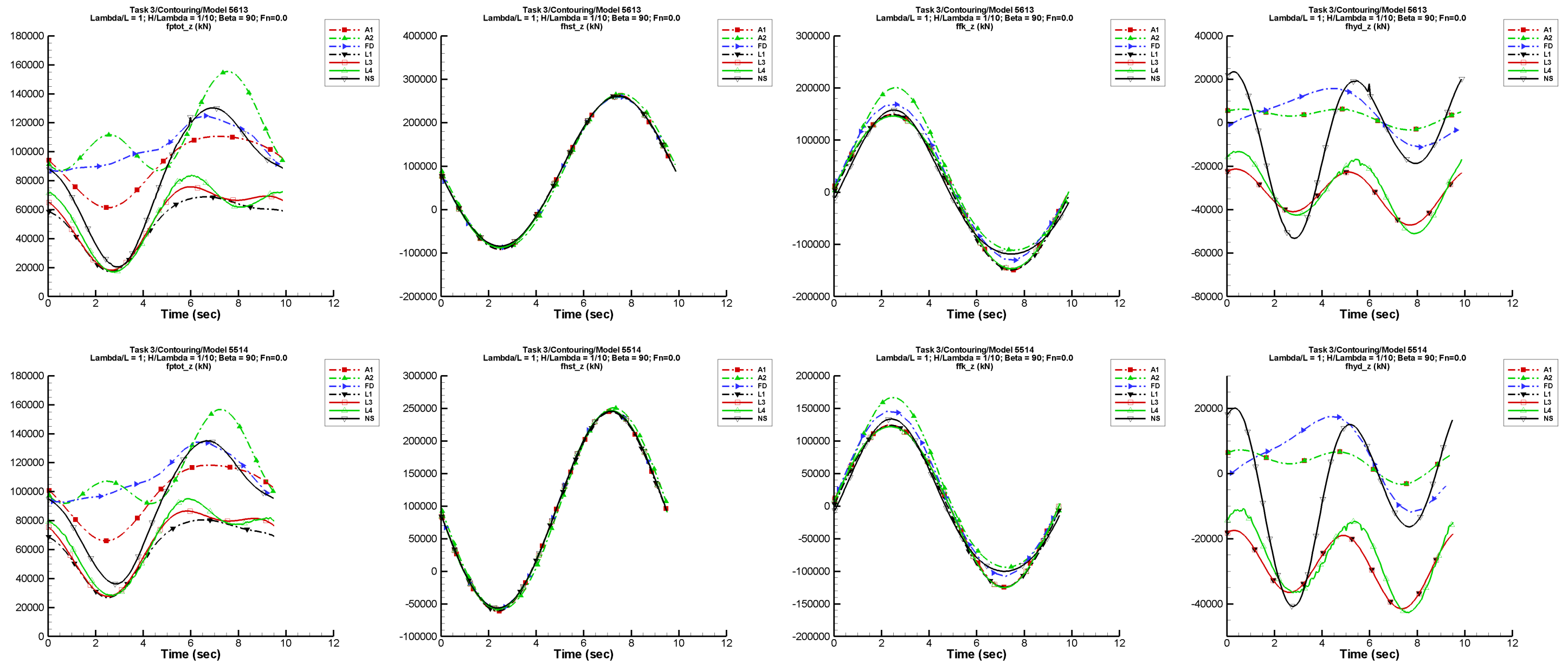


Fig. 25. Ship-fixed vertical component of the total (left), hydrostatic (center left), Froude-Krylov (center right), and hydrodynamic (right) force experienced by Models 5613 (top) and 5514 (bottom) while contouring waves in beam seas at zero forward speed.

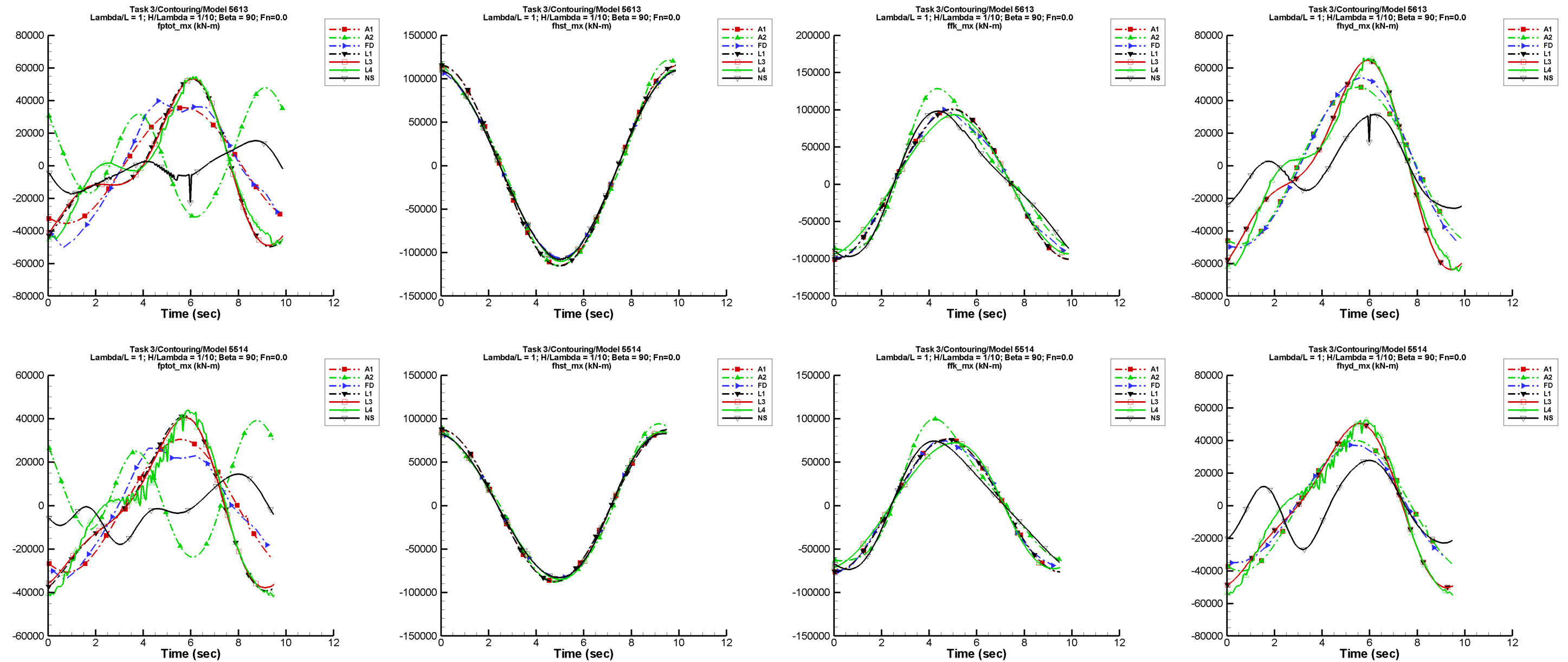


Fig. 26. Total (left), hydrostatic (center left), Froude-Krylov (center right), and hydrodynamic (right) roll moment experienced by Models 5613 (top) and 5514 (bottom) while contouring waves in beam seas at zero forward speed.

5514, NSHIPMO lacks the peak present in the results from other codes in that part of the cycle where the wave height at the center of gravity decreases from its maximum to its minimum. The peak is present in the results from NSHIPMO for Model 5613. A similar discrepancy between NSHIPMO and the other codes is seen in the hydrostatic pitch moment for the same simulation. Most likely these discrepancies are related to how hull sections are repeneled each time step. In some cases the hydrostatic forces and moments from AEGIR-1 are orders of magnitude different from those computed by other codes. (See Fig. 28 for an example.) Since the hydrostatic force and moment from AEGIR-1 were obtained from waterplane quantities as part of postprocessing and the hydrostatic force and moment from AEGIR-2 agree with those from other codes, the discrepancy is probably due to an error in postprocessing.

Hydrostatic forces and moments from linear theory will be inaccurate for large amplitude motions, but not to the degree shown in the Fig. 28 where the ship-fixed vertical hydrostatic force is plotted for prescribed pitch motion of Model 5514 of amplitude 1.75° at the frequency 0.2079 rad/sec. The hydrostatic force is

$$\begin{aligned}\vec{F}^{\text{hst}} &= - \iint_{S_B} \rho g z \vec{n} dS = \rho g V(z) \vec{k} = \rho g V(0) \vec{k} + \rho g \left. \frac{\partial V}{\partial z} \right|_{z=0} z \vec{k} + \dots \\ &\approx \rho g V(0) \vec{k} + \rho g z \left[\int_{x_{\text{stern}}}^{x_{\text{bow}}} B(x) x dx \right] \vec{k} = \rho g V(0) \vec{k} - C_{33} z \vec{k}\end{aligned}$$

where $V(z)$ is the volume of the hull beneath the waterline at z and $z = 0$ is at the calm waterline, $B(x)$ is the beam at the longitudinal position x and C_{33} is the usual hydrostatic restoring coefficient in the vertical direction due to vertical motion. In the time history plots of F_z^{hst} , the hydrostatic force from the linear codes AEGIR-1 and LAMP-1 was obtained from waterplane quantities such as is given after the last equals sign of the equation. When z_e approaches the draft of the ship, the displacement volume $V(z)$ is not approximated well by the Taylor series in z truncated after the linear term. It is physically impossible to obtain the negative values for F_z^{hst} shown in plots such as that of Fig. 29 where the vertical hydrostatic force experienced by Model 5613 (scaled to $L = 154$ m) heaving at 0.2079 rad/sec with an amplitude 80% of the mean draft at zero forward speed is plotted. This figure also shows that the hydrostatic force from AEGIR-1 is orders of magnitude off only for some cases, but not the case plotted in Fig. 29.

Submerged Deck

For the prescribed pitch and roll motions at the highest amplitudes in task 1, parts of the deck submerge below the calm water level periodically. For the pitch motion at the highest amplitude, the amplitude of the vertical motion at the bow and stern exceeds the draft of the ship. The nonlinear codes try to resolve the geometric nonlinearities and the computed forces and moments show oscillations which are very likely not physical. (See Fig. 30 where the vertical force experienced by Model 5613 at zero forward speed in pitch motion of frequencies 0.2079 rad/sec, 0.3831 rad/sec, and 1.1 rad/sec is plotted. Also see the sequence of plots in Fig. 31 where the vertical force is plotted for Model 5514 at zero forward speed in pitch motion of frequency 0.2079 rad/sec with amplitudes 1.00° , 1.75° , 2.50° , 3.75° , and 5.00° .) The top plot in Fig. 32 depicts the ship-fixed vertical force on Model 5613 for forced sinusoidal roll of amplitude 45° and frequency 0.2079 rad/sec at zero forward speed. The results from NSHIPMO and LAMP-4 would be more or less near one

another if the result from NSHIPMO had been smoothed. (The figure also shows what may be unresolved issues with respect to the definition of the roll angle since some results are out of phase from others.) The next higher amplitude is in the bottom plot of Fig. 32.

Steep Large Amplitude Waves

At higher wave steepness, some of the codes had difficulty. For either ship, the amplitude of the waves exceeds the draft of the ship at the highest wave steepness. Results from AEGIR-2 were provided for only short periods of time in a few of these cases. Results from LAMP-4 and NSHIPMO are sometimes noisy as can be seen in the plots of Fig. 33 which depict the vertical component of the diffraction force in head seas of wave steepness $1/15$ and $1/10$ for Model 5613 at Froude number 0.0. The plots in Fig. 34 are also of interest. They show the vertical force in following seas for Model 5613 at Froude number 0.3 for wave steepnesses varying from $1/60$ to $1/10$. Unfortunately at the time of writing, there was no result from NSHIPMO at the highest wave steepness, but the results from NSHIPMO are at variance from the results from all other codes at the three lower wave steepnesses.

Nonlinear Strip Theory and 3D Nonlinear Theory

For low frequencies, one might conclude from a few of the figures that codes based on strip theory and 3D nonlinear theory are close to one another but are out of phase from the results of other codes. One might expect that nonlinear theory is required more for the large amplitude motions at high frequencies. Some of the plots corroborate that notion. The results from NSHIPMO and LAMP-4 frequently show common features in the time history plots for large amplitude motions.

Nonlinear Versus Linear Strip Theory

At Froude number 0.3, nonlinearity in strip theory makes little difference for the computed vertical radiation force in prescribed pitch motion at the lowest frequency 0.2079 rad/sec in Figs. 35 and 36. To see this, one should compare the results from FREDYN and NSHIPMO. On the other hand, at zero forward speed, nonlinearity makes a difference as can be seen in Figs. 37 and 38. Before inferring too much from the figures, it should be noted that the magnitude of the force at forward speed is an order of magnitude larger than at zero forward speed.

For the highest pitch amplitude of Model 5613 at zero forward speed, nonlinear and linear strip theory seem to give results that are close when the stern is submerged below its equilibrium position in (the right half of) the bottom right plot in Fig. 37. At the same time results from all three versions of LAMP are fairly close to one another but are not close to the results from the strip theory codes. On the other hand, when the bow is submerged (in the left half of the plot), the result from nonlinear strip theory given by NSHIPMO agrees with the result from LAMP-4, but disagrees with the result from FREDYN which is based on linear strip theory. The corresponding results for Model 5514 are depicted in the bottom right plot in Fig. 38. They are very different. Perhaps the difference is due to the difference in the geometry between a tumblehome and a flared hull. Perhaps cases such as this ought to be rerun to determine the source of the difference. The discrepancies may be due to limited capabilities in handling geometry.

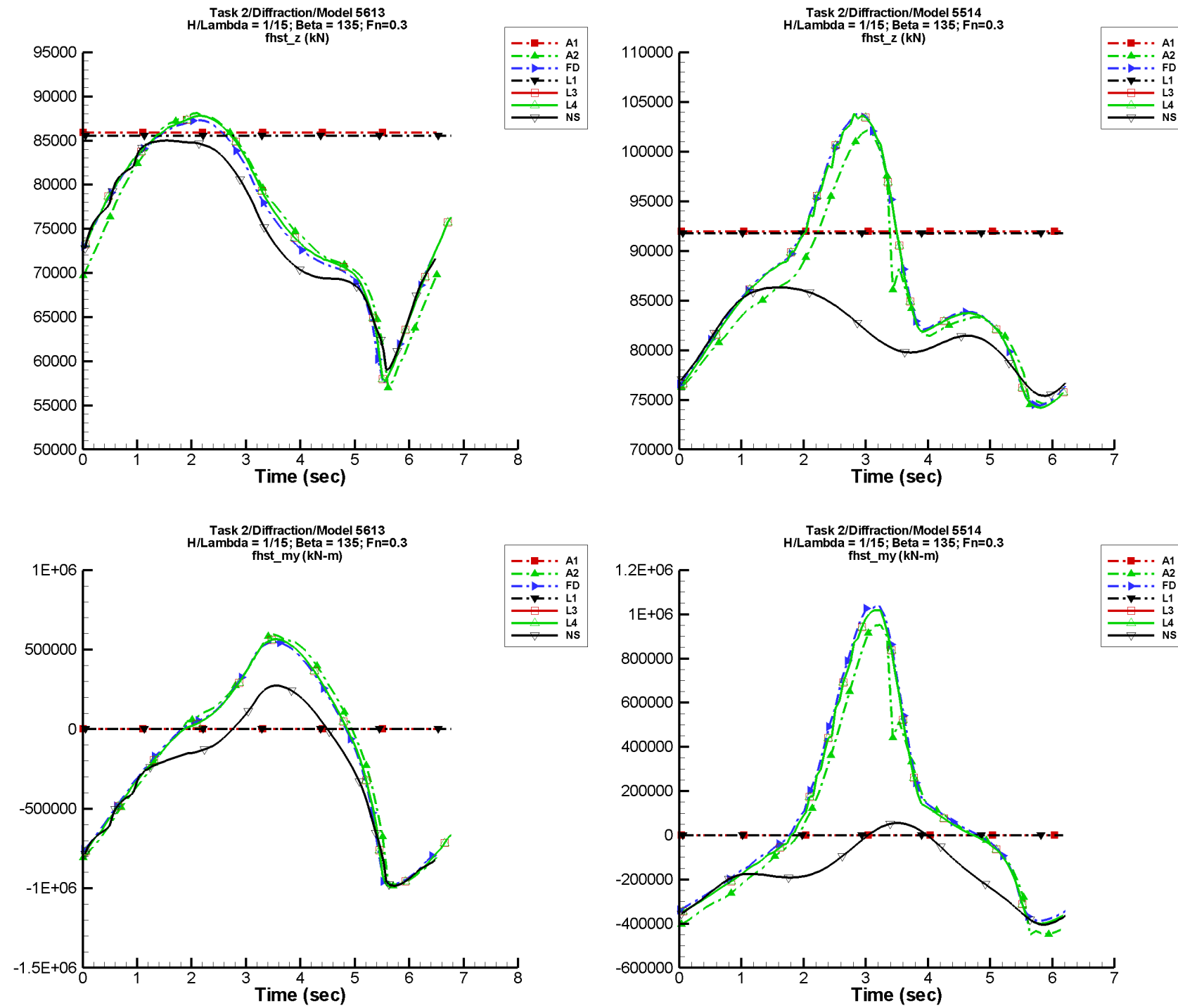


Fig. 27. Vertical hydrostatic force (top) and hydrostatic pitch moment (bottom) acting on Models 5613 (left) and 5514 (right) advancing at forward speed $F_n = 0.3$ in waves of steepness $H/\lambda = 1/15$ at the heading $\beta = 135^\circ$.

THIS PAGE INTENTIONALLY LEFT BLANK.

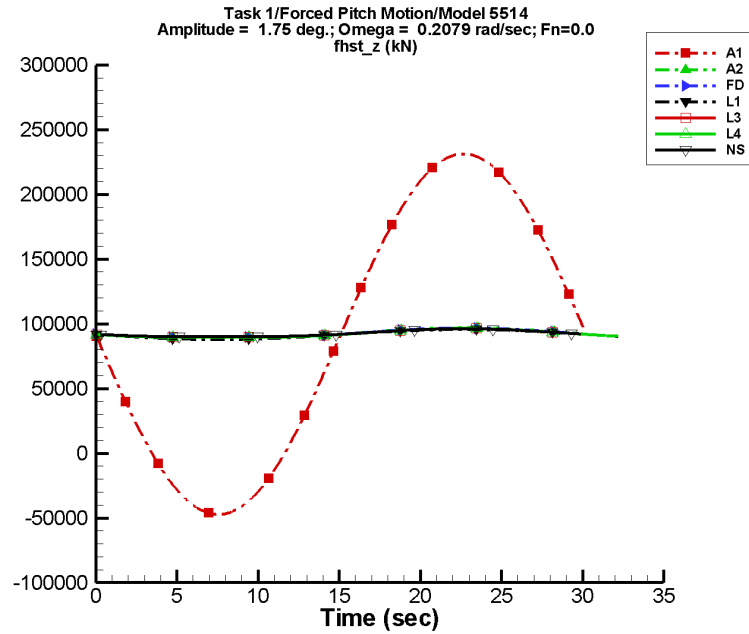


Fig. 28. Ship-fixed vertical hydrostatic force acting on Model 5514 pitching at frequency 0.2079 rad/sec and amplitude 1.75° at zero forward speed.

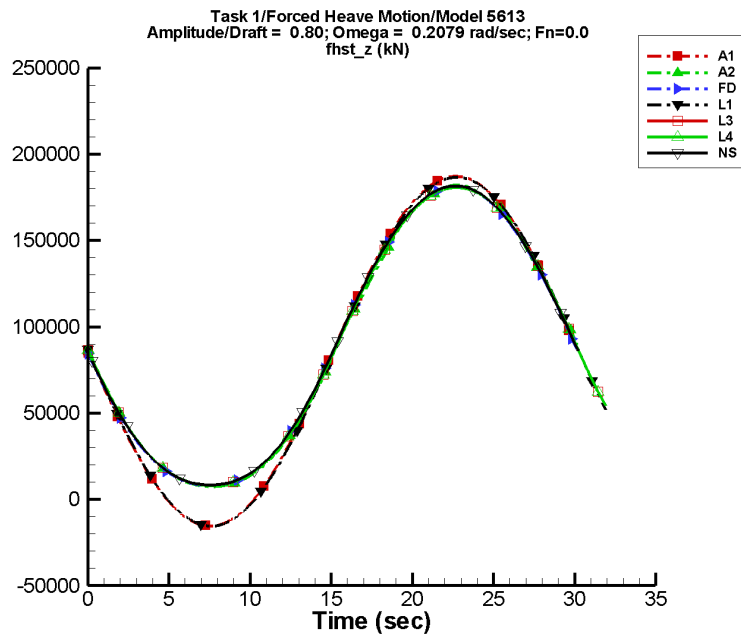


Fig. 29. Ship-fixed vertical hydrostatic force acting on Model 5613 heaving at frequency 0.2079 rad/sec and amplitude 80% of draft at zero forward speed.

Effect of Grid Velocity Term

Figures 35–38 show that the radiation force computed by LAMP–1 and LAMP–3 agree but differ from the radiation force computed by AEGIR–1 and AEGIR–2. The results from AEGIR–1 and AEGIR–2 are from pure linear theory; the results from LAMP–1 and LAMP–3 include the grid velocity term discussed earlier in the report. Unfortunately, LAMP–1 includes a Kelvin component in the hydrodynamic force, which includes both the radiation and diffraction components of the force. Consequently, the difference in computed force due to $|\nabla\Phi_T|^2/2$ is not clear at forward speed. Plots of results for task 2 and task 3 at zero forward speed show that there can be a significant difference due to the quadratic term in the pressure.

Wave Contouring

The result from FREDYN for the vertical hydrodynamic force acting on Model 5613 as it contours a following wave is out of phase with the results from other codes at Froude number 0.3. This is not the case for Model 5514 (Fig. 39). Perhaps there is an error in processing although the result from NSHIPMO is also quite different from the linear results at forward speed. The results from the linear codes AEGIR–1 and AEGIR–2 are grouped together as are the results from the three LAMP codes. The result from FREDYN might be in line with the results from the linear codes if the phase discrepancy at Froude number 0.3 can be cleared up for Model 5613.

Minimum and Maximum in Forced Pitch Motion

20. The nonlinear behavior of the maximum of the ship-fixed vertical radiation force experienced by Model 5613 as it undergoes prescribed sinusoidal pitch motion of frequency 1.1 rad/sec at zero forward speed is clear in the plot of the results from LAMP–4 and NSHIPMO in Fig. 40. This plot corresponds to the time-history plots in Fig. 41 where time histories for the amplitudes 1° , 1.75° , 2.5° , 3.75° , and 5° are depicted. A noisy spike occurs in the time history plots when the ship returns to the equilibrium position after the bow has been down.

FREDYN

Considering the crude approximations it uses, FREDYN does fairly well. Questions about the phase sometimes arise when the time-history plots are examined. This is particularly the case for the radiation force and moment for pitch and heave motions. Most of the total potential force and moment acting on a ship arises from the hydrostatic and Froude-Krylov components. These components are handled well by FREDYN.

CONCLUSION

Thousands of comparative plots of the time histories of many variables for the last full period of motion have been provided for the simulations in the potential flow force study. The figures containing the plots and associated tables of information have been placed in Appendices A–J. These appendices are in the form of bookmarked PDF files to ease navigation through them. Comparative plots of many variables as a function of the nonlinearity of the problem have been provided for the radiation problems in task 1 and the diffraction problems in task 2. The figures and associated

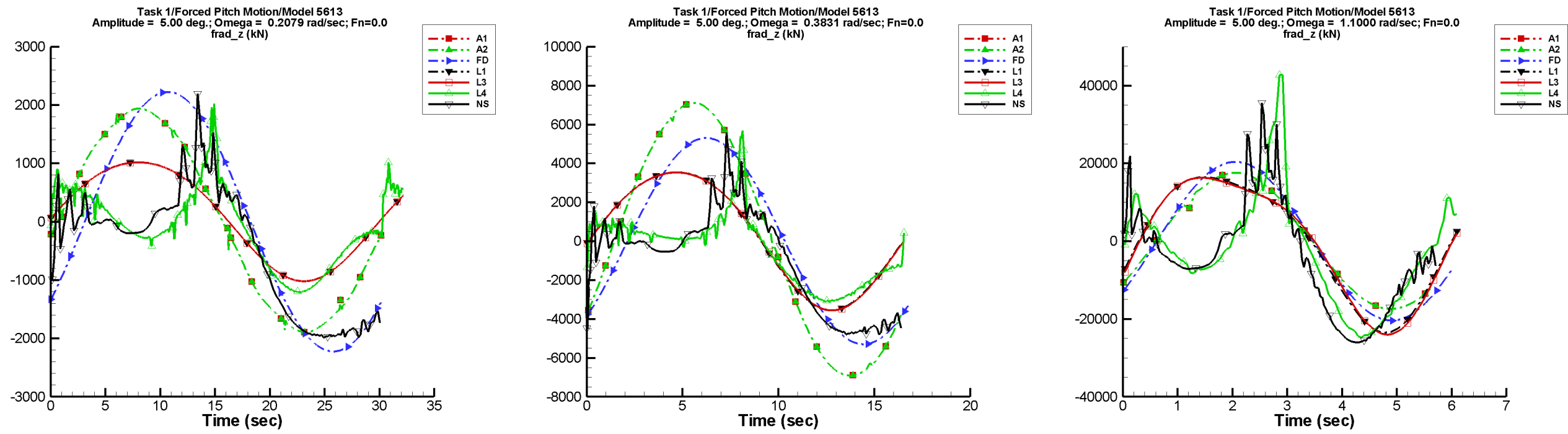


Fig. 30. Ship-fixed vertical component of the radiation force experienced by Model 5613 in prescribed pitch motion of amplitude 5° and frequencies 0.2079, 0.3831, and 1.1 rad/sec at zero forward speed.

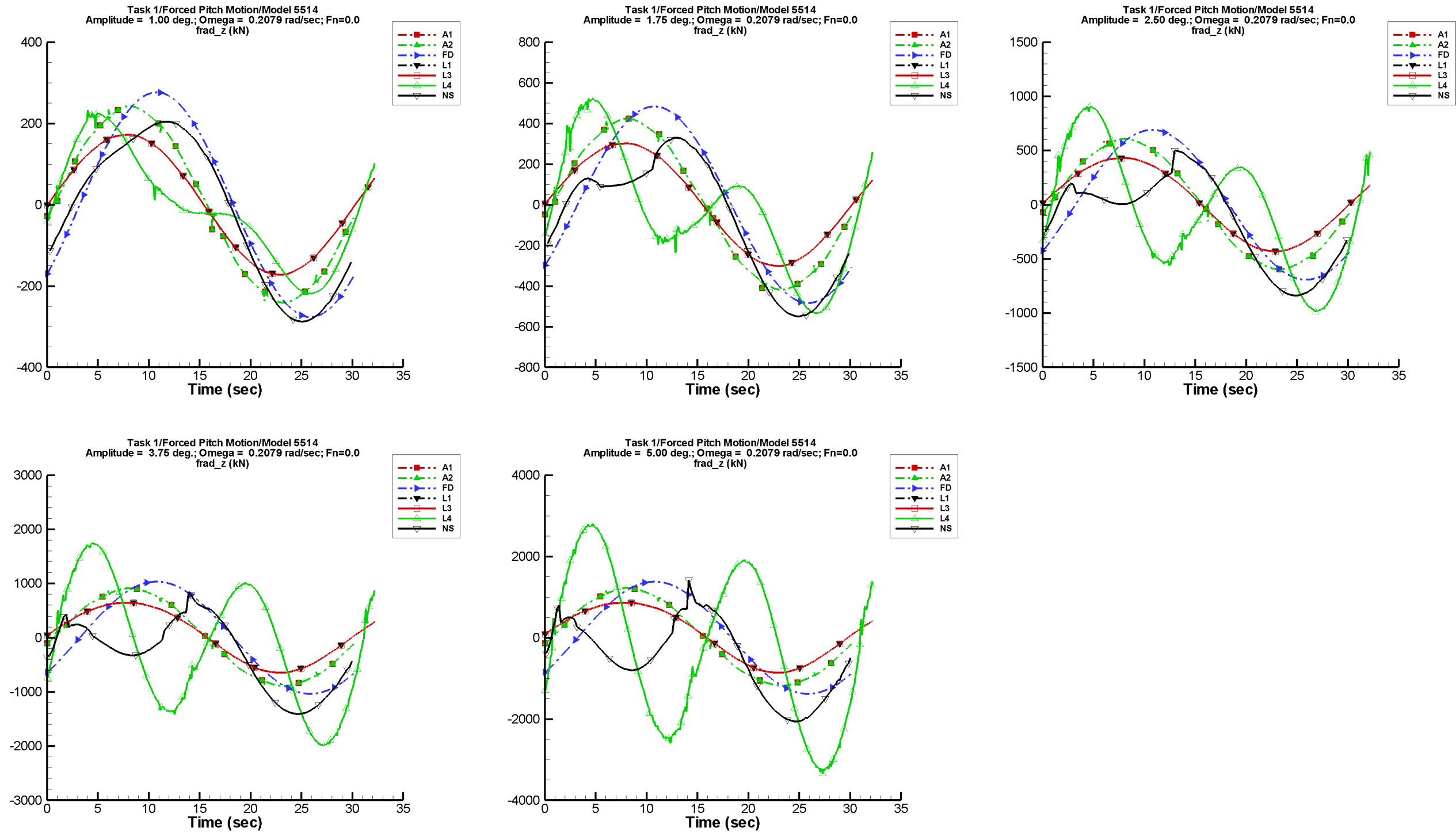


Fig. 31. Ship-fixed vertical component of the radiation force experienced by Model 5514 at zero forward speed in prescribed pitch motion of frequency 0.2079 rad/sec at the pitch amplitudes 1.00°, 1.75°, 2.50°, 3.75°, and 5.00°.

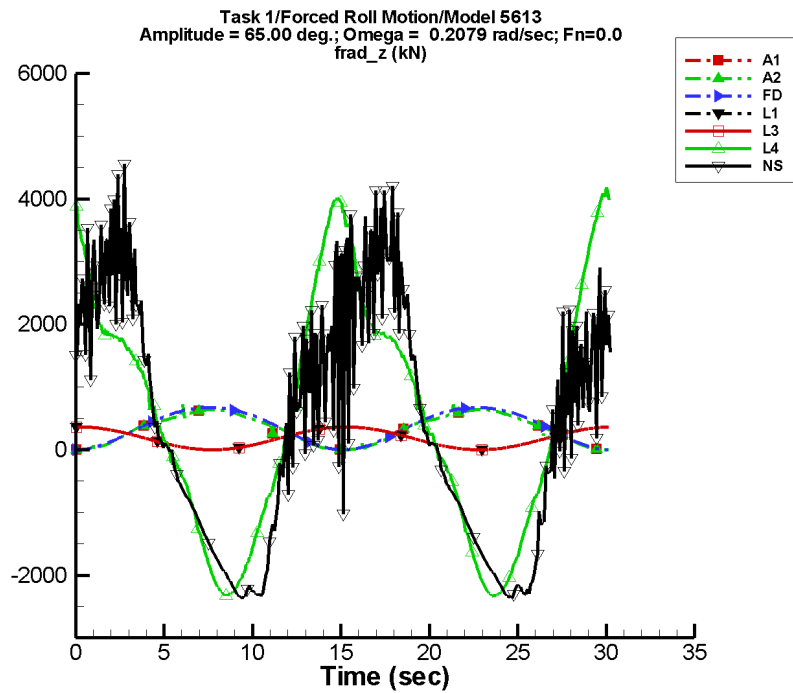
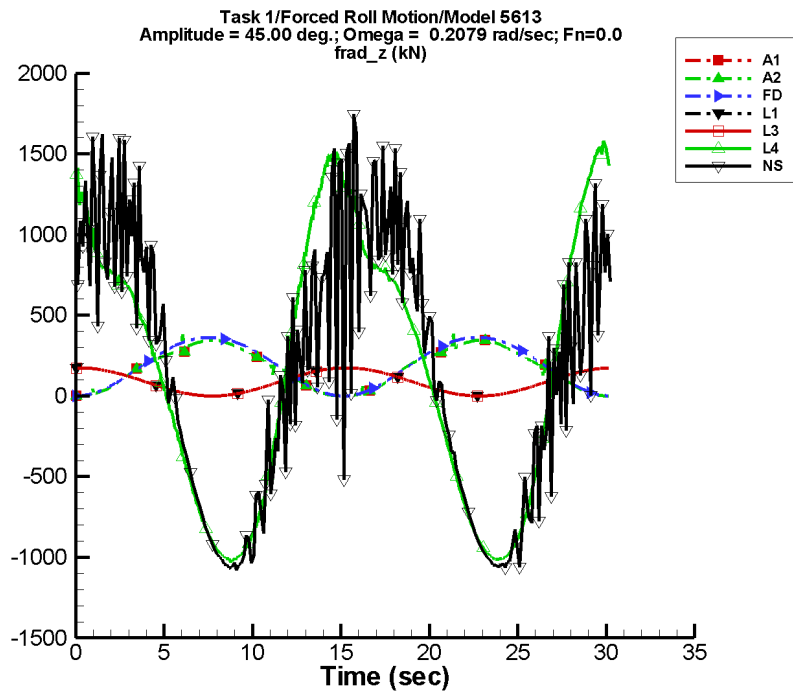


Fig. 32. Ship-fixed vertical component of the radiation force experienced by Model 5514 in prescribed roll motion of amplitude 45° (left) and 65° (right) at zero forward speed.

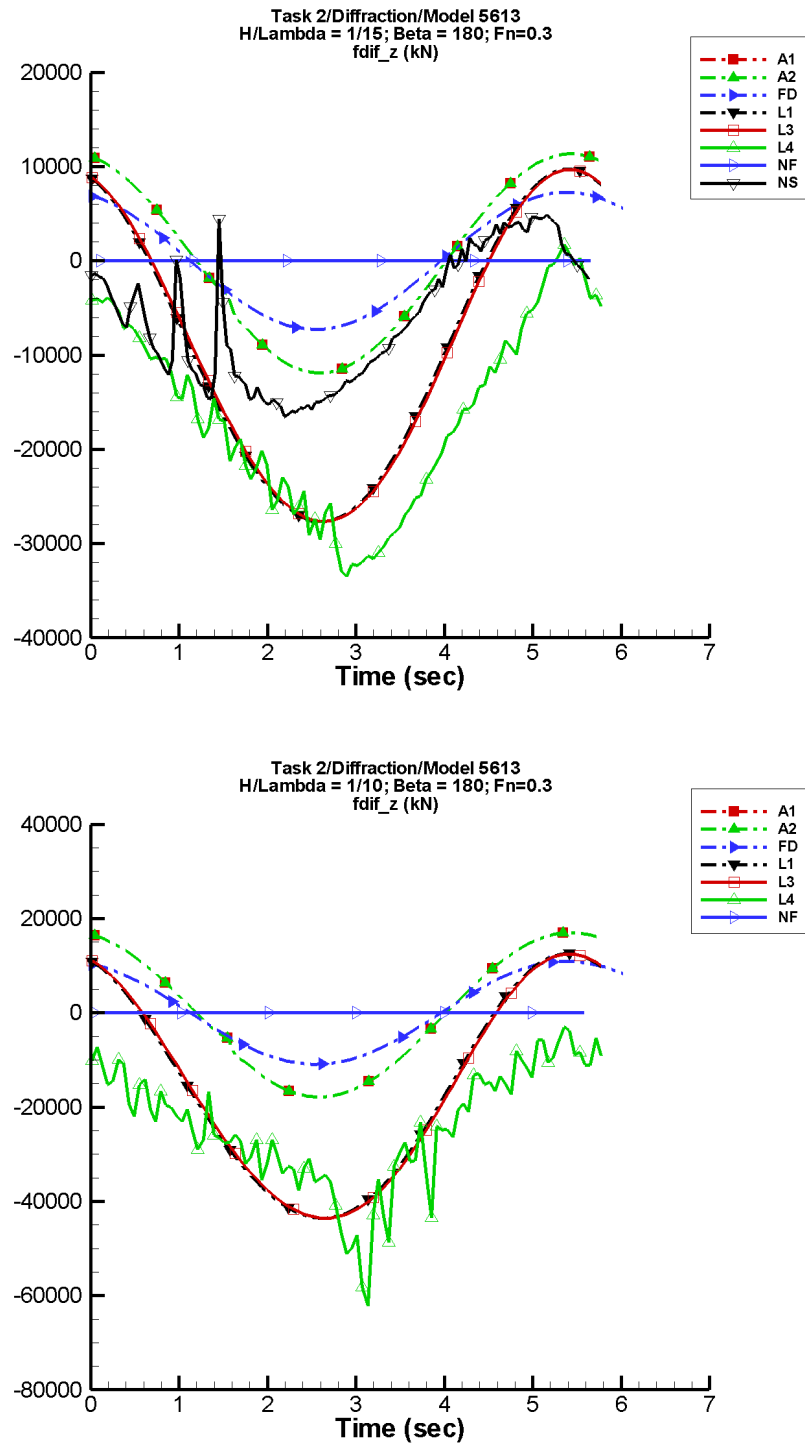


Fig. 33. Vertical diffraction force experienced by Model 5613 advancing in 0-DOF motion ($F_n = 0.3$) in head seas of wave steepness $H/\lambda = 1/15$ (top) and $H/\lambda = 1/10$ (bottom).

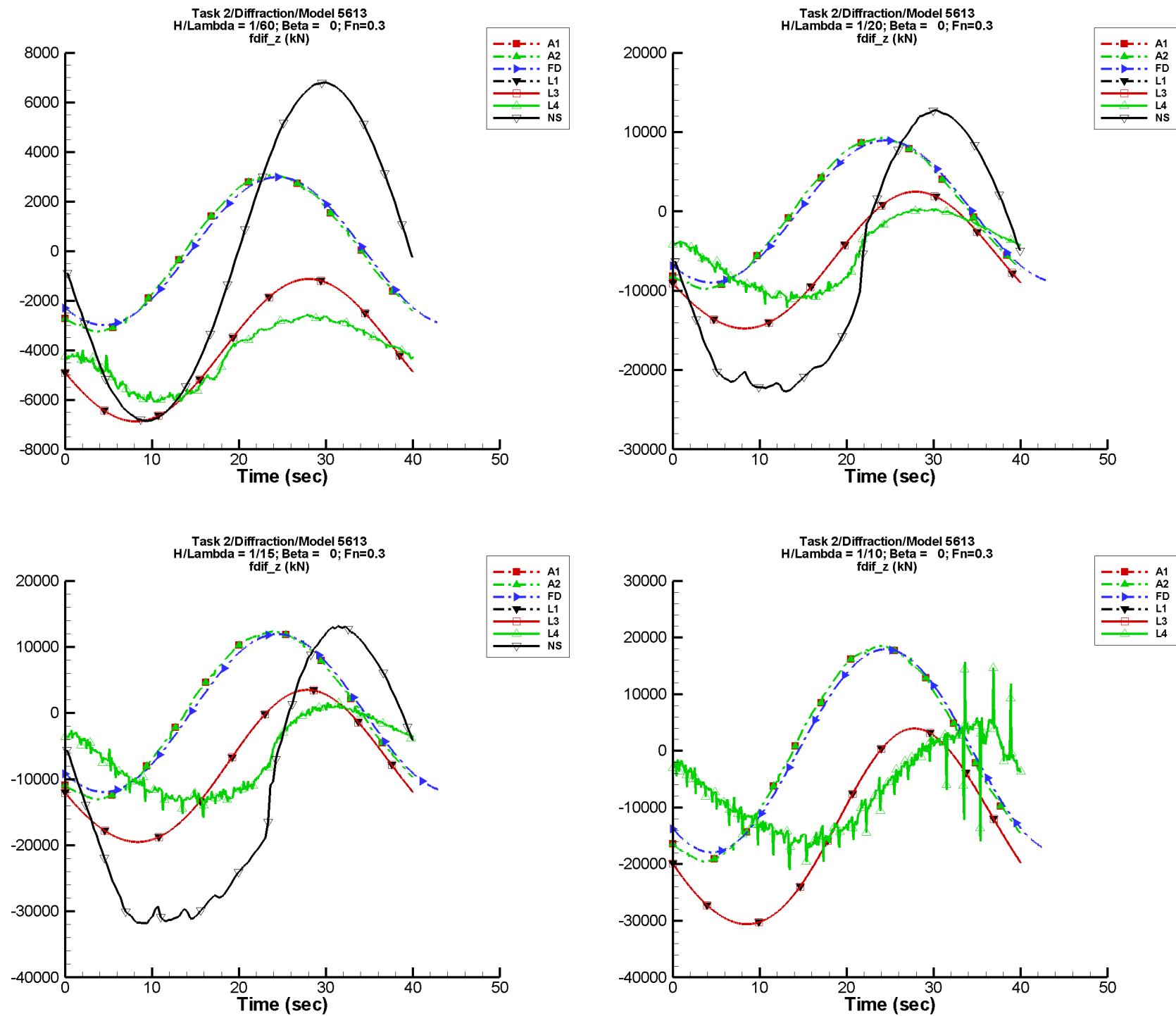


Fig. 34. Vertical diffraction force experienced by Model 5613 advancing in 0-DOF motion ($F_n = 0.3$) in following seas of wave steepness $H/\lambda = 1/60$ (top left), $1/20$ (top right), $1/15$ (bottom left), and $1/10$ (bottom right) where $\lambda = L$.

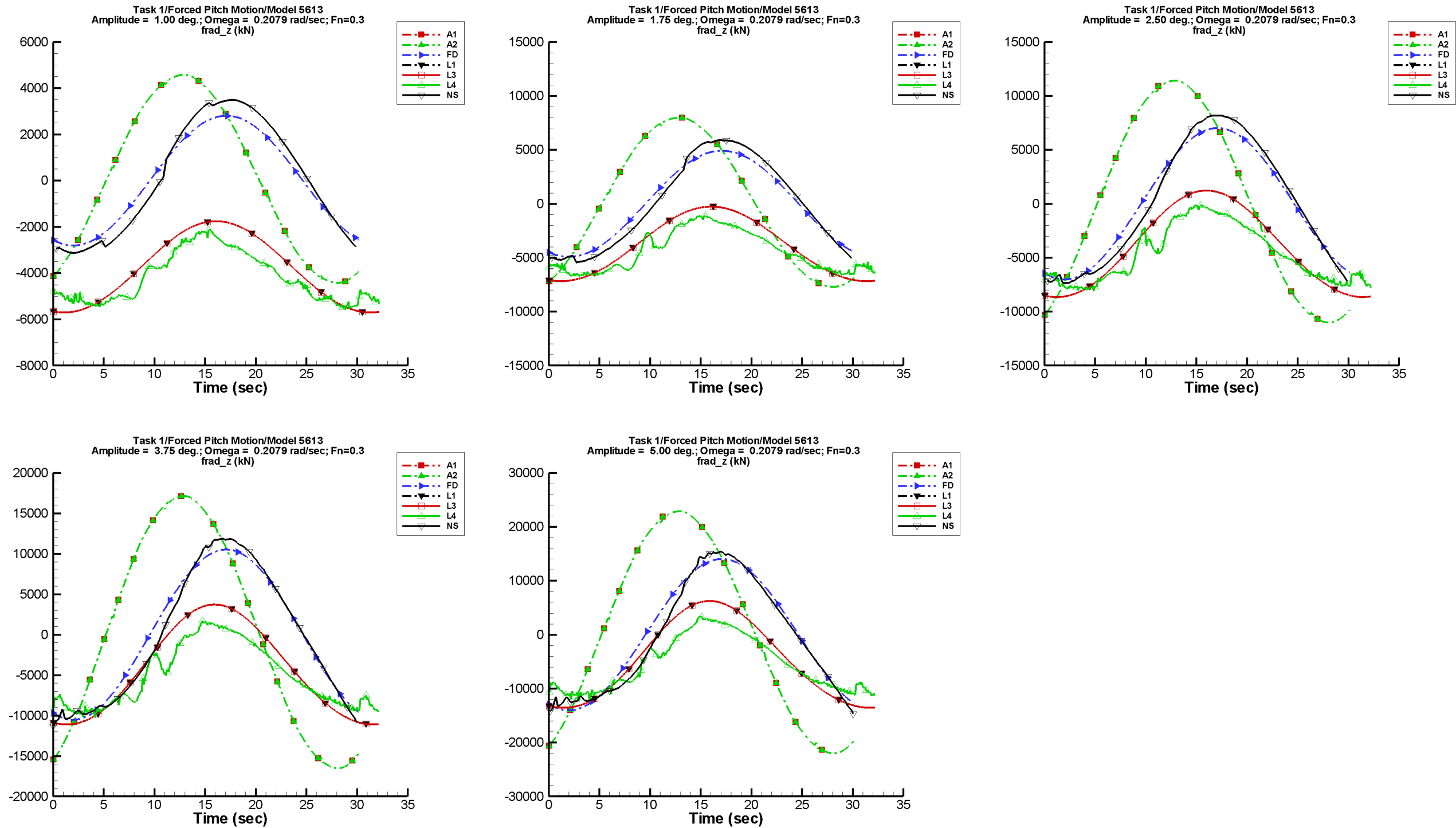


Fig. 35. Ship-fixed vertical component of radiation force experienced by Model 5613 advancing in calm water ($F_n = 0.3$) with 1-DOF pitch motion of frequency 0.2079 rad/sec and amplitudes 1.00°, 1.75°, 2.50°, 3.75°, and 5.00°.

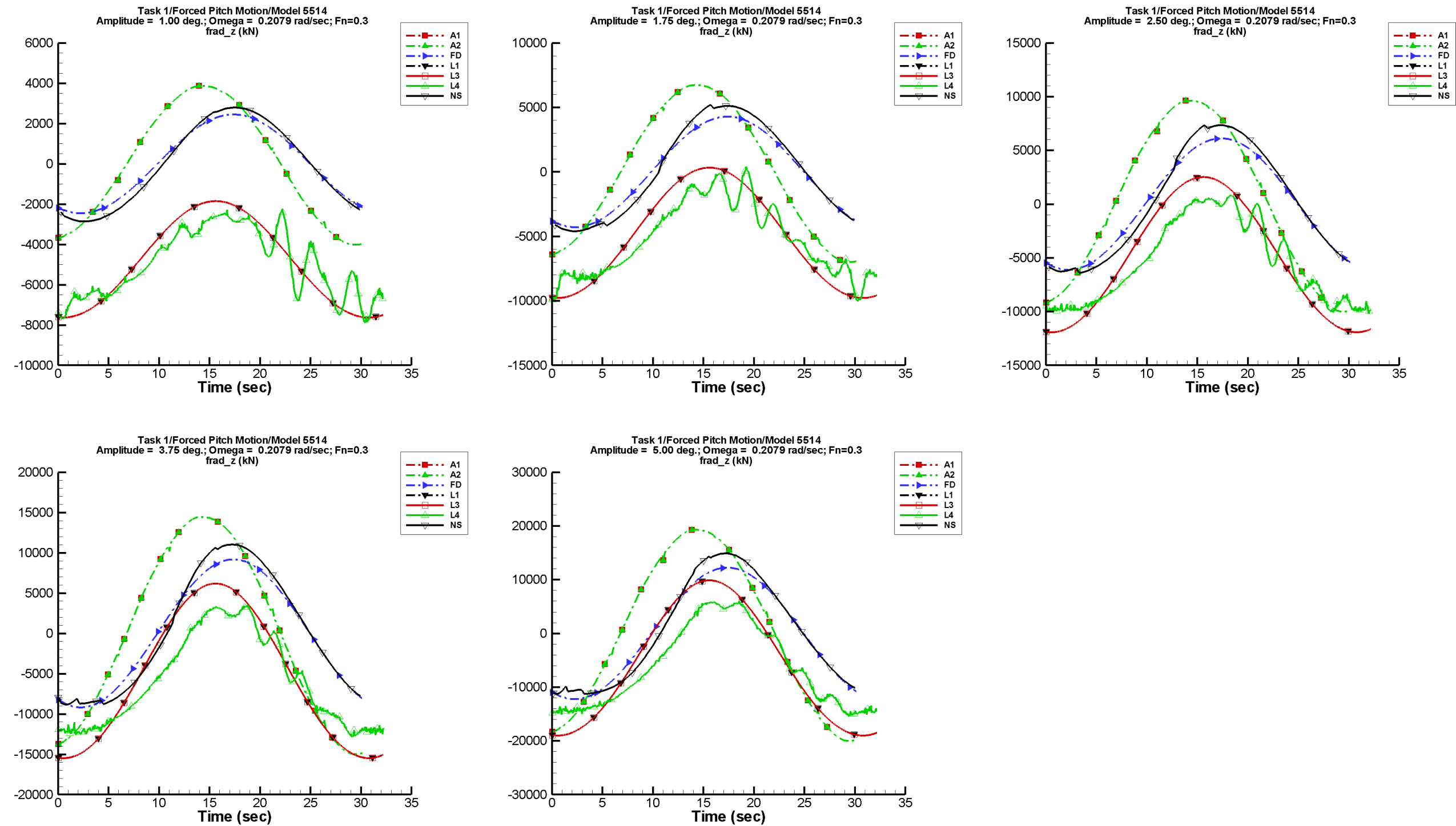


Fig. 36. Ship-fixed vertical component of radiation force experienced by Model 5514 advancing in calm water ($F_n = 0.3$) with 1-DOF pitch motion of frequency 0.2079 rad/sec and amplitudes 1.00°, 1.75°, 2.50°, 3.75°, and 5.00°.

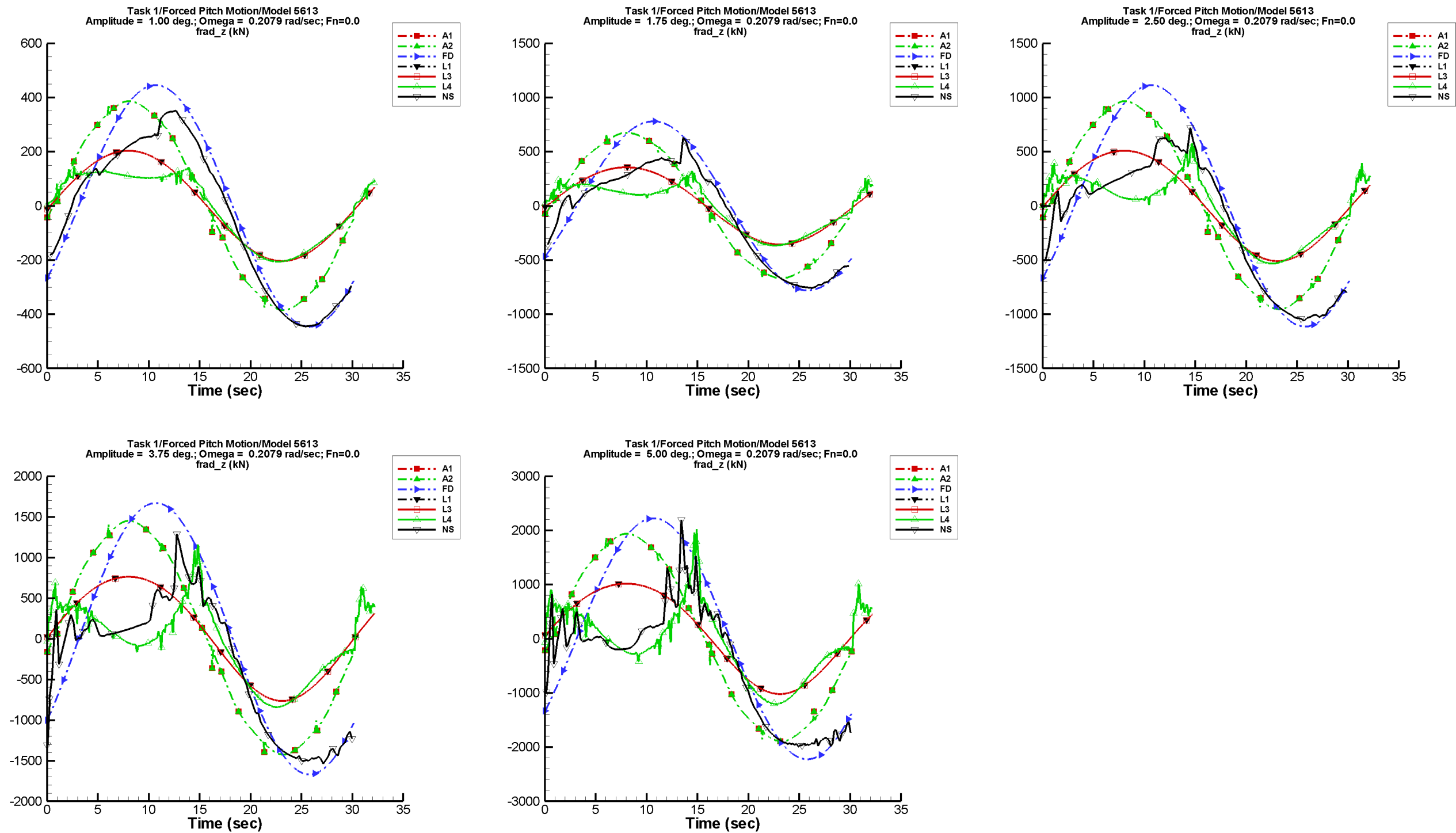


Fig. 37. Ship-fixed vertical component of radiation force experienced by Model 5613 at zero forward speed in calm water with 1-DOF pitch motion of frequency 0.2079 rad/sec and amplitudes 1.00°, 1.75°, 2.50°, 3.75°, and 5.00°.

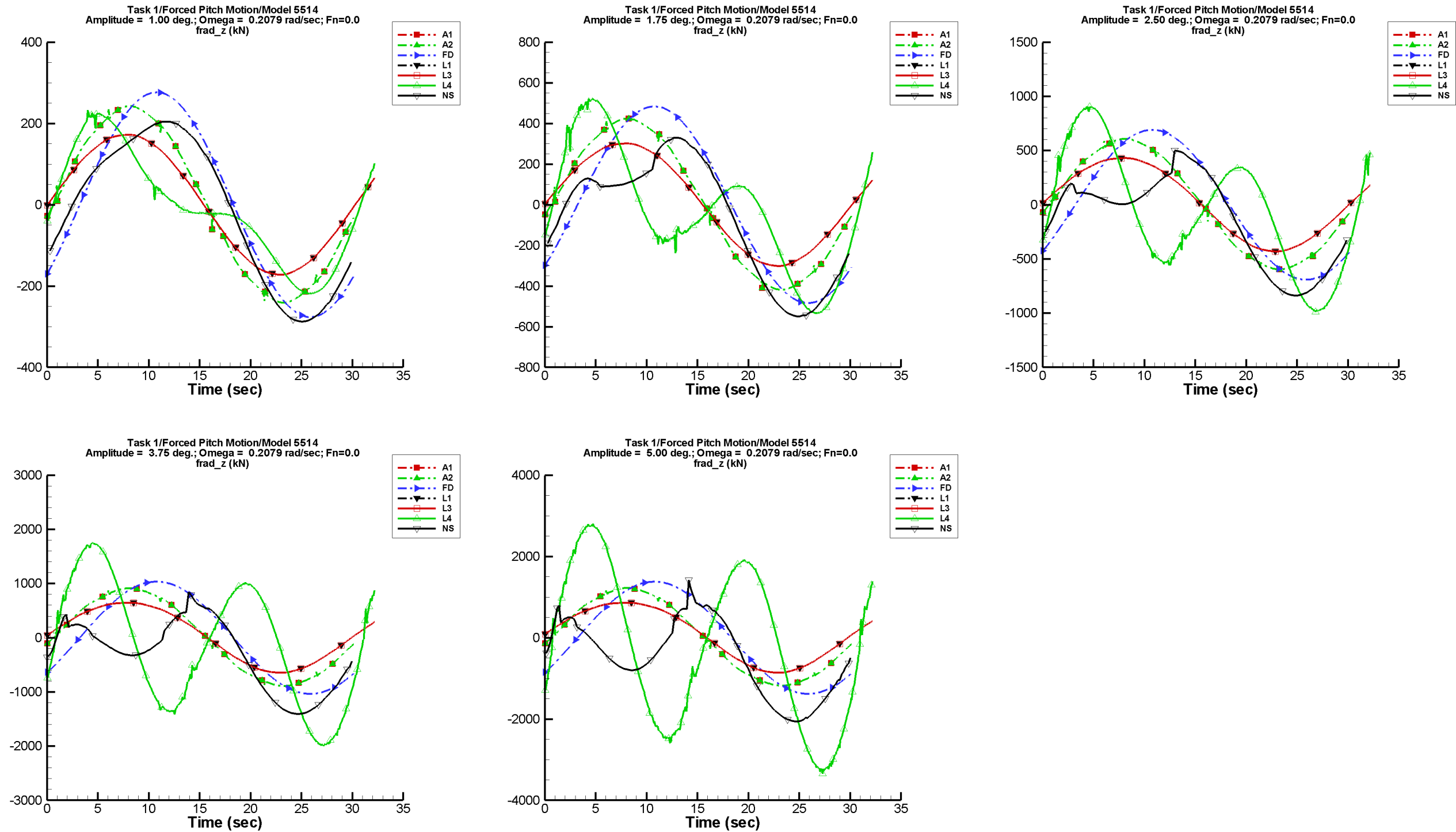


Fig. 38. Ship-fixed vertical component of radiation force experienced by Model 5514 at zero forward speed in calm water with 1-DOF pitch motion of frequency 0.2079 rad/sec and amplitudes 1.00°, 1.75°, 2.50°, 3.75°, and 5.00°.

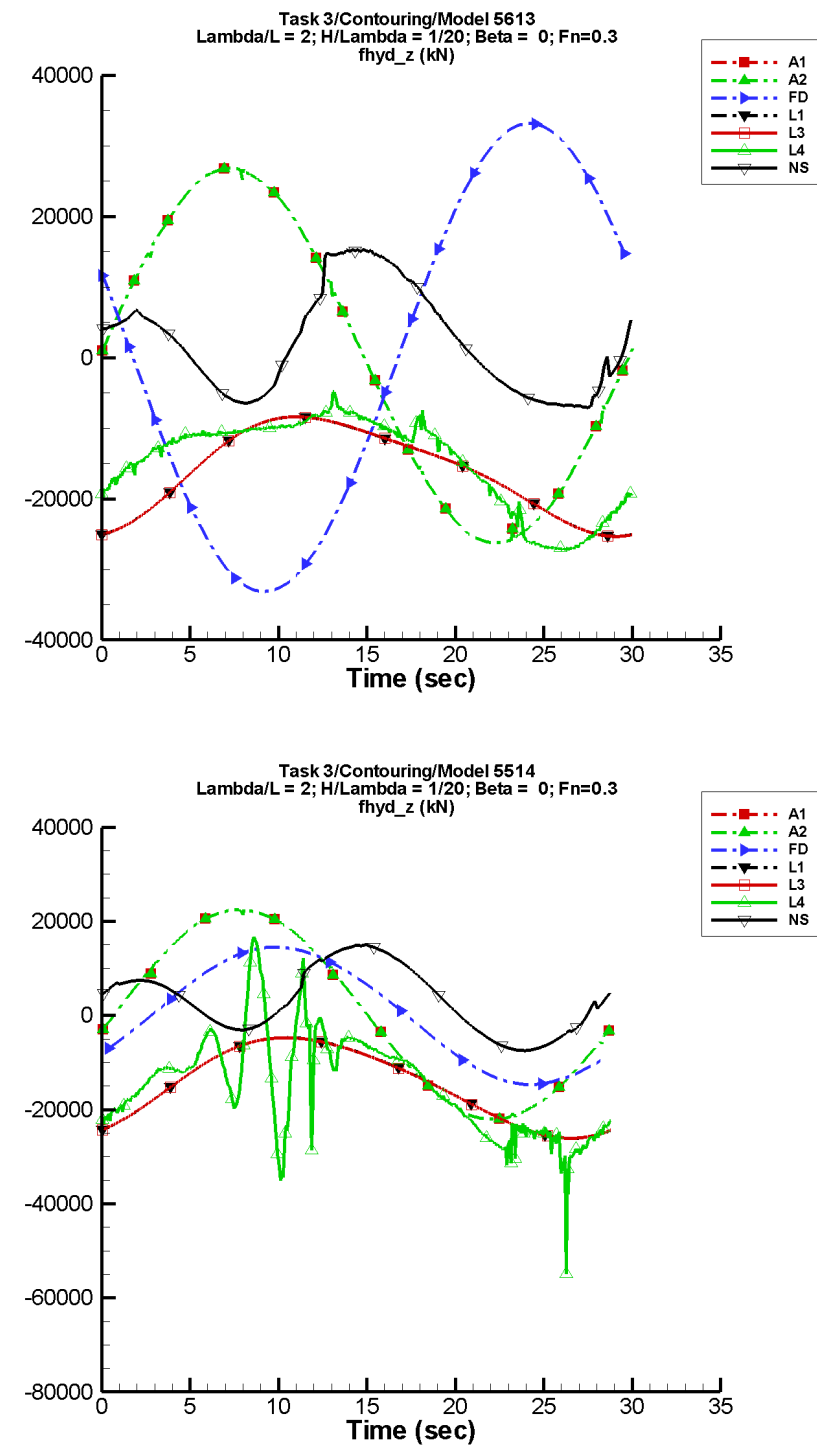


Fig. 39. Ship-fixed vertical component of hydrodynamic force experienced by Models 5613 (top) and 5514 (bottom) as they contour a wave at forward speed ($F_n = 0.3$) in following seas (task 3, condition 1).

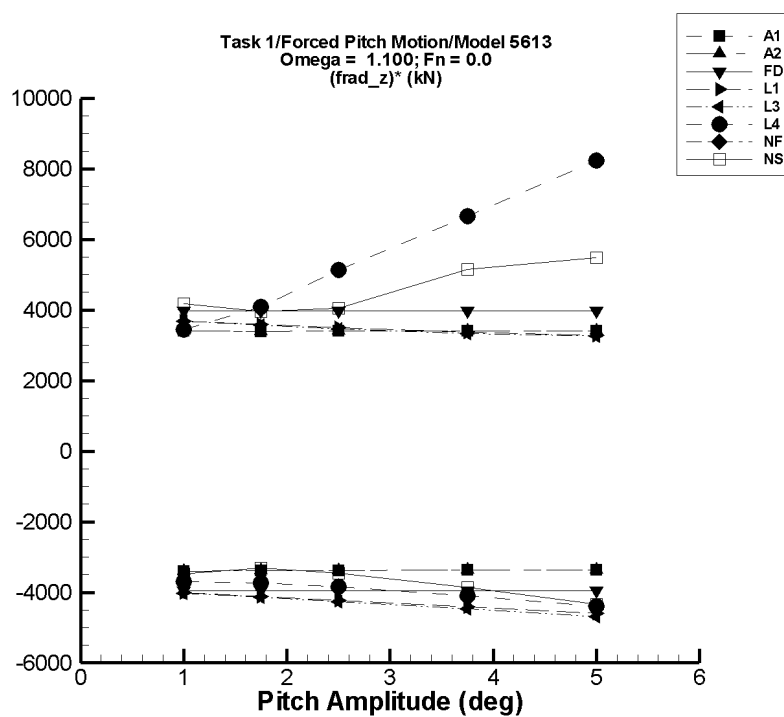


Fig. 40. Minimum and maximum of the ship-fixed vertical component of the radiation force experienced by Model 5613 in pitch motion at zero forward speed in otherwise undisturbed water at the frequency 1.1 rad/sec.

tables of data are in Appendices K–R, which also take the form of bookmarked PDF files. The time-history plots should be compared with one another. The plots of the minimum and maximum found in Appendices K–R should be compared with the time-history plots in Appendices A–H. Here Appendix A is associated with Appendix K, Appendix B with Appendix L, and so forth. Given the amount of data in the appendices, time is required to digest the results to draw definitive conclusions about robustness and accuracy of the codes, the importance of nonlinearities, and how well various computer codes calculate nonlinearities.

Many of the results in this report reflect on the immaturity of the codes in handling geometry and do not necessarily say anything about whether a code based on this or that theory would suffice instead of one based on a fully nonlinear theory. In some cases, the code runners were challenged to provide a suitable free-surface paneling for low frequency forced motion where two length scales ought to be resolved — one of the order of the length of the ship and one of the order of a wavelength which is more than ten times the length of the ship. In some of those cases one cannot be sure if the fluctuations in the results are due to inadequate paneling or some other cause. LAMP-1 ought to have been modified for all the runs so that the grid velocity term is identically zero. Of course, the results will no longer be from LAMP-1, but part of the purpose of this study is to determine the adequacy of various theories. Most codes require filtering to maintain numerical stability, and the result of such filtering is obvious in some cases. Other causes of noise in the results may be related to discontinuous jumps in geometry from time step to time step. A volume-of-fluid code such as NFA might be able to handle such changes more robustly, but not without an extra computational burden. Results from it should be compared more closely with results from other codes. Unfortunately, code within NFA was developed to compute forces and moments as the tasks of the potential flow force study were executed. Hence, results from NFA have not been thoroughly validated. If the codes mature a bit more, it might be interesting to rerun selected cases from this study.

Despite the unexpected disparity in the results due to code immaturity, differing definitions of quantities, and so forth, one can say that the importance of nonlinearity is demonstrated in the results that have been presented in plots. An obvious indicator of nonlinearity is the departure of the components of force and moment from simple trigonometric form, an indicator seen in most of the plots presented. Spikes present in some components may originate in geometric nonlinearities. Accurately defining the incident wave's kinematics and pressures near the free surface is critical to determining the total fluid force. In large steep waves, using second order pressure results in significant changes to the predictions (as, for example, can be seen in Fig. 42 where the results from NSHIPMO and the four LAMP codes are compared with the results from the other codes). Higher order nonlinear wave theory must be used in such cases. Cancellation of forces and moments arising from the wave radiation and diffraction components, the Froude-Krylov component, and hydrostatics component contributes to the importance of determining all components accurately even when they are relatively small. For task 3, examples of such cancellation are seen in Figs. 24–26 where it is seen that the hydrostatic and Froude-Krylov components of the force and moment nearly cancel for a ship contouring waves in beam seas. The remaining hydrodynamic component of the force and moment must be calculated accurately. If there is relative motion between the ship and the water, a body-exact theory is required.

Unfortunately, codes based on body-exact three-dimensional theory are computationally inten-

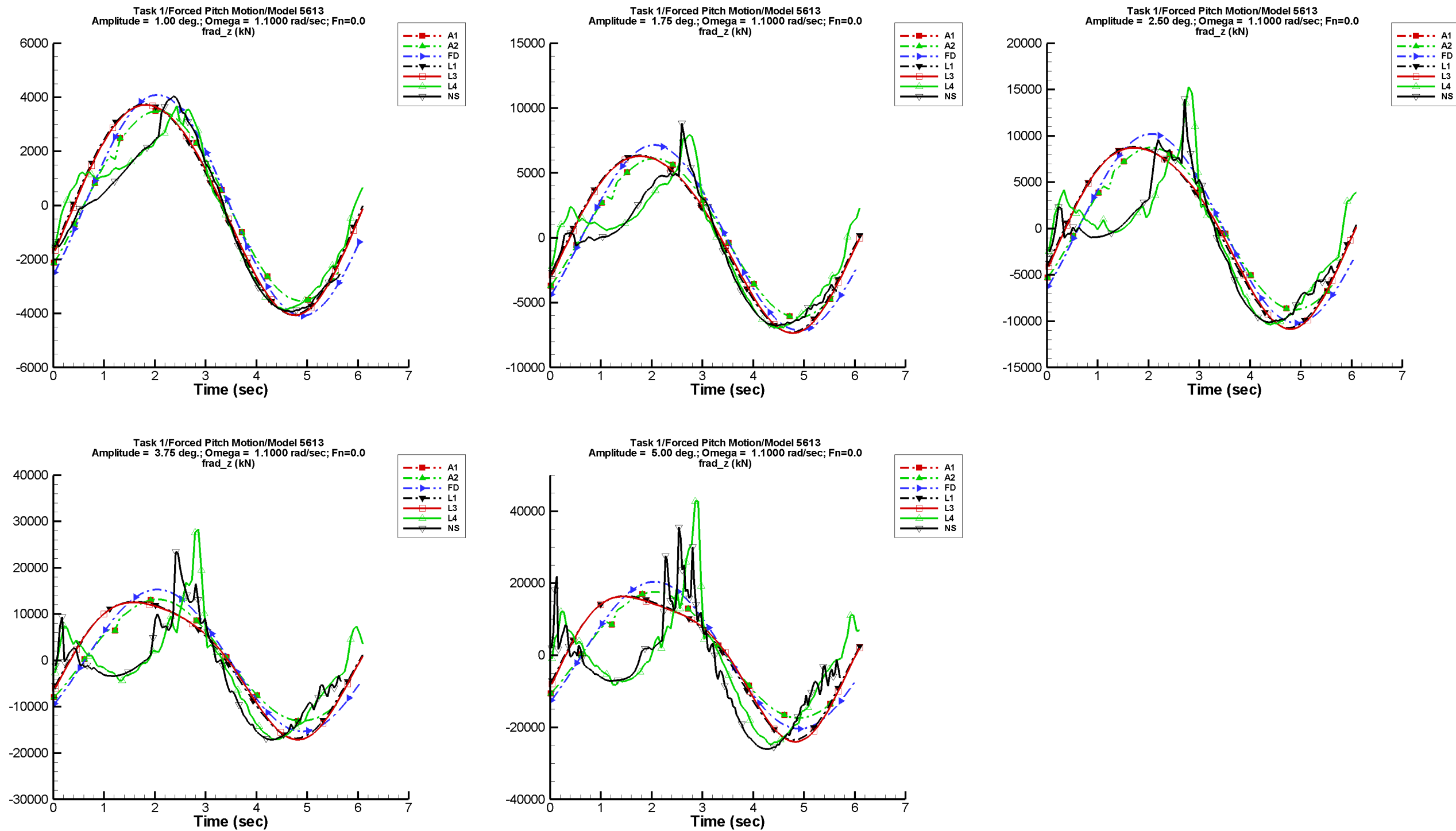


Fig. 41. Time-history plots of the ship-fixed vertical component of the radiation force experienced by Model 5613 at zero forward speed in forced pitch motion of amplitudes 1.0°, 1.75°, 2.5°, 3.75°, and 5° and frequency 1.1 rad/sec.

THIS PAGE INTENTIONALLY LEFT BLANK.

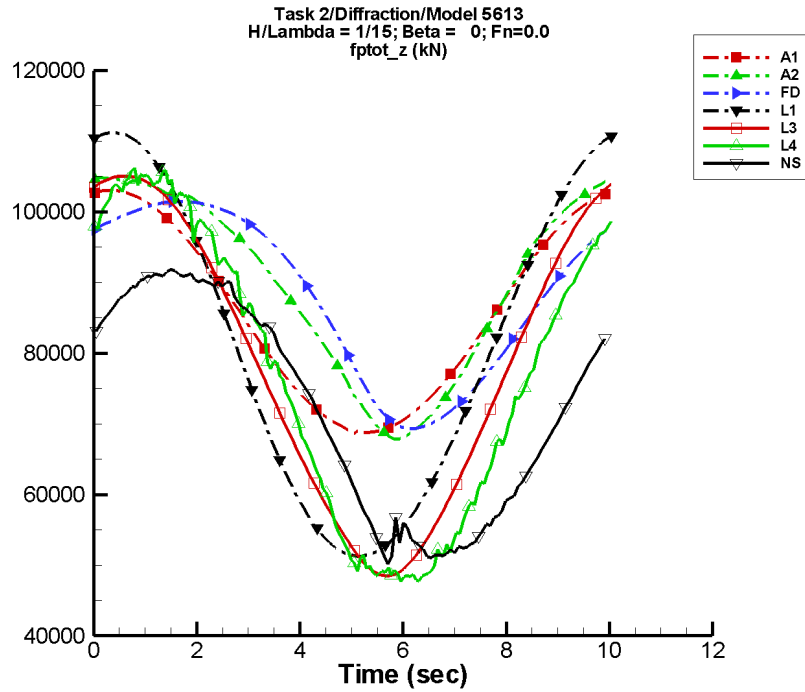


Fig. 42. Time-history plot of the vertical component of the total force experienced by Model 5613 in 0-DOF motion at zero forward speed in following seas with wavelength $\lambda/L = 1$ and amplitude $H/\lambda = 1/15$.

sive. In the plots of results shown in Figs. 13, 14, 16, and 18, the nonlinear two-dimensional strip theory of NSHIPMO appears to capture details predicted by the nonlinear three-dimensional code LAMP-4 that are not present in the results of the other codes. Further, Fig. 43 shows a comparison of NSHIPMO with LAMP-4 and NFA for the total vertical force experienced by Model 5613 in forced heave motion. In this figure, the curves depicting the results from NSHIPMO, LAMP-4, and NFA share features not present in the curves corresponding to the results from the other codes. Figure 44 shows a comparison of the yaw component of the computed total moment for one case of Model 5514 in forced roll motion. Peaks predicted by NSHIPMO, LAMP-4, and NFA agree although details between the peaks do not agree so well. The results in these figures suggest that the use of fully nonlinear body-exact codes like LAMP-4 and NFA can be avoided. Using the type of strip theory present in NSHIPMO would provide a substantial speedup in the calculations while maintaining increased accuracy.

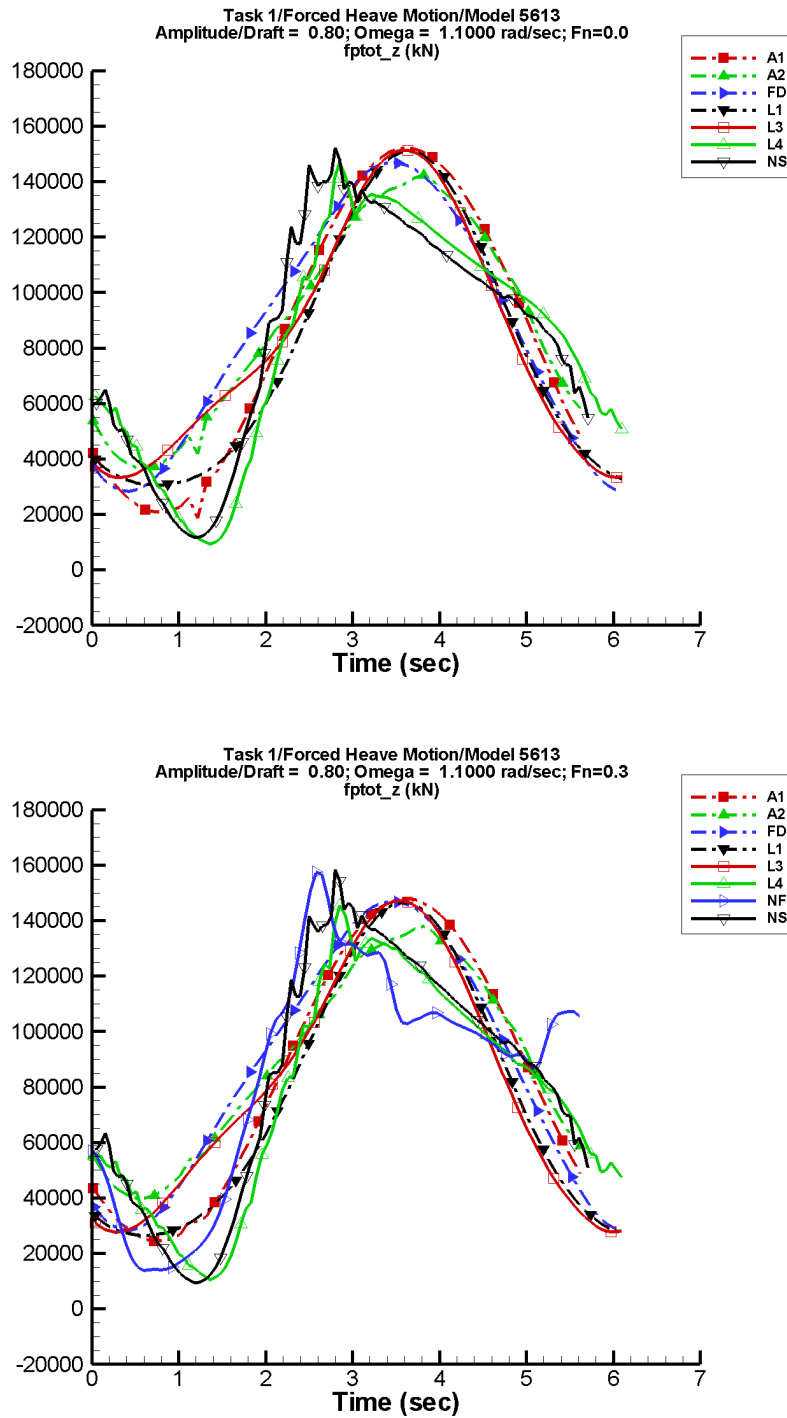


Fig. 43. Time-history plot of the vertical component of the total force experienced by Model 5613 in forced heave motion at frequency 1.1 rad/sec and amplitude 80 per cent of the draft for zero forward speed (top) and forward speed corresponding to Froude number 0.3 (bottom).

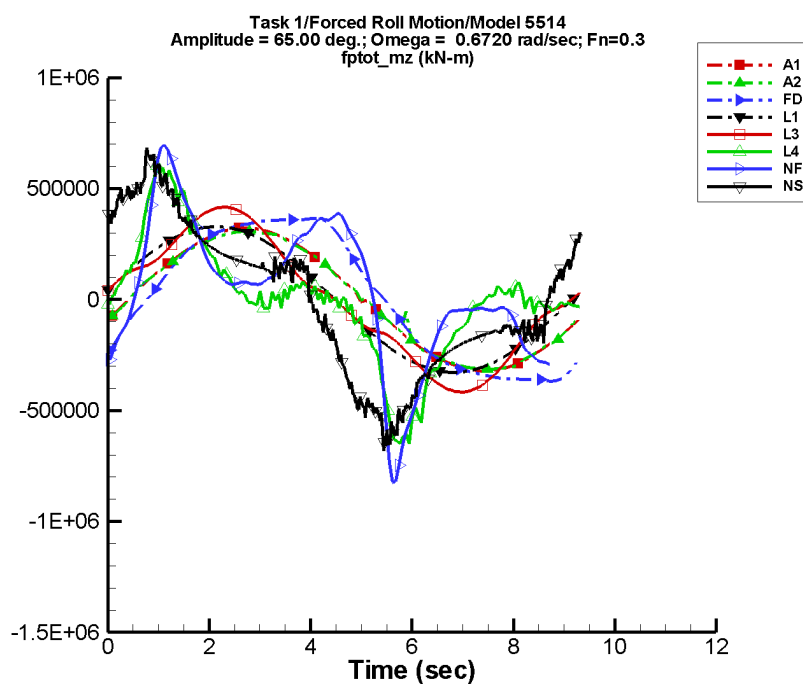


Fig. 44. Time-history plot of the yaw component of the computed total moment experienced by Model 5514 in forced roll motion at frequency 0.672 rad/sec and amplitude 65° at forward speed corresponding to Froude number 0.3.

THIS PAGE INTENTIONALLY LEFT BLANK

REFERENCES

1. Beck, R. F., and A. M. Reed, "Modern Computational Methods for Ships in a Seaway," *SNAME Transactions*, Vol. 109, pp. 1-51, 2001.
2. Hayden, D. D., R. C. Bishop, J. T. Park, and S. M. Lavery, "Model 5514 Capsize Experiments Representing the Pre-Contract DDG 51 Hull Form at End of Service Life Conditions," Naval Surface Warfare Center Carderock Division Report NSWCCD-50-TR-2006/020, April 2006.
3. Bishop, R. C., W. F. Belknap, C. Turner, B. Simon, and J. H. Kim, "Parametric Investigation on the Influence of GM, Roll Damping, and Above-Water Form on the Roll Response of Model 5613," Naval Surface Warfare Center Carderock Division Report NSWCCD-50-TR-2005/027, August 2005.
4. Kring, D. C., W. M. Milewski, and N. E. Fine, "Validation of a NURBS-Based BEM for Multihull Ship Seakeeping," *Proc. 25th Symposium on Naval Naval Hydrodynamics*, St. John's, Newfoundland and Labrador, Canada, 8–13 August 2004.
5. Liut, D. A., K. W. Weems, and W.-M. Lin, "Nonlinear Green Water Effects On Ship Motions and Structural Loads," *Proc. 24th Symposium on Naval Hydrodynamics*, Fukuoka, Japan, 8–13 July 2002.
6. Dommermuth, D. G., T. T. O'Shea, D. C. Wyatt, T. Ratcliffe, G. D. Weymouth, K. L. Hendrikson, D. K. P. Yue, M. Sussman, P. Adams, and M. Valenciano, "An Application of Cartesian-Grid and Volume-of-Fluid Methods to Numerical Ship Hydrodynamics," *Proc. 9th International Conference on Numerical Ship Hydrodynamics*, Ann Arbor, MI, 5–8 August 2007.
7. Dommermuth, D. G., T. T. O'Shea, D. C. Wyatt, M. Sussman, G. D. Weymouth, D. K. P. Yue, P. Adams, and R. Hand, "The Numerical Solution of Ship Waves Using Cartesian-Grid and Volume-of-Fluid Methods," *Proc. 26th Symposium on Naval Hydrodynamics*, Rome, Italy, 17–22 September 2006.
8. de Kat, J. O., and J. R. Paulling, "The Simulation of Ship Motions and Capsizing in Severe Seas," *SNAME Transactions*, 97:139–68, 1989.
9. de Kat, J., "Irregular Waves and their Influence on Extreme Ship Motions," *Proc. 20th Symposium on Naval Hydrodynamics*, Santa Barbara, CA, pp. 48–67, 1994.
10. de Kat, J. O., R. Brouwer, K. A. McTaggart, and W. L. Thomas, III, "Intact Ship Survivability in Extreme Waves: New Criteria from a Research and Navy Perspective," *Proc. 5th International Conference on Stability of Ships and Ocean Vehicles (STAB 94)*, Melbourne, FL, 7–11 November 1994.
11. Salvesen, N., E. O. Tuck, and O. Faltinsen, "Ship Motions and Sea Loads," *SNAME Transactions*, vol. 78, 1970.
12. Abramowitz, M., and I. A. Stegun, *Handbook of Mathematical Functions with Formulas, Graphs, and Mathematical Tables*, New York: Dover, 1964.

13. Whittaker, E., and G. Robinson, *The Calculus of Observations: A Treatise on Numerical Mathematics*, 4th ed., London: Blackie & Son, Ltd., 1944.
14. Press, W. H., B. P. Flannery, S. A. Teukolsky, and W. F. Vetterling, *Numerical Recipes: The Art of Scientific Computing*, New York: Cambridge University Press, 1986.

Report Distribution

Number of Copies		
1	NAVSEA PMS 500T	J. Horvath
1	NAVSEA 05D2	M. Garner
2	NAVSEA 05Z11	R. Crocket/R. Waters
2	NAVSEA 05Z12	D. Cimino/P. Alman
1	DTIC	
1	ONR 331	P. Purtell
1	CSC	J. O'Dea
1	MIT	P. Slavounos
2	SAIC/Annapolis	W.-M. Lin/K. Weems
2	SAIC/La Jolla	D. Dommermuth/C. Scragg
1	VA Tech	L. McCue
1	Penn State/ARL	E. Paterson
1	Flight Safety Technology	D. Kring
1	Applied Physical Sciences	W. Milewski
1	UC Berkeley	R. Paulling
2	University of Michigan	R. Beck/A. Troesch
NSWCCD INTERNAL DISTRIBUTION		
Number of Copies	NSWCCD Code	Individual
1	3452	TIC
1	504	Reed
1	5060	Walden
1	5080	Brown
5	5500	Applebee, Belknap, Campbell, Hughes, Telste
1	5800	Hurwitz

